MICROCOPY RESOLUTION TEST CHART
NATIONAL BUREAU OF STANDARDS-1963-A

AD-A141 962

Below-Room-Temperature Water-Vapor Continuum Absorption within the 8- to 12-μm Atmospheric Transmission Window

G. L. LOPER, M. A. O'NEILL, and J. A. GELBWACHS
Chemistry and Physics Laboratory
Laboratory Operations
The Aerospace Corporation
El Segundo, Calif. 90245

11 May 1984

APPROVED FOR PUBLIC RELEASE;
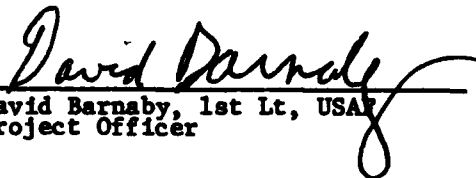DISTRIBUTION UNLIMITED

DTIC
ELECTE
JUN 1 1 1984
B

Prepared for

SPACE DIVISION
AIR FORCE SYSTEMS COMMAND
Los Angeles Air Force Station
P.O. Box 92960, Worldway Postal Center
Los Angeles, Calif. 90009

84 06 08 006

This report was submitted by The Aerospace Corporation, El Segundo, CA 90245, under Contract No. F04701-83-C-0084 with the Space Division, P.O. Box 92960, Worldway Postal Center, Los Angeles, CA 90009. It was reviewed and approved for The Aerospace Corporation by S. Feuerstein, Director, Chemistry and Physics Laboratory. First Lieutenant David Barnaby, SD/YNCS, was the project officer for the Mission-Oriented Investigation and Experimentation Program.

This report has been reviewed by the Public Affairs Office (PAS) and is releasable to the National Technical Information Service (NTIS). At NTIS, it will be available to the general public, including foreign nationals.

This technical report has been reviewed and is approved for publication. Publication of this report does not constitute Air Force approval of the report's findings or conclusions. It is published only for the exchange and stimulation of ideas.

David Barnaby, 1st Lt, USAF
Project Officer

Joseph Hess, Director, West Coast Office
Air Force Space Technology Center

REPORT DOCUMENTATION PAGE		READ INSTRUCTIONS BEFORE COMPLETING FORM
1. REPORT NUMBER SD-TR-84-14	2. GOVT ACCESSION NO. AD-A141962	3. RECIPIENT'S CATALOG NUMBER
4. TITLE *(and Subtitle)* BELOW-ROOM-TEMPERATURE WATER-VAPOR CONTINUUM ABSORPTION WITHIN THE 8- to 12-μm ATMOSPHERIC TRANSMISSION WINDOW		5. TYPE OF REPORT & PERIOD COVERED
		6. PERFORMING ORG. REPORT NUMBER TR-0084(4945-09)-1
7. AUTHOR(s) G. L. Loper, M. A. O'Neill, and J. A. Gelbwachs		8. CONTRACT OR GRANT NUMBER(s) F04701-83-C-0084
9. PERFORMING ORGANIZATION NAME AND ADDRESS The Aerospace Corporation El Segundo, Calif. 90245		10. PROGRAM ELEMENT, PROJECT, TASK AREA & WORK UNIT NUMBERS
11. CONTROLLING OFFICE NAME AND ADDRESS Space Division Los Angeles Air Force Station Los Angeles, Calif. 90009		12. REPORT DATE 11 May 1984
		13. NUMBER OF PAGES 94
14. MONITORING AGENCY NAME & ADDRESS *(if different from Controlling Office)*		15. SECURITY CLASS. *(of this report)* Unclassified
		15a. DECLASSIFICATION/DOWNGRADING SCHEDULE

16. DISTRIBUTION STATEMENT *(of this Report)*

Approved for public release; distribution unlimited.

17. DISTRIBUTION STATEMENT *(of the abstract entered in Block 20, if different from Report)*

18. SUPPLEMENTARY NOTES

19. KEY WORDS *(Continue on reverse side if necessary and identify by block number)*

Atmospheric infrared transmission
CO_2 laser transmission
Water continuum absorption
Water dimer models
Collisional-broadening model
CO_2 laser photoacoustic technique

20. ABSTRACT *(Continue on reverse side if necessary and identify by block number)*

Described are the results of a laboratory study of the weak water-continuum absorption within the 8- to 12-μm atmospheric transmission window. The highly sensitive photoacoustic detection technique was used in conjunction with a line-tunable CO_2 laser to measure water continuum absorption throughout the CO_2 laser 10.4-μm band. These measurements were performed over a range of atmospheric temperatures and water pressures important to the attenuation of radiation for long-slant atmospheric transmission paths. Water continuum CO_2 laser absorption spectra are reported for

DD FORM 1473
(FACSIMILE)

19. KEY WORDS (Continued)

20. ABSTRACT (Continued)

temperatures between 27 and -10°C. Below room temperature, spectra of this type have not been determined previously.

The water continuum absorption was found to possess a negative temperature dependence between 27 and -10°C that is similar to that observed between 100 and 27°C by previous investigators. The temperature, pressure, and wavelength dependences observed for the 8- to 12-μm water continuum in this study, and in previous studies reviewed thoroughly here, are best modeled by assuming simultaneous contributions of water-dimer and collisional-broadening mechanisms to the continuum. At room temperature and below, the water dimer mechanism becomes more important than the collisional-broadening mechanism.

CONTENTS

FIGURES

TABLES

I. INTRODUCTION

Quantitative information on the propagation efficiency of infrared radiation through the earth's atmosphere is important for a variety of current and possible future Air Force Space Division (SD) missions. These include remote sensing, missile and aircraft detection, and the use of infrared lasers in weapons and communication systems.

Atmospheric propagation of infrared radiation is most efficient at wavelengths between 3 and 5 μm and between 8 and 12 μm, where major atmospheric transmission windows are present. The wavelength limits of these windows are defined primarily by strong absorption bands for atmospheric water vapor and carbon dioxide. The predominant contribution to the attenuation of radiation within the windows, under high-visibility conditions, results from a weak background absorption that is continuous with wavelength and is associated with water vapor. This continuum absorption remains upon subtraction of the absorption contributions from the weak water-vapor lines located in the windows. Although the magnitude of continuum absorption per unit length of the atmosphere is small, it can cause significant attenuation of infrared radiation for long atmospheric transmission path lengths.[1-4] Accurate data on the magnitude of the continuum absorption within the 3- to 5-μm and 8- to 12-μm wavelength regions under a variety of possible atmospheric conditions are thus required to ensure the optimum design of future infrared military systems and to better evaluate the performance of existing systems.

This report describes the results of laboratory measurements of the weak water-continuum absorption within the 8- to 12-μm window. The measurements were performed using mixtures of water vapor and air over a range of water partial pressures and temperatures that simulate those found in the atmosphere. The data obtained in this program will help to establish a data base from which appropriate models can be developed to predict accurately water continuum absorption within the 8- to 12-μm region under all possible atmospheric conditions of temperature, water-vapor and air partial pressure, and transmission path length and zenith angle.

Most studies of the 8- to 12-µm water continuum absorption have been performed in the laboratory with long-path absorption techniques using multipass spectroscopic gas cells.[5-12] The inherent sensitivity limitations of these techniques have generally allowed these studies to be performed only on water-vapor—air mixtures of high relative humidity at room temperature or above. Such conditions, however, do not represent the entire atmosphere that must be traversed in certain space-based detection schemes for which atmospheric temperatures may range from above room temperature to -60°C (213 K).[13] For detection schemes involving long-slant transmission paths through the atmosphere, it may be necessary to account for water continuum absorption at temperatures of -10°C or below.

We have used the highly sensitive photoacoustic detection technique in conjunction with a line-tunable CO_2 laser to measure water-vapor CO_2 laser absorption spectra at significantly lower temperatures than employed previously. The CO_2 laser photoacoustic detection technique has been used to accurately measure water continuum absorption spectra within the 8- to 12-µm transmission window.[14-16] These measurements, however, were made primarily on water-vapor—air mixtures at temperatures above 20°C.

The origin of the water continuum absorption within either transmission window has not been well characterized. Collisional-broadening or water-vapor aggregate (mainly water dimer) mechanisms, or both, have been most frequently proposed to account for water continuum absorption within the 8- to 12-µm window. The most thoroughly developed collisional-broadening[17,18] and water dimer models[19,20] can predict the proper magnitude of the 8- to 12-µm continuum absorption near room temperature. These models, however, predict different dependences of the continuum absorption on temperature and water partial pressure. Thus, extension of the continuum measurements to lower temperatures than previously studied and determination of the continuum's water-pressure dependence below room temperature should permit better quantification of the relative contributions of the collisional-broadening and water aggregate mechanisms to 8- to 12-µm continuum absorption. Knowledge of the relative importance of each of these mechanisms, or other possible mechanisms,[21] as a function of temperature, and water-vapor—air partial pressure is needed to permit the continuum-absorption phenomenon to be modeled and accurately predicted under various atmospheric conditions.

Section II describes the contributions to the atmospheric attenuation of infrared radiation and reviews previous studies of the water-vapor continuum absorption within the 8- to 12-μm atmospheric transmission window. It also briefly describes the CO_2-laser-based photoacoustic technique used in the present program. Section III describes the experimental apparatus and procedures used to measure the water continuum under various simulated atmospheric conditions. Section IV presents and discusses the water continuum data determined in this study. Conclusions to the study are outlined in Section V.

II. BACKGROUND

A. ATMOSPHERIC ATTENUATION OF INFRARED RADIATION

The efficiency with which infrared radiation is transmitted through the atmosphere depends upon various properties of both the radiation field (viz., wavelength, spectral bandwidth, radiance, and coherence) and the propagation media over the transmission path (viz., type, abundance, and distribution of gases, aerosols, and particles, as well as the atmospheric temperature and pressure). The atmospheric attenuation of infrared radiation primarily results from absorption by molecular atmospheric constituents and scattering by aerosols and particles. Under normal atmospheric conditions of high visibility, molecular absorption makes a significantly greater contribution to the attenuation of radiation throughout the infrared region (wavelengths between approximately 1 μm and 1 mm) than does aerosol or particle scattering. Attenuation due to Rayleigh scattering from molecules and scattering at locations of turbulence-induced atmospheric refractive-index inhomogeneities is generally much less important in the infrared than molecular absorption or aerosol and particle scattering.

The magnitude of the attenuation caused by scattering from aerosols and particles is determined by their number density, size distribution, and composition. These factors are influenced by geographical locat'on and time-varying meteorological conditions. The phenomena of scattering of infrared radiation from aerosols and particles, such as found in clouds, fog, rain, and haze, have been reviewed by Zuev.[22]

The earth's atmosphere can be divided into a number of different layers based on its vertical temperature profile and other properties. Almost all of the water vapor and over three-fourths of the other atmospheric gases are contained in the troposphere.[13] In the troposphere, the lowest layer of the atmosphere, average temperatures generally decrease rapidly with increasing altitude and convection mixing of gases occurs. The vertical thickness of the troposphere varies with latitude and season; it may extend to 18 km at tropical latitudes and to 10 km at polar latitudes. The troposphere is bounded by the stratosphere, which may extend to altitudes of 50 km. Temperatures in the

stratosphere are nominally constant with increasing altitude to about 25 km but then increase rapidly above 25 km.

The infrared-active atmospheric species present in the greatest natural abundance and causing the most intense integrated absorption over the infrared-wavelength region are water vapor and carbon dioxide. The wavelength regions of high relative transmittance in combined infrared spectra of these compounds generally correspond to the wavelength regions of the atmospheric infrared transmission windows, as Fig. 1 indicates. The integral absorption of atmospheric ozone throughout the infrared is much weaker than that of water vapor or carbon dioxide. However, ozone does possess some strong, sharp absorption lines between about 9.4 and 9.8 μm. The minor infrared-active constituents of the atmosphere -- methane, nitrous oxide, carbon monoxide, nitric oxide, nitrogen dioxide, nitric acid, ammonia, sulfur dioxide, and partially deuterated water -- contribute negligibly to the integral absorption of infrared radiation by the atmosphere. However, their attenuation effects[2,23] may have to be considered for applications involving the propagation or detection of narrow-band infrared radiation within the 3- to 5-μm and 8- to 12-μm atmospheric transmission windows.* Under clear atmospheric conditions, water-vapor continuum absorption is the most important contributor to the attenuation of infrared radiation within these transmission windows. The mechanisms proposed as being responsible for this absorption are described in Section II.D.

Nitrogen and oxygen, the major components of the atmosphere, are vibrationally infrared inactive in their isolated molecule state, because they do not have permanent dipole moments that can couple their vibrations to a radiation field. In the atmosphere, however, the fundamental vibrational transitions in nitrogen and oxygen (centered at 4.24 and 6.33 μm, respectively) may become very weakly allowed during nitrogen--oxygen molecular collisions and collisions of nitrogen or oxygen with other atmospheric

---

*The wavelength centers of the strongest absorption bands in the vapor-phase infrared spectra of the minor atmospheric constituents are methane (3.31 and 7.66 μm), nitrous oxide (4.50, 7.78, and 16.98 μm), carbon monoxide (4.67 μm), nitric oxide (5.33 μm), nitrogen dioxide (3.44, 6.17, and 15.43 μm), nitric acid (2.82, 5.85, 7.51-7.55, 11.38, and 13.12 μm), ammonia (3.00, 6.14, and 10.53 μm), sulfur dioxide (7.33, 8.68, and 19.23 μm), and partially deuterated water (3.68, 7.13, and > 12 μm).
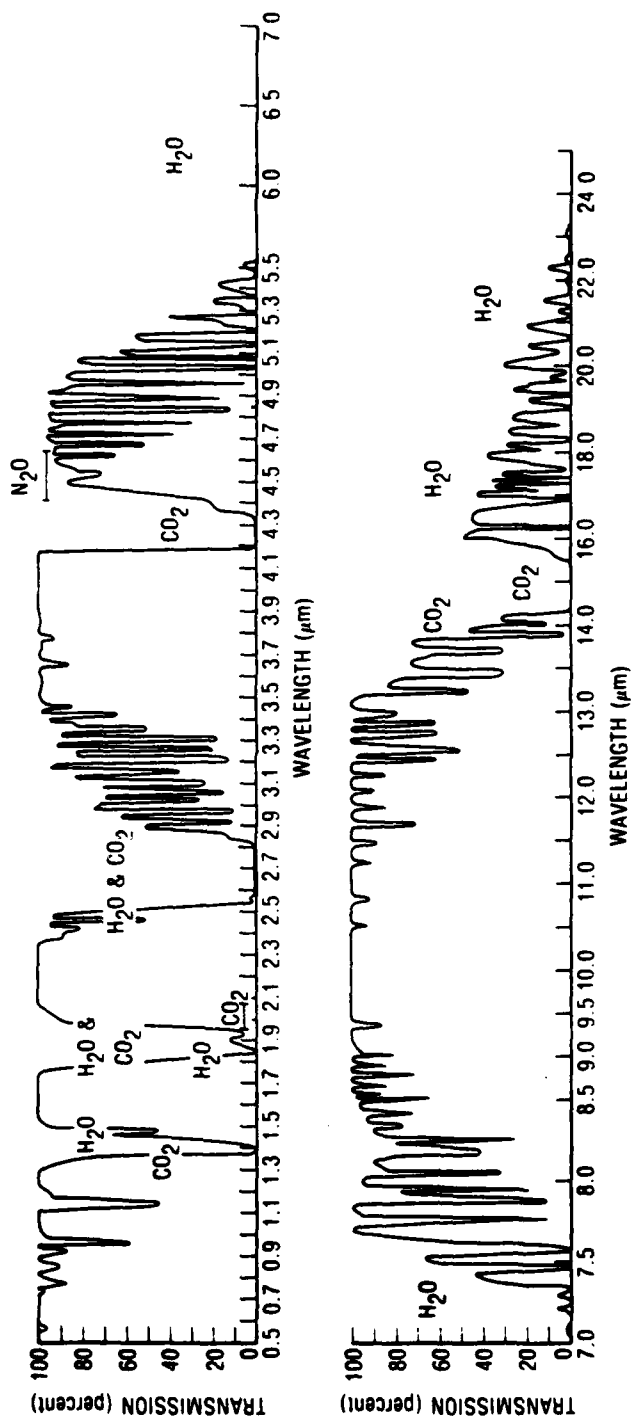
Fig. 1. Transmission of 0.305-m horizontal air path at sea level. Temperature, 26°C; 5.7 mm precipitable water. Spectrum taken from "Infrared Detection" chart prepared by Santa Barbara Research Center. Absorption contributions by ozone, the nitrogen continuum, oxygen, and most of the minor atmospheric constituents are not observed here for the short, 0.305-m path employed.

13

gases.[24] Consequently, the effect of a collision-induced nitrogen continuum absorption needs to be considered for applications involving the long-path transmission of 3.7- to 4.7-μm radiation.[25,26] The attenuation effect of the corresponding collision-induced oxygen continuum absorption near 6 μm, on the other hand, can be neglected relative to the strong attenuation produced by water vapor in this region. Molecular oxygen does possess two weak absorption bands that must be taken into account for applications involving the atmospheric transmission of near-infrared radiation. These bands are centered at 1.27 μm and 1.07 μm and correspond to the 0--0 and 0--1 vibrational transitions, respectively, of the O_2^{16} $a(^1\Delta_g)$-$X(^3\Sigma_g^-)$ electronic absorption band.[22]

B. CALCULATION OF ATMOSPHERIC ABSORPTION

To calculate accurately the long-path atmospheric absorption of infrared radiation, information is needed on the concentrations of the absorbers as well as conditions of temperature and pressure over the transmission path. Information is also required on the infrared spectral properties of these absorbers as a function of atmospheric temperature and pressure for the wavelength region of interest.

Nitrogen, oxygen, methane, and nitrous oxide are uniformly mixed by convection in the atmosphere, so their specific concentrations can be considered constant with altitude for the bottom 90-km atmospheric layer.[13,22,25,26] Carbon dioxide and carbon monoxide can be produced by natural processes and by the burning of fossil fuels.[27] Higher-than-background levels of these gases may be present at source locations. However, for the purpose of atmospheric transmission calculations, their mixing ratios can generally also be considered constant with altitude for the bottom 90-km portion of the atmosphere.[22,25,26]

Ozone, nitric oxide, nitrogen dioxide, nitric acid, ammonia, and sulfur dioxide are also produced by natural processes and fossil-fuel burning. These gases and water vapor, however, are not uniformly mixed in the atmosphere, and their concentrations may vary greatly with altitude. In addition, significant diurnal, seasonal, and geographical variations may be observed in the concentrations of these gases.[27-30]

14

Water-vapor concentrations vary greatly in the troposphere. The maximum concentration of water vapor at a given altitude is governed by the air temperature at that point. Water-vapor pressures above 30 Torr (1 Torr = 0.1333 kPa) are possible near the earth's surface in tropical climates. The allowable water-vapor pressures decrease rapidly with decreasing temperature. Water-vapor pressures of 0.1 Torr or less are observed in air samples at temperatures near -40°C, such as found in the colder regions of the troposphere at altitudes above about 8 km.

When important in atmospheric transmission calculations, the transmission-path-dependent concentrations of nonuniformly mixed absorbers are established independently, e.g., through radiosonde measurements, or are predicted using model concentration profiles. Only small temporal and geographical variations are observed in atmospheric pressure in the lower 30-km layer of the atmosphere. For example, sea-level pressures measured at various global locations generally vary by less then ±3% from the average value of 760 Torr.[22] The same vertical atmospheric-pressure profile can always be used for various locations around the world. Vertical atmospheric-temperature profiles, however, vary with season and geographical location. Vertical profiles for pressure and temperature as assumed in a standard model of the atmosphere are listed in Table I as a function of altitude up to 30 km.[13]

The most useful infrared spectral parameters for accurately calculating the contributions of different atmospheric absorbers are the absorber vibration-rotation line-center frequencies, lower state vibrational-rotational energy levels, absorption line strengths, air-broadened line widths as a function of temperature, and line shapes. With the exception of line-shape data, which are not available for all atmospheric species in the desired spectral regions, the Air Force Geophysics Laboratory (AFGL) has compiled an extensive set of such data on magnetic tape from high-resolution spectral measurements for the atmospheric species water vapor, ozone, oxygen, methane, nitrous oxide, carbon monoxide, carbon dioxide, nitric oxide, nitrogen dioxide, nitric acid, ammonia, and sulfur dioxide.[31,32]

Several highly useful computer codes have been developed at AFGL[25,26,33-36] and elsewhere[37-39] that make use of this AFGL data set, called the Atmospheric Line Parameters Compilation,[31,32] to compute synthetic atmospheric transmission and emission spectra. AFGL developed the computer

15

TABLE I. TEMPERATURE AND PRESSURE AS A FUNCTION OF ALTITUDE IN ARDC[a] MODEL ATMOSPHERE

Altitude (km)	Temperature (K)	Temperature (°C)	Atmospheric Pressure (Torr)	Approximate Saturation Water Pressure (Torr)
0	288.16	15.01	760.00	12.79
1	281.66	8.51	674.13	8.30
2	275.16	2.01	596.31	5.29
3	268.67	−4.48	525.95	3.29
4	262.18	−10.97	462.49	2.00
5	255.69	−17.46	405.39	0.98
6	249.20	−23.95	354.16	0.53
7	242.71	−30.44	308.31	0.29
8	236.23	−36.92	267.41	0.13
9	229.74	−43.41	231.02	0.069
10	223.26	−48.89	198.76	0.034
11	216.78	−56.37	170.26	0.014
12	216.66	−56.49	145.51	0.014
14	216.66	−56.49	106.29	0.014
16	216.66	−56.49	77.65	0.014
18	216.66	−56.49	56.74	0.014
20	216.66	−56.49	41.47	0.014
22	216.66	−56.49	30.32	0.014
24	216.66	−56.49	22.17	0.014
25	216.66	−56.49	18.96	0.014
26	219.34	−53.81	16.23	0.018
28	225.29	−47.86	11.96	0.030
30	231.24	−41.91	8.89	0.087

[a]Model atmosphere developed for Air Research Development Command (ARDC) in 1959 by Air Force Cambridge Research Center (now Air Force Geophysics Laboratory).

code HITRAN to calculate high-resolution transmission and radiance over atmospheric paths.[33] The original HITRAN code convolved the Lorentz line shape with the molecular lines of the different atmospheric species to calculate transmission by summing the absorption contributions of each line. This code had the disadvantage of requiring large amounts of computer time and subsequent runs for emission calculations. A newer HITRAN code (FASCODE) convolves a Voigt profile with the molecular lines to more rapidly calculate the transmission spectra.[25,34] FASCODE can also simultaneously calculate the overall radiance of a multilayer path. In the FASCODE program, the atmosphere is represented by a 33-layer model between 0 and 100 km. Each layer is assumed to be in thermal equilibrium. The temperature, pressure, and concentration of water vapor and ozone in each model layer are selected to reflect their variations with altitude. The mixing ratios of nitrogen, oxygen, methane, nitrous oxide, carbon monoxide, and carbon dioxide are assumed to remain constant with altitude. Altitude profiles of the nonuniformly mixed gases can be incorporated into the code.

The HITRAN codes can be used to calculate atmospheric absorption spectra at any spectral resolution. Because HITRAN computation times can become excessive for low-resolution applications, AFGL developed the much simpler and faster LOWTRAN computer code with a fixed 20 cm^{-1} spectral resolution for transmittance and radiance calculations.[35,36,26] The HITRAN and LOWTRAN codes currently cover wavelengths longer than 0.69 μm and the range 0.25 to 28.5 μm, respectively.

The LOWTRAN calculation is similar to several previous single-parameter band model* calculations. LOWTRAN uses an atmospheric layer model similar to that used in HITRAN, except that the LOWTRAN calculation combines the molecular abundance and pressure dependence of absorption and neglects the temperature dependence. The replacement of these independent variables by a single parameter results in a reduction in the computational accuracy of the LOWTRAN code compared to the HITRAN code.[35] The major limitation in the accuracy of HITRAN is due to lack of adequate information concerning the shapes of the

---

*A band model is an idealized mathematical representation of the frequency dependence and intensity distribution of the vibrational-rotational spectral lines of a molecular absorption band.[40]

17

wings of molecular absorption lines for various atmospheric species, particularly water vapor. In those wavelength regions where absorption contributions from molecular lines are much more important than water-vapor or nitrogen continuum absorption contributions and aerosol attenuation, HITRAN can provide transmittance accuracies of ± 1 to 2% at 20 cm^{-1} resolution for most atmospheric paths; the faster LOWTRAN code can generally provide transmittance accuracies of about ± 5%. Because the temperature dependence of molecular line absorption is neglected in LOWTRAN calculations, larger uncertainties may exist in spectral regions near absorption lines having large temperature dependences.[35]

In addition to the absorption contributions of molecular lines, the contributions of aerosol attenuation and continuum absorption by water vapor and nitrogen must be modeled within the atmospheric transmission windows in both the HITRAN and LOWTRAN codes. Because it is difficult to accurately model continuum absorption and aerosol contributions, the largest uncertainties in HITRAN and LOWTRAN calculations of transmittance and radiance occur within the transmission windows. In these regions, the accuracy of both codes is a function of (1) the accuracy of the laboratory measurements of water and nitrogen continuum absorption over the range of possible atmospheric conditions, and (2) how well available aerosol models can be matched to the actual atmospheric conditions. Thus, the accuracies with which computer codes such as HITRAN and LOWTRAN can calculate transmittance and radiance in the window regions will improve once reliable water and nitrogen continuum data bases are established and improved aerosol models are developed.

C. CO$_2$ LASER PHOTOACOUSTIC DETECTION TECHNIQUE FOR
WATER CONTINUUM ABSORPTION MEASUREMENTS

Since the development of the CO$_2$ laser in 1964[41] there has been increasing interest in accurately determining the atmospheric transmission properties of its output, particularly at the highest gain lines, for a number of applications. The $C^{12}O_2^{16}$ laser has a spectral output of greater than 100 discretely tunable lines between 9.1 and 11.0 μm, and other CO$_2$ isotopic species can produce discretely tunable output at wavelengths as long as 12.0 μm;[42] therefore, such lasers are well suited to function as excitation sources for the study of water continuum absorption throughout much of the 8- to 12-μm

18

transmission window. For these reasons, CO_2 lasers have been used as excitation sources in water absorption studies with conventional long-path absorption detection systems[5,8-10] and with photoacoustic detection systems.[14-16,43]

The very weak nature of the 8- to 12-μm water continuum absorption requires highly sensitive absorption-measurement techniques to precisely determine its magnitude under different laboratory-simulated atmospheric conditions. The water continuum absorption coefficient is only about 10^{-6} cm^{-1} in the 10-μm wavelength region for air mixtures containing 10-Torr water vapor at room temperature.[14-16] Techniques capable of measuring absorption coefficients of 10^{-8} cm^{-1} or smaller are required to reliably study 8- to 12-μm water continuum contributions to atmospheric attenuation over various long-slant atmospheric transmission paths.

Photoacoustic detection systems are capable of measuring much smaller absorption coefficients than can be measured by practical long-path absorption detection systems.[44-48] The sensitivity of the long-path absorption technique is ultimately limited by the difficulty in measuring the small difference in the intensities of the incident and transmitted light beams through the absorber being studied. Measurement of absorption coefficients on the order of 10^{-8} cm^{-1} by the long-path absorption technique would require the use of 5-km absorption path lengths if a practical detector capable of measuring light intensity differences down to 0.5% could be employed. A multipass absorption cell of this type would be large and expensive, and it would require lengthy pump-down and sample-mixing procedures.

The photoacoustic technique is inherently more sensitive than the long-path absorption technique because it can measure small absorption signals against a null background. Laser photoacoustic systems designed to minimize photoacoustic cell window absorption can measure absorption coefficients of 10^{-10} to 10^{-9} cm^{-1}.[44-48] Such detection sensitivities can be obtained with absorption path lengths of only several centimeters. This allows the use of small-volume cells, enabling rapid cell pump down and sample mixing. By the CO_2 laser photoacoustic technique, the output beam from a wavelength-tunable, continuous-wave (cw) CO_2 laser is intensity-modulated and passed through a photoacoustic cell containing the gas sample whose absorption is to be measured. Radiation periodically absorbed by the species of interest (in this study, by water molecules) is converted through collisions with nonabsorbing

19

buffer gas molecules (N_2 and O_2) in the cell into periodic increases in thermal motion of the entire gas mixture. The result is a periodic increase in cell pressure, which can be sensitively detected at the precise light-modulation frequency by a microphone or other sensitive pressure transducer, such as a capacitance manometer, in conjunction with a lock-in amplifier.

D.   PREVIOUS 8- TO 12-μm WATER CONTINUUM ABSORPTION STUDIES

The existence of a water-vapor continuum absorption in the 8- to 12-μm atmospheric transmission window was first proposed by Elsasser in 1938.[49] Elsasser attributed the continuum to contributions of the collisionally broadened extreme wings of strong absorption lines located in the water-vapor vibrational-rotational band centered at 6.3 μm and in its pure rotational band located at wavelengths longer than 12 μm. The presence of such continuum absorption was later confirmed by measurements of the attenuation of solar radiation,[50] artificial radiation,[51,5] and atmospheric emission,[52] over long horizontal or slant atmospheric transmission paths. These measurements, however, did not allow an accurate determination of the dependence of the continuum absorption on temperature and water-vapor partial pressure. This was due, in these studies, to uncertainties in the magnitudes of the latter quantities over the transmission path and the lack of accurate information on the attenuation caused by such variable atmospheric factors as aerosols and clouds.

To better ascertain the dependence of the 8- to 12-μm water continuum on temperature and water-vapor--air partial pressures, several groups have measured continuum absorption in the laboratory on synthetic water-vapor--air mixtures. These measurements have primarily been performed over long absorption paths through the use of White-type multipass absorption cells in conjunction with either conventional incoherent infrared sources[6,7,11] or infrared laser sources.[5,8-10,12] Recently, the CO_2 laser photoacoustic technique was employed in the study of the water continuum in the 8- to 12-μm region.[14-16] The observations from these various laboratory studies are outlined in Subsection II.D.1 below. In each study, measurements were performed on mixtures of water vapor in either nitrogen or synthetic air (80% N_2--20% O_2) to eliminate absorption contributions in this spectral region from carbon dioxide in natural air. In Subsection II.D.2, we describe some of the models developed to account for the 8- to 12-μm water continuum.

20

1. EXPERIMENTAL STUDIES OF 8- TO 12-μm WATER CONTINUUM

In 1969, McCoy, Rensch, and Long[5] reported the results of a study on the dependence of water continuum absorption on water partial pressure at the CO_2 laser 9.4- and 10.4-μm band P(20) lines (wavelengths 9.553 and 10.591 μm, respectively). These measurements were performed at temperatures of 23 to 26°C using a multipass gas cell with a 1-km path length. When the cell was filled with water vapor only, the continuum absorption dependence on water-vapor pressure was purely quadratic. When the cell was filled with mixtures of water vapor and air at total pressures of 700 Torr, the continuum had dependence on water-vapor pressure that included both linear and quadratic terms. McCoy et al.[5] attributed the continuum absorption to collisional broadening of the far wings of strong water-absorption lines located on each side of the 8- to 12-μm window as proposed earlier by Elsasser.[49] The linear water-pressure term was associated with collisional broadening of water lines by air (foreign broadening), whereas the quadratic water-pressure term was associated with broadening caused by collisions between water molecules (self-broadening).

In 1970, Bignell[7] reported the results of water-vapor absorption measurements at selected wavelengths between 8.9 and 20.9 μm. These measurements were performed with a grating-spectrometer-equipped, multipass-absorption cell that gave path lengths up to 0.5 km. A Nernst glower was the infrared source. The absorption data obtained were regarded as representing true water continuum absorption, because the wavelengths used were considered to be free of local water absorption lines and their near wings. Measurements were performed on 750-Torr total pressure air mixtures containing up to 26 Torr of water vapor at various temperatures between 21 and 45°C. Only limited absorption data could be determined at wavelengths between 8 and 12 μm, owing to sensitivity limitations in the absorption measurements. More extensive data were obtained within the 17- to 21-μm region, where the absorption was about an order of magnitude more intense than the 8- to 12-μm absorption. The absorption attributed to the continuum in the 17- to 21-μm region had a noticeable positive curvature from a pure linear dependence on water-vapor partial pressure and was reported to have a negative temperature coefficient. The absorption increased in magnitude by about 2% for every degree-Celsius decrease over the 21 to 45°C temperature range studied. The limited

21

absorption data determined between 8 and 12 μm were reported to have a dependence on water-vapor partial pressure and temperature similar to that of the 17- to 21-μm data. To explain his observations, Bignell suggested that two mechanisms of continuum absorption may be involved. These included absorption contributions due to (1) foreign broadening of water lines, and (2) the formation of water-vapor dimers. The water dimer mechanism had been proposed previously by Varanasi et al.[53] to account for the continuum absorption observed between 10 and 17 μm in high-pressure (2-5 atm) and high-temperature (177-227°C) steam samples.

Burch, in 1970,[6] was able to measure, more accurately and extensively than Bignell,[7] absorption on water-vapor—nitrogen mixtures at several selected wavelengths between 8 and 12.5 μm. To obtain his data, Burch employed a Nernst glower source combined with a grating-equipped, multipass absorption cell with a total path length up to 1.2 km. The temperatures used were 23, 85, and 115°C. As in the measurements of Bignell, the wavelengths selected were believed to correspond to regions where local water-line absorption contributions were negligible compared with continuum absorption. Similar measurements were made by Burch and coworkers in 1973[54] and 1974[55] at selected wavelengths between 12.2 and 30 μm. A temperature coefficient of approximately -2%/°C was observed for the 8- to 30-μm continuum between 23 and 115°C. The magnitude of the continuum absorption increased with increasing wavelength between 8 and 30 μm. An increase of about a factor of 3 was observed between 8 and 12 μm, and an increase of over two orders of magnitude was observed between 8 and 30 μm.[6,11,54-57] Burch and coworkers interpreted their water continuum absorption data in terms of a mechanism involving the collisional broadening of the far wings of strong water-absorption lines. They showed that a simple Lorentzian line shape for the water lines could not account for the continuum's magnitude and concluded that a super-Lorentzian line shape with larger far-wing absorption contributions must be employed.[11,56,57]

In 1975, Arefev and coworkers[8] reported the results of CO_2 laser absorption measurements on pure water-vapor samples at 20 ± 1°C, using a multipass absorption cell with a total transmission path of 3 km and water pressures up to 17 Torr. Because the CO_2 laser output occurred alternately at the 10.4-μm band laser lines P(16), P(20), P(22), and P(24), the absorption wavelength was

regarded as being 10.60 ± 0.05 μm. They observed that their 20°C transmission data for pure-water samples had a dependence on water pressure that was within experimental uncertainty of the quadratic dependence observed earlier by McCoy et al.[5] at 23 to 26°C.

Arefev and Dianov-Klokov[9] reported additional absorption measurements with the long-path cell in 1977. Measurements were performed on pure water-vapor samples between 11 and 80°C and on 760-Torr total pressure water-vapor—nitrogen mixtures at 20 and 50°C. Water pressures up to 20 Torr were employed. The absorption coefficient at 10.60 ± 0.05 μm could be fit by an expression of the form

$$\text{absorption (abs.)} = k_1 p_{H_2O}(1 + a p_{N_2}) + k_2 p_{H_2O}^2 e^{-\Delta H/RT}$$

where p_{H_2O} is the water partial pressure, p_{N_2} is the nitrogen partial pressure, R is the gas law constant, and T is the temperature in degrees Kelvin. The terms k_1, k_2, a, and ΔH are constants determined in the fit [$k_1 = 1.86$ Torr^{-1}, $k_2 = 0.47$ Torr^{-2}, $a = 2.3 \times 10^{-3}$ Torr^{-1}]. Thus, as in previous studies,[5-7] the absorption had both a linear and a quadratic dependence on water pressure. Because ΔH was determined to be -4.5 kcal/mol (-18.84 kJ/mol), the quadratic water-pressure term was concluded to have a negative temperature coefficient equal to the approximately -2%/°C dependence at room temperature and above reported by Bignell[7] and Burch et al.[6,54-57] Arefev and Dianov-Klokov[9] attributed the continuum to absorption contributions due to the formation of water-vapor dimers.

Shumate and coworkers[14] employed the CO_2 laser photoacoustic technique in 1976 to measure the absorption of synthetic water-vapor—air mixtures at $27 \pm 1°C$. These measurements were performed at 49 different CO_2 laser wavelengths from 9.2 to 10.7 μm on mixtures containing 5.0-, 10.0-, and 15.0-Torr water vapor. As observed in earlier studies by Burch et al.,[6,54-57] the magnitude of the continuum in this spectral region gradually increased with increasing wavelength. This was most noticeable for water partial pressures of 10 Torr or more. As also observed in previous water continuum studies,[5-9] the magnitude of the continuum absorption within this wavelength region had a dependence on water pressure that could be modeled as a sum of linear and quadratic terms. The quadratic dependence on water pressure was of greater

23

relative importance for wavelengths within the 10.4-μm band than within the laser 9.4-μm band, and was concluded to account for the larger continuum absorption observed at longer wavelengths when air mixtures containing partial pressures of 10 Torr or more were employed.

In 1978, Montgomery[12] reported the results of measuring water-vapor continuum absorption at 8.313 μm as a function of temperature between 60 and 200°C. The measurements, on 760-Torr nitrogen mixtures containing water partial pressures of 80 Torr or more, were made with a multipass cell whose total path length was 40 m. The infrared source was a lead-tin-telluride diode laser, which could be tuned to the 8.313-μm region, where absorption contributions from local water lines were concluded to be negligible. His continuum data overlapped and extended the 27 to 115°C continuum data obtained earlier by Burch[6] in the 8- to 12-μm region. The water continuum absorption coefficient over the 60 to 200°C range studied deviated only slightly from a purely quadratic dependence on water partial pressure, as expected at the > 80-Torr water partial pressures employed. In the 60 to 115°C range, the water continuum data at 8.313 μm were in good agreement with the corresponding data obtained by Burch.[6] Between 27 and 100°C, the continuum data of Montgomery, like the 8- to 12-μm data of Burch, possessed a temperature coefficient of about -2%/°C. However, a nearly constant or very weak positive temperature coefficient was observed for the continuum from ~ 100 to 200°C. To interpret the 27 to 200°C continuum data of Burch[6] and Montgomery,[12] Montgomery suggested that, near room temperature, the water dimer contribution to the continuum is more important than a contribution from the collisional-broadening of wings of waterlines. He hypothesized that, with increasing temperature, the dimer contribution would decrease and eventually become smaller than the collisional-broadening contribution. At temperatures above approximately 100°C, the dimer mechanism was concluded to become of negligible importance relative to the collisional-broadening mechanism. The collisional-broadening mechanism was thought to remain nearly independent of temperature between about 100 and 200°C.

In 1978 and 1979, Long's group extended their previous studies of water continuum absorption.[10,15,16] Nordstrom et al.[10] reported the results of pressure-broadened, room-temperature (22.5°C) transmittance measurements on water-vapor samples at five wavelengths within the CO_2 laser 10.4-μm band.

24

Selected water partial pressures between 6 and 16 Torr and the same long-path absorption cell used earlier by McCoy et al.[5] were employed in these measurements. With the buffer gases pure nitrogen, 80% N_2--20% O_2, and 60% N_2--40% O_2, Nordstrom et al.[10] found that oxygen is a less efficient broadener of water absorption lines than nitrogen. The results of this study indicate that the buffer-gas mixture 80% N_2--20% O_2 should be employed rather than pure nitrogen as a collisional broadener in laboratory studies designed to model atmospheric transmission.

More extensive pressure-broadened measurements of water-vapor absorption at CO_2 laser wavelengths were reported by Peterson et al.[15,16] These measurements were performed as a function of temperature and water partial pressure with this same long-path absorption cell, as well as with a photoacoustic detection system. Absorption measurements were made on mixtures of water vapor in nitrogen at a total pressure of 760 Torr at 27 CO_2 laser wavelengths between 9.24 and 10.70 μm. These measurements were performed in the 22.5-to-24.5°C temperature range. As in previous studies, the water continuum in this wavelength region was observed to increase slowly with increasing wavelength. Peterson[15] also studied the temperature dependence of the water continuum absorption between 16 and 27.6°C at the 10.4-μm band laser lines P(16) and P(20) when an 80% N_2--20% O_2 mixture was used as the buffer gas. A temperature coefficient of approximately -1.7%/°C was observed for this continuum at 22°C. Long's group also interpreted their water continuum data in terms of a mechanism involving the collisional broadening of the far wings of strong water-absorption lines. A collisional-broadening model developed by Nordstrom and Thomas[17,18] of Long's group is outlined in the following description of water continuum models.

2. WATER CONTINUUM MODELS

The water continuum absorption in the 8- to 12-μm window, most often explained in terms of collisional-broadening[5-7,10-12,14-16] and water-vapor dimer[7-9,12,4] mechanisms, has also been attributed by a few researchers to water aggregates that are much larger than dimers and to various large hydrated-ion clusters.[21] However, the recent studies[19,20] discussed below indicate that, compared with water dimer species, trimer and higher-order water oligomers and various hydrated-ion clusters contribute negligibly to water continuum absorption. We will use the term "water cluster" as a general

25

expression to refer to water dimers, higher-order water oligomers, and hydrated-ion clusters. The most thoroughly developed water-cluster[19,20] and collisional-broadening[58,17,18] continuum models are described here.

a. Water-Cluster Models

The hypothesis that the water dimer mechanism[53,59,19,20] causes the 8- to 12-μm continuum absorption has been based primarily on the dimer model's ability to predict the negative-temperature and pure quadratic water-pressure dependences observed for the water continuum in several of the above-described experimental studies. Suck and coworkers[19,20] recently performed theoretical estimates of the magnitude of the water continuum absorption that would be produced in the 8- to 12-μm window by the formation of both homomolecular $[(H_2O)_n]$ and heteromolecular $[A^{\pm}(H_2O)_n$, where $A^{\pm}$ is a positive or negative ion] water clusters. Water aggregate models were proposed and expressions derived to calculate (1) the partial pressures of water dimers, higher-order water oligomers, and hydrated-ion clusters as a function of temperature and water pressure, and (2) the wavelength positions, intensities, and spectral profiles of new infrared absorption bands proposed to develop from the formation of these water clusters.

Molecular orbital calculations[60,61] and molecular beam microwave spectroscopic experiments[62] have indicated that the most energetically favorable equilibrium structure of the water-vapor dimer is the translinear geometric configuration shown in Fig. 2. Suck and coworkers based their dimer model on this proposed structure. They calculated the equilibrium concentration of water dimers $C_{(H_2O)_2}$ as a function of water concentration C_{H_2O} through the relationship $C_{(H_2O)_2} = K_2 C_{H_2O}^2$, where K_2 is the temperature-dependent equilibrium constant for water dimer formation. K_2 was calculated by the simple statistical mechanical theory of equilibrium.[63] This involved constructing molecular partition functions for the water dimer and water monomer species. K_2 was concluded to vary approximately with temperature by the factor

$$\frac{T^{-3} \prod_{i=1}^{6} \exp\left(-h\nu_i/2kT\right) \exp\left(-\Delta H^\circ/RT\right)}{\left[1 - \exp\left(-h\nu_i/kT\right)\right]}$$

26

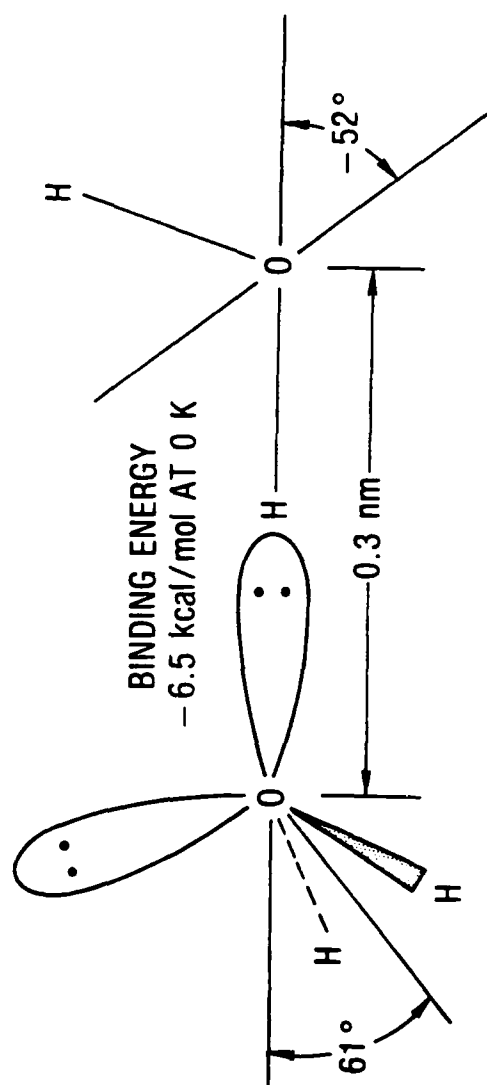BINDING ENERGY
−6.5 kcal/mol AT 0 K

−52°

0.3 nm

61°

Fig. 2. Water-vapor dimer translinear geometric configuration.19,20,62

27

where h is Planck's constant, k is Boltzmann's constant, and the ν_i correspond to the frequencies of the six intermolecular vibrational modes of the water dimer. Here $\Delta H°$ is the water-vapor dimer electronic binding energy at 0 K; R is the gas law constant; and T is the temperature in K. On the basis of molecular orbital calculations, Suck and coworkers[19,20] chose the binding energy to be -6.5 kcal/mol.

Of the six intermolecular vibrational modes available to the water dimer, the highest-frequency mode was concluded to be the out-of-plane bending mode about the hydrogen bond axis. The vibrational-rotational absorption band associated with this mode was calculated to be centered near 16 μm and concluded to have a Lorentzian-shaped intensity profile with a half-power bandwidth of 200 cm^{-1}.* The integrated absorption strength of this band was predicted numerically. Molecular orbital theory was used to calculate the square of the dipole-moment variation with respect to the dimer out-of-plane bending normal coordinate. Suck et al.[19,20] estimated, with their dimer model, that the high-frequency tail of the out-of-plane dimer absorption band should produce water continuum absorption coefficients of between 1×10^{-7} cm^{-1} and 1.7×10^{-6} cm^{-1} at a wavelength of 10 μm for air mixtures containing between 4- and 14-Torr water vapor at 23°C. These values are in reasonable agreement with the water continuum absorption coefficients of between about 4×10^{-7} cm^{-1} and 1.8×10^{-6} cm^{-1} obtained by Shumate et al.[14] in air mixtures containing between 5- and 15-Torr water vapor at 27°C. Suck et al.[19,20] thus concluded that the water-vapor dimer mechanism may be an important contributor to water continuum absorption in the 8- to 12-μm window.

Suck and coworkers demonstrated that the concentration of the water oligomer $(H_2O)_n$ in a water-vapor sample can be expressed by the general relationship $C_{(H_2O)_n} = K_n C_{H_2O}^n$, where K_n is the temperature-dependent equilibrium constant for formation of $(H_2O)_n$. They estimated that at 23°C and

---

*To date, no direct spectroscopic measurements have been made on the vibrational-rotational band contours of the water dimer in the vapor phase. The prediction by Suck et al.[19,20] that the out-of-plane bending mode is located near 16 μm is in agreement with calculations of other workers[61] and is within the 12.5- to 25-μm range in which hindered rotational absorption bands caused by dimer formation are observed in liquid water. The hindered rotational bands in liquid water are reported to have 200- to 250-cm^{-1} bandwidths.[64]

its water saturation pressure of 21 Torr, the dimer-to-monomer concentration ratio C_2/C_1 is 2.4×10^{-3}. Under the same conditions, the trimer-to-monomer concentration ratio C_3/C_1 was estimated to be 1.9×10^{-6}. The concentration ratios C_n/C_1 for $n > 3$ were similarly calculated to decrease by several orders of magnitude for each incremental increase in cluster size n. Because the computed integrated absorption strengths increased with increasing cluster size at a much slower rate than C_n/C_1 decreased, it was concluded that, unlike water dimers, trimers and larger water clusters should not contribute significantly to absorption in the 8- to 12-μm window.

Given typical ion concentrations in the atmosphere, the concentration of hydrated-ion clusters, such as H_3O^+--$(H_2O)_n$, were further concluded to be less than 10^{-10} times the water dimer concentration in the lower atmosphere Since the absorption cross sections of these ion clusters were calculated to not be several orders of magnitude larger than that of the dimer, these ion clusters, unlike the water dimer, were also concluded by Suck et al.[19,20] to be unable to account for the observed magnitude of the 8- to 12-μm water continuum absorption.

Figure 3 compares the experimental temperature dependence of the component of the water continuum absorption coefficient that is quadratic in water partial pressure with that predicted by the water-vapor dimer mechanism and, as discussed in the following section, by the collisional-broadening mechanism. The experimental data shown here were determined by Burch et al.[6,54,55] in the 8- to 12-μm region between about 27 and 100°C and by Montgomery[12] in the 8-μm region between 60 and 200°C. The quadratic water-pressure component, which results from either the binary association of water molecules to form water dimer species or the broadening of water absorption lines by binary collisions between water molecules, or both, is expressed in Fig. 3 in terms of the so-called continuum absorption self-broadening coefficient* used extensively in the literature. Although the water dimer

---

*The so-called self-broadening coefficient $C_s(\lambda, T)$, plotted versus temperature in Fig. 3, is most often defined in the literature through the relation

$$\text{abs.}(\lambda, T) = C_s(\lambda, T) w_{H_2O} [P_{H_2O} + \gamma(\lambda, T)(P - P_{H_2O})]$$

[Footnote continued on page 31.]

29
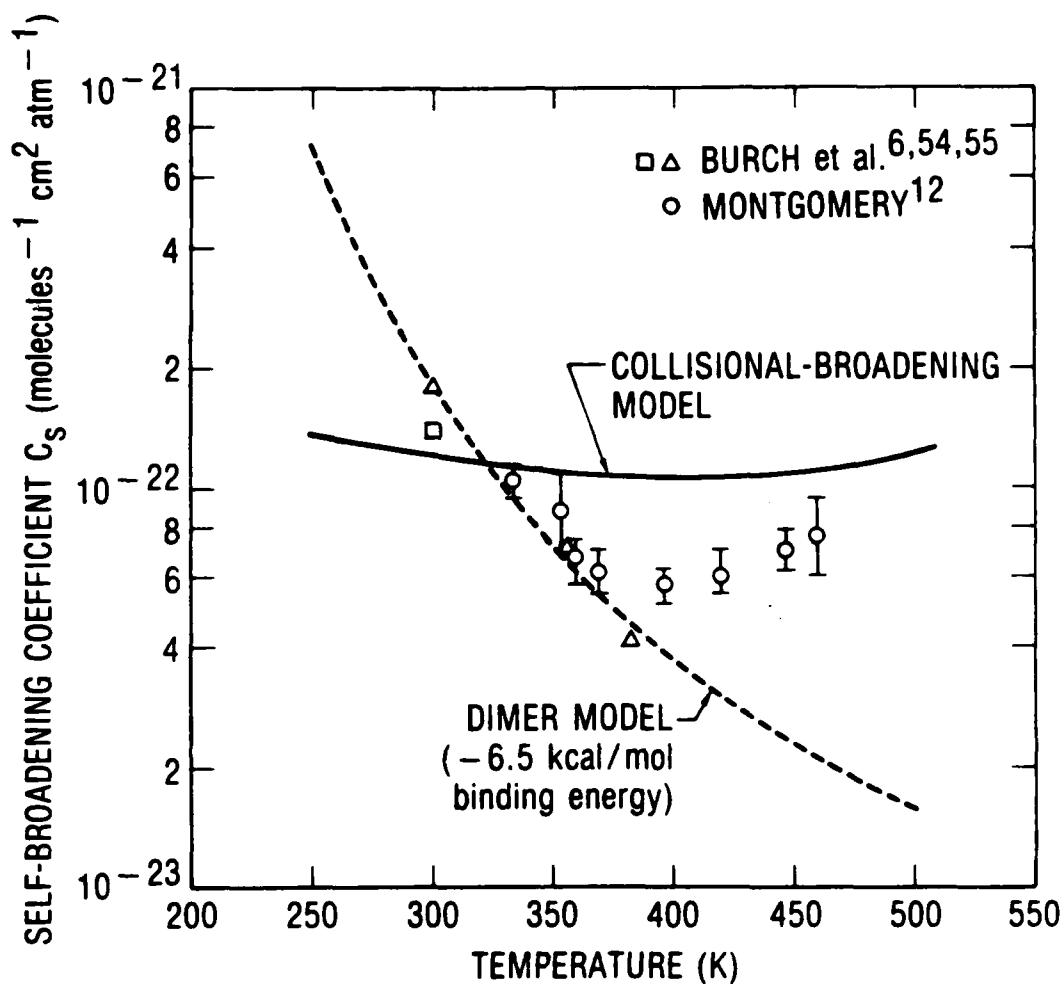
Fig. 3. Comparison of experimental and predicted temperature dependences of the water-pressure quadratic component of the 8- to 12-μm water continuum absorption. The dimer intermolecular frequencies predicted by Owicki et al.[61] (593, 496, 189, 168, 161, and 98 cm^{-1}) were assumed in the dimer model used here. The dimer model predicts a C_s value of 2.0×10^{-22} molecules^{-1} cm^2 atm^{-1} at 296 K. This value is based on the 1.7×10^{-6} cm^{-1} absorption strength estimated by Suck et al.[19,20] at 10 μm for air mixtures containing 14-Torr water at 23°C.

mechanism fails to predict the observed positive temperature coefficient above about 100°C, it predicts a negative temperature coefficient that is close to the measured value between room temperature and 100°C.

b. Water Collisional-Broadening Models

Clough and coworkers[58] and Nordstrom and Thomas[17,18] have recently employed molecular absorption line-shape theory in an attempt to predict the magnitude of the water continuum absorption throughout the infrared region. They treated the water continuum as resulting entirely from absorption contributions from the collision-broadened wings of strong absorption lines of water molecules. The shapes of these wings (spectral line profiles) were derived by considering self-broadening and foreign-broadening collisions. The strong water monomer lines whose wing absorption contributions were summed by both groups[18,58] to calculate the continuum were (1) the pure rotational lines at wavelengths longer than 12 μm and centered at about 50 μm, (2) the vibrational-rotational lines within the ν_2 fundamental band (due to bending) centered at 6.27 μm, and (3) the vibrational-rotational lines within the ν_1 and ν_3 fundamental bands (due to symmetric and asymmetric stretching) centered at 2.73 and 2.66 μm, respectively. The AFGL absorption-line listing for water vapor,[31] compiled from previous extensive spectroscopic studies, was used by both groups to calculate the positions and intensities of these strong water lines for specified atmospheric conditions. The models of Clough and coworkers and Nordstrom and Thomas differ in the way they were developed and the range of atmospheric conditions for which they are applicable.

To describe the collision-broadened shapes of the water lines in the AFGL compilation, Clough and coworkers[58] employed the impact approximation[65] and the Van Vleck and Huber line-shape formalism.[66] Assigning the self-broadened water line widths as five times the foreign-broadened widths, they summed the contributions from line wings 25 cm^{-1} from the center of each line. In their approximation, the calculated continuum at 23°C was five times too small at

---

Here abs.(λ, T) is the water continuum absorption coefficient at a particular wavelength and temperature, w_{H_2O} is the density of water vapor in molecules per cubic centimeter, p_{H_2O} is the water partial pressure and P the total pressure in atmospheres, and $\gamma(\lambda, T) = C_f(\lambda, T)/C_s(\lambda, T)$ is the "foreign-broadening to self-broadening" coefficient ratio.

31

wavelengths longer than 20 μm and two times too large at 10 μm. The wavelength dependence of the continuum could be properly modeled by modifying the impact theory to include a duration of collision time. Clough et al. did not attempt to treat the temperature dependence of the continuum. However, they suggested that it should be possible to account for the observed negative temperature coefficient by including the effects of the intermolecular potential in the collisional-broadening theory.

To calculate the magnitude of the water continuum absorption in the 3- to 5-μm and 8- to 12-μm transmission windows as a function of water partial pressure, total pressure, and temperature, Nordstrom and Thomas[17,18] included the effects of intermolecular potential in their collisional-broadening model. They developed expressions for the spectral line profiles through the use of the binary collision and adiabatic approximations. Time correlation functions for the upper and lower transition energy levels of the collisionally perturbed absorbing molecules were described in terms of collisional scattering operators. Rotationally averaged dipole-dipole interactions were used as the intermolecular potentials in the collisional scattering operators to model collisions between water molecules. Dipole-quadrupole intermolecular potentials were used to model collisions between water and nitrogen or oxygen. The total line-shape expressions were then obtained by taking the inverse Fourier transform of the time correlation functions.

Nordstrom and Thomas concluded that the line-shape and correlation functions could be divided into three regions, corresponding to near-line-center, intermediate-wing, and far-wing regions. Weakly perturbing collisions, such as occur at large impact parameters, produced long-duration correlation functions. From the time-bandwidth product of Fourier transform pairs, these weak collisions were concluded to be primarily responsible for near-line-center behavior. Strongly perturbing collisions, such as occur at small impact parameters, produced short-duration correlation functions and were concluded to be primarily responsible for far-wing behavior. They treated the weak-collision or near-line-center case in the impact (interruption-broadening) approximation[65] and the strong-collision or far-wing case in the quasi-static (statistical-broadening) approximation,[67] as has been done in previous theories of collision-broadened line shapes. The intermediate-wing region is difficult to treat analytically. Nordstrom and Thomas described the

32

intermediate-wing line shape as a linear combination of near-line-center and far-wing line shapes. They used a frequency-dependent weighting function to increase gradually the far-wing contribution while decreasing the near-line-center contribution as the frequency from line center was increased.

The far-wing components of the total line-shape expressions derived by Nordstrom and Thomas[17,18] each contained a set of 16 parameters (four different types of parameters corresponding to each of the four fundamental absorption bands of water). These parameters were evaluated from room-temperature water absorption data determined within the wavelength regions of the fundamental water-absorption bands.[17,18] The 12.2- to 30-μm grating spectrometer measurements by Burch et al.[54,55] were used to obtain far-wing line-shape parameters for the pure rotational band of water vapor. The parameters for the ν_2 band were determined from CO laser water absorption measurements by Long et al.,[68] whereas the parameters for the ν_1 and ν_3 bands were obtained from HF laser water-absorption measurements by White et al.[69] The parameters were determined by trial and error by summing wing absorption contributions within ± 1000 cm^{-1} ranges from selected frequencies until a good fit to the absorption data was obtained in the fundamental band regions. Continuum absorption data in the 3- to 5-μm and 8- to 12-μm window regions were not used in the determination of these parameters.

With the line-shape parameter fit to the absorption band regions, Nordstrom and Thomas were able to use their collisional-broadening model to predict the correct magnitude of the room-temperature water-vapor absorption coefficients at DF laser frequencies within the 3- to 5-μm window and at CO_2 laser frequencies within the 8- to 12-μm window. The dependence of the magnitude of the water absorption coefficients on water partial pressure can also be accurately predicted at DF and CO_2 laser frequencies with this model. The model is also able to predict a negative absorption coefficient at temperatures below 100°C and a positive temperature coefficient at higher temperatures, as observed experimentally by Burch et al.[6] and Montgomery.[12] However, even though the model can predict the proper magnitude of the positive temperature coefficient above 100°C, Fig. 3 shows that it significantly underestimates the magnitude of the negative temperature coefficient measured between 100°C and room temperature. The lack of agreement between the predicted and actual temperature dependences was attributed primarily to

limitations in the shapes of the absorption lines in the pure rotational band below 12 μm. The latter was thought to be related to approximations in the interaction potentials and perturbation expansions used in the collisional scattering operators. On the basis of the ability of their continuum model to predict the observed water-pressure dependence and to qualitatively predict the positive and negative temperature dependences above and below 100°C, respectively, Nordstrom and Thomas[17,18] concluded that the mechanism of far-wing absorption contribution must be carefully considered before other mechanisms, such as water dimers, are introduced to account for the water continuum.*

Figure 3 demonstrates that the temperature dependences of the continuum water-pressure quadratic component predicted by the collisional-broadening model of Nordstrom and Thomas[17,18] and the water dimer model of Suck et al.,[19,20] described above, diverge significantly below room temperature. Thus, the below-room-temperature water continuum absorption data determined in this study will permit further testing of the predictive capabilities of these, or other, water continuum absorption models.

---

*This conclusion has also been reached by Burch and coworkers,[56,57] who determined the shape of the water continuum between 12.2 and 30 μm in order to examine whether absorption maxima indicative of dimer absorption bands could be observed in this wavelength region. They calculated an "empirical continuum" between 12.2 and 30 μm by subtracting theoretical water continuum self-broadening coefficients (predicted on the basis of the AFGL line listing and a simple Lorentzian line shape) from their measured water continuum self-broadening coefficients between 12.2 and 30 μm. The resulting empirical continuum increased smoothly from 12.2 to 30 μm and showed no evidence of absorption maxima in the 14- to 20-μm region that could be attributed to intermolecular vibrational bands of vapor-phase water dimers. Burch et al. concluded that the shape of this empirical continuum indicated the need to use super-Lorentzian line profiles to describe the self-broadened shapes of water-vapor absorption lines.

III. EXPERIMENTAL

We determined the water-vapor continuum absorption spectra reported here with the CO_2 laser photoacoustic detection system shown schematically in Fig. 4. The excitation source for the system was a Laakmann Electro-Optics Inc. model RF-4400D PZTG cw waveguide $C^{12}O_2^{16}$ laser, which was generally selectively tuned over 23 wavelengths of its 10.4-μm band [R(32) to R(10) and P(10) to P(30)]. The line-tunable laser output was intensity-modulated at 13 Hz by a mechanical chopper, focused to a 2- to 3-mm beam diameter, and passed through matched, nonresonant sample and reference photoacoustic cells. The photoacoustic cells were connected to the differential pressure head of a capacitance manometer that served as the photoacoustic system's pressure transducer. The sample cell was filled with the water-vapor—air mixture; the reference cell was filled with dry air. The differential pressure signal detected between the two cells by the capacitance manometer was measured at the exciting-light-modulation frequency with a lock-in amplifier (PAR model 5404). A power meter (Coherent model 210) determined the intensity of the laser exciting light, and a CO_2 laser spectrum analyzer (Optical Engineering model 16A) monitored its wavelength. The laser provided a TEM_{00} mode output power of greater than 6 W on its strongest lines. The chopper average power throughput was 50% of the incident power.

The photoacoustic system's capacitance manometer was an MKS Instruments, Inc., Baratron type 170 pressure meter with a 10-Torr full-range differential pressure head. Differential absorption measurements were made between the matched photoacoustic cells to minimize the effects of spurious absorption at the cell windows. Each photoacoustic cell was constructed of stainless steel and had an optical path length of 14.9 cm and a bore of 0.99 cm. The cells were equipped with zinc selenide (ZnSe) windows mounted at Brewster's angle.

The photoacoustic cells fit tightly into a trough in an aluminum cell-holder block. The cell holder provided good thermal contact with the cells and kept the cell optical axes aligned. The cells were maintained at selected fixed temperatures by circulating heat-exchange fluid from an external constant-temperature bath (Neslab LT50) through a channel that extended the length of the cell-holder block. The cell-holder assembly was placed in a compartment that could be flushed with gaseous dry nitrogen, preventing
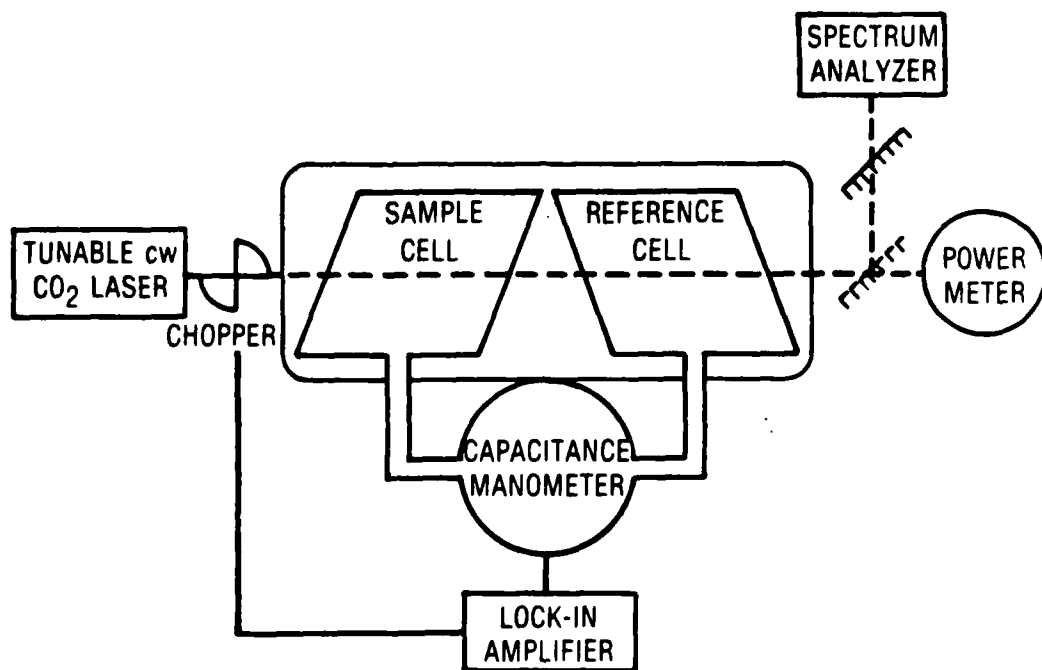
35

Fig. 4. CO_2 laser photoacoustic detection system.

moisture in the ambient air from condensing on the outside of the cell windows during below-room-temperature measurements.

Gas samples were prepared and added to the sample and reference photo-acoustic cells with a mercury-free, greaseless vacuum line. The responsivity of the photoacoustic detection system was measured over a several-order-of-magnitude concentration range of ethylene (as a calibration gas) in 1-atm pressure of nitrogen at the CO_2 laser 10.4-μm band lines P(12), P(14), P(16), and P(22). The detector responsivity was calculated from ethylene-absorption cross sections determined by us for these CO_2 laser lines. The cross sections $\sigma(\lambda)$ were determined by measuring the transmittance $T(\lambda)$ of CO_2 laser light, at each of the desired wavelengths, through a gas cell containing a known low pressure of ethylene buffered with nitrogen to 1-atm total pressure. The $\sigma(\lambda)$ were obtained by evaluating the relationship $T(\lambda) = \exp[-\sigma(\lambda)pL]$, where p is the ethylene pressure (in atmospheres) and L is the cell path length in centimeters. The absorption measurements were performed in a 5-1 spherical glass cell of low surface-to-volume ratio (0.28 cm^{-1}) to minimize ethylene adsorption losses on the cell walls. The cell had a path length of 32.0 cm and was equipped with ZnSe Brewster's angle windows.

Water-vapor—air mixtures of known concentration were added to the photo-acoustic detection system by first expanding the desired pressure of water vapor into the sample cell and then closing the cell. The photoacoustic system capacitance manometer was used to measure the steady-state pressure of water vapor after the sample sat in the cell for several minutes while the photoacoustic system was maintained at the temperature selected for the absorption measurements. A synthetic-air sample (80% N_2—20% O_2) was next bled into the sample cell containing the water vapor until the desired total pressure of water vapor and air was obtained. The water-vapor—air mixture was then heated to 50°C and maintained at temperatures above ambient for 2 hr or more to ensure thorough sample mixing before the cells were cooled to the desired temperature. Finally, synthetic air was added to the reference cell until a pressure balance between both cells was obtained.

The ethylene—nitrogen mixtures and synthetic-air samples used to fill the photoacoustic cells were prepared in a calibrated 12-1 flask equipped with a convection mixing loop. The oxygen, nitrogen, and synthetic-air pressures were measured with a 0-to-800-Torr Wallace and Tiernan pressure gauge.

37

Ethylene pressures were measured with an MKS Baratron pressure gauge with a 77 H-10 pressure head. Research-purity ethylene, nitrogen (99.9995%), oxygen (> 99.996%), and water (Baker AR Grade for HPLC use) were used throughout the study.

Two or more spectral runs were made on different water-vapor--air mixtures at each temperature and water-vapor partial pressure for which water-vapor CO_2 laser absorption spectra were determined. The replicate water-vapor spectra were in good agreement.

IV. RESULTS AND DISCUSSION

This section presents and discusses the results of measurements of water-vapor CO_2 laser absorption spectra performed by the CO_2 laser photoacoustic technique. Water-vapor absorption data were obtained at numerous wavelengths within the 10.4-μm CO_2 laser band at selected temperatures as low as -10°C. Section IV.A describes ethylene absorption cross-section measurements and photoacoustic responsivity measurements on ethylene—nitrogen calibration mixtures for the purpose of placing the water absorption data on an absolute basis. Section IV.B presents and discusses the results of extensive measurements to determine the dependence of water continuum absorption on temperature and water-vapor partial pressure.

A. CALIBRATION OF ABSOLUTE MAGNITUDE OF WATER-VAPOR ABSORPTION

1. ETHYLENE ABSORPTION CROSS-SECTION MEASUREMENTS

Photoacoustic detection systems do not directly measure absolute absorption strengths. The responsivity of such a system must first be calibrated with a reference gas for which absorption cross-section data are available. Its highly structured CO_2 laser absorption profile and low adsorptivity on cell walls make ethylene an ideal calibration gas for CO_2 laser photoacoustic detection systems. Photoacoustic detector responsivity measurements are typically made over a several-order-of-magnitude concentration range of ethylene in nitrogen or synthetic air at selected CO_2 lines. The accurate application of this approach requires that the ethylene-absorption cross sections be accurately known at these CO_2 laser wavelengths.

Several groups of workers have measured ethylene-absorption cross sections at many[70,71] or, in some cases,[72] just a few CO_2 laser wavelengths. The largest absorption cross section occurs at the CO_2 laser 10.4-μm band P(14) line on account of its wavelength proximity to the Q-branch of the ethylene $\nu_7(b_{1u})$ out-of-plane bending mode.[73] The ethylene absorption signal can be easily recognized through the use of this laser line together with a few nearby lines where ethylene cross sections are a factor of 6 or more smaller.

In this study, photoacoustic responsivity measurements were carried out at the CO_2 laser 10.4-μm band lines P(12), P(14), P(16), and P(22). To obtain

another independent determination of the absorption cross sections at these lines, transmission measurements were made through ethylene—nitrogen mixtures in a 32.0-cm-path-length cell (see Section III) at a total pressure of 760 Torr and at room temperature (24°C). The cross-section data obtained as a function of ethylene partial pressure are shown in Fig. 5. The ethylene-absorption cross sections at the P(12), P(16), and P(22) laser lines increase by 10% or less as the ethylene pressure is decreased over the ~ 5.5- to 0.5-Torr range. The absorption cross sections in the limit of low (i.e., < 0.1 Torr) ethylene pressure at these lines are 5.06, 6.15, and 1.95 cm^{-1} atm^{-1}, respectively. The ethylene-absorption cross section at the P(14) line, on the other hand, is independent of ethylene pressure over the 0.306- to 3.08-Torr range studied. The cross section at the P(14) line, furthermore, remained constant (at 34.76 ± 0.27 cm^{-1} atm^{-1}) for 12 measurements over an approximately 5- to 50-W cm^{-2} laser irradiance range (beam diameter ~ 2 mm).

The constancy of the P(14) line cross section with irradiance indicates that ethylene-absorption saturation effects are unimportant at the laser lines employed in the cross-section measurements for irradiances below 50 W cm^{-2}. The photoacoustic system responsivity measurements described below were performed at laser irradiances below 50 W cm^{-2}.

The ethylene-absorption cross-section data determined here are compared in Table II with similar data determined by other groups on ethylene—air mixtures maintained at 760-Torr total pressure and room temperature. Christy and Faller[72] obtained an absorption cross section of 35 cm^{-1} atm^{-1} for ethylene at the CO_2 laser 10.4-μm band P(14) line by performing transmission measurements through dilute ethylene—air mixtures. Patty and coworkers[70] obtained cross sections of 4.35, 29.10, 4.55, and 1.09 cm^{-1} atm^{-1} at the 10.4-μm band laser lines P(12), P(14), P(16), and P(22), respectively. They measured transmission through ethylene—air mixtures in a 60-m-total-path-length multipass gas cell, employing ethylene partial pressures between 7.6×10^{-3} and 0.27 Torr. Persson and coworkers[71] obtained cross sections of 5.29, 38.99, 6.42, and 1.78 cm^{-1} atm^{-1} at the P(12), P(14), P(16), and P(22) laser lines, respectively. They obtained these data by measuring transmission through a 1.5-m-path-length gas cell containing ethylene—air mixtures at ethylene partial pressures between 0.29 and 12.2 Torr.
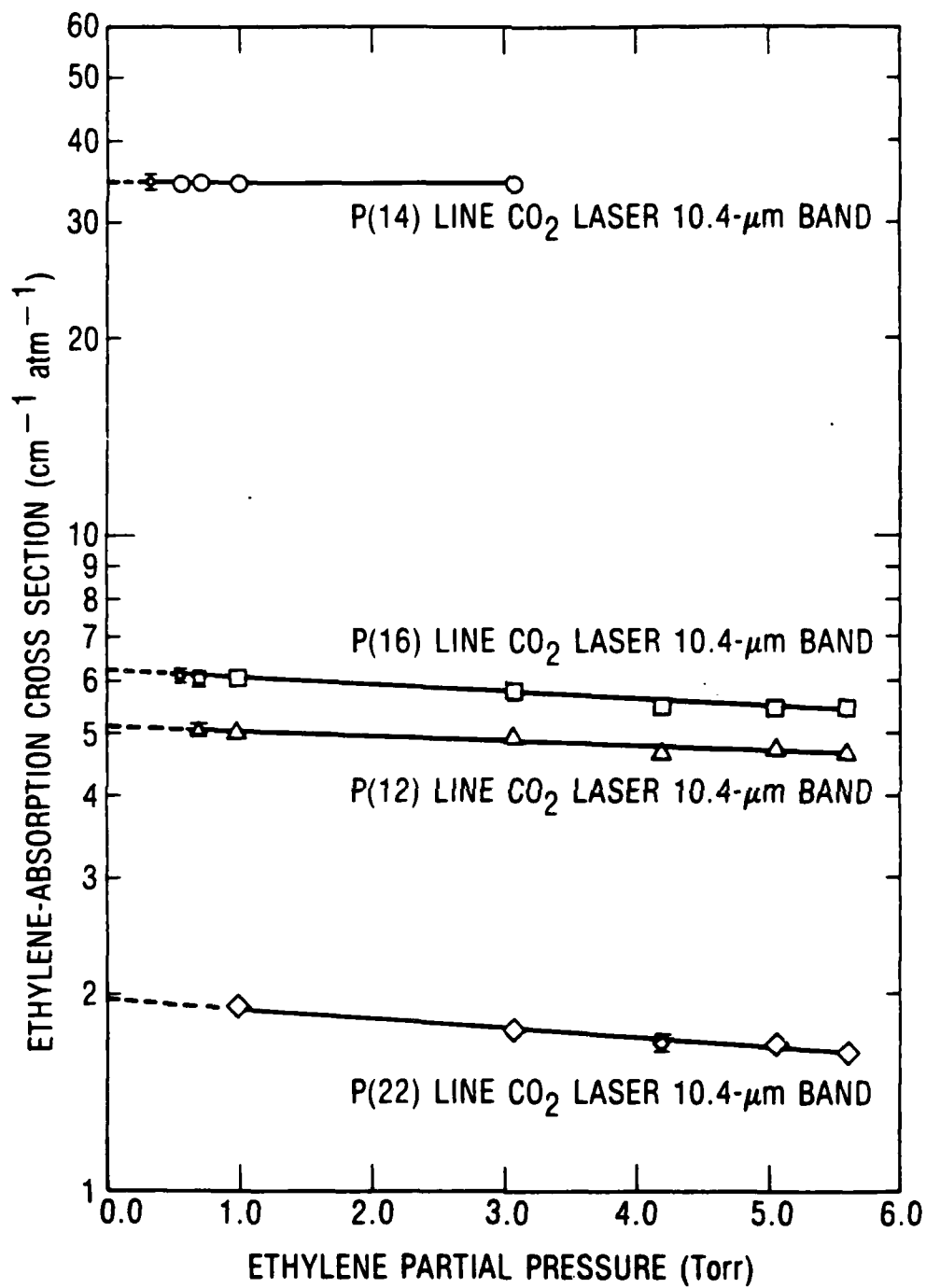
Fig. 5. Ethylene-absorption cross sections versus ethylene
partial pressure in samples buffered to 760-Torr
total pressure with nitrogen.

41

TABLE II. ETHYLENE-ABSORPTION CROSS SECTIONS σ (in cm^{-1} atm^{-1})
AT SELECTED CO_2 LASER WAVELENGTHS

| $C^{12}O_2^{16}$ Laser 10.4-μm (00°1–10°0) Band | | Reference | | | | | | |
| | | This work | | Christy and Faller[72] | Patty et al.[70] | | Persson et al.[71] | |
Transition	λ (μm)	$\sigma_{P(n)}$	$\dfrac{\sigma_{P(n)}}{\sigma_{P(14)}}$ ratio	$\sigma_{P(n)}$	$\sigma_{P(n)}$	$\dfrac{\sigma_{P(n)}}{\sigma_{P(14)}}$ ratio	$\sigma_{P(n)}$	$\dfrac{\sigma_{P(n)}}{\sigma_{P(14)}}$ ratio
P(12)	10.513	5.06	0.146	—	4.35	0.149	5.29	0.136
P(14)	10.532	34.76	1.000	35	29.10	1.000	38.99	1.000
P(16)	10.551	6.15	0.177	—	4.55	0.157	6.42	0.165
P(22)	10.611	1.95	0.056	—	1.09	0.037	1.78	0.046

Our ethylene-absorption cross section determined at the 10.4-μm band P(14) laser line agrees closely with the corresponding value obtained by Christy and Faller.[72] The cross sections determined in this study at the P(12), P(14), and P(16) laser lines fall between the corresponding values determined by Patty et al.[70] and those of Persson et al.[71] Our P(12), P(14), and P(16) laser-line cross sections are, respectively, 4.5, 11.0, and 3.5% lower than those of Persson and coworkers. The cross section reported here at the P(22) laser line is 9.5% higher than that determined by Persson and coworkers but nearly 80% higher than the value obtained by Patty and coworkers.

2. PHOTOACOUSTIC SYSTEM RESPONSIVITY MEASUREMENTS

Relative photoacoustic responsivity measurements were made on ethylene—nitrogen mixtures as a function of ethylene concentration with the CO_2 laser photoacoustic system used in the water absorption measurements. Figure 6 shows the results for ethylene concentrations between about 30 ppm and 10 ppb. A linear photoacoustic response is observed at the laser lines P(12), P(14), P(16), and P(22) for absorption signals as small as about 0.4 μV W^{-1}.* A linear least-squares fit to the relation

$$\log \text{ (signal)} = m \log(p_{C_2H_4}) + b$$

was performed on the photoacoustic response data at each laser line for absorption signals greater than 1.0 μV W^{-1}. The values of the coefficients m and b (and their corresponding standard deviations) determined in the fits at these laser lines are:

line	m	b
P(12)	0.977 ± 0.006	−1.872 ± 0.019
P(14)	0.974 ± 0.005	−1.018 ± 0.015
P(16)	0.984 ± 0.008	−1.829 ± 0.026
P(22)	0.974 ± 0.005	−2.334 ± 0.016

---

*An approximately 0.1 μV W^{-1} larger absorption signal in the sample photoacoustic cell compared with the reference cell results in the development of curvature below 0.4 μV W^{-1} in Fig. 6. The larger absorption signal in the sample cell compared with that of the reference cell (see Fig. 4) is believed to result from an approximately 1% larger incident laser intensity on the sample cell than the reference cell.
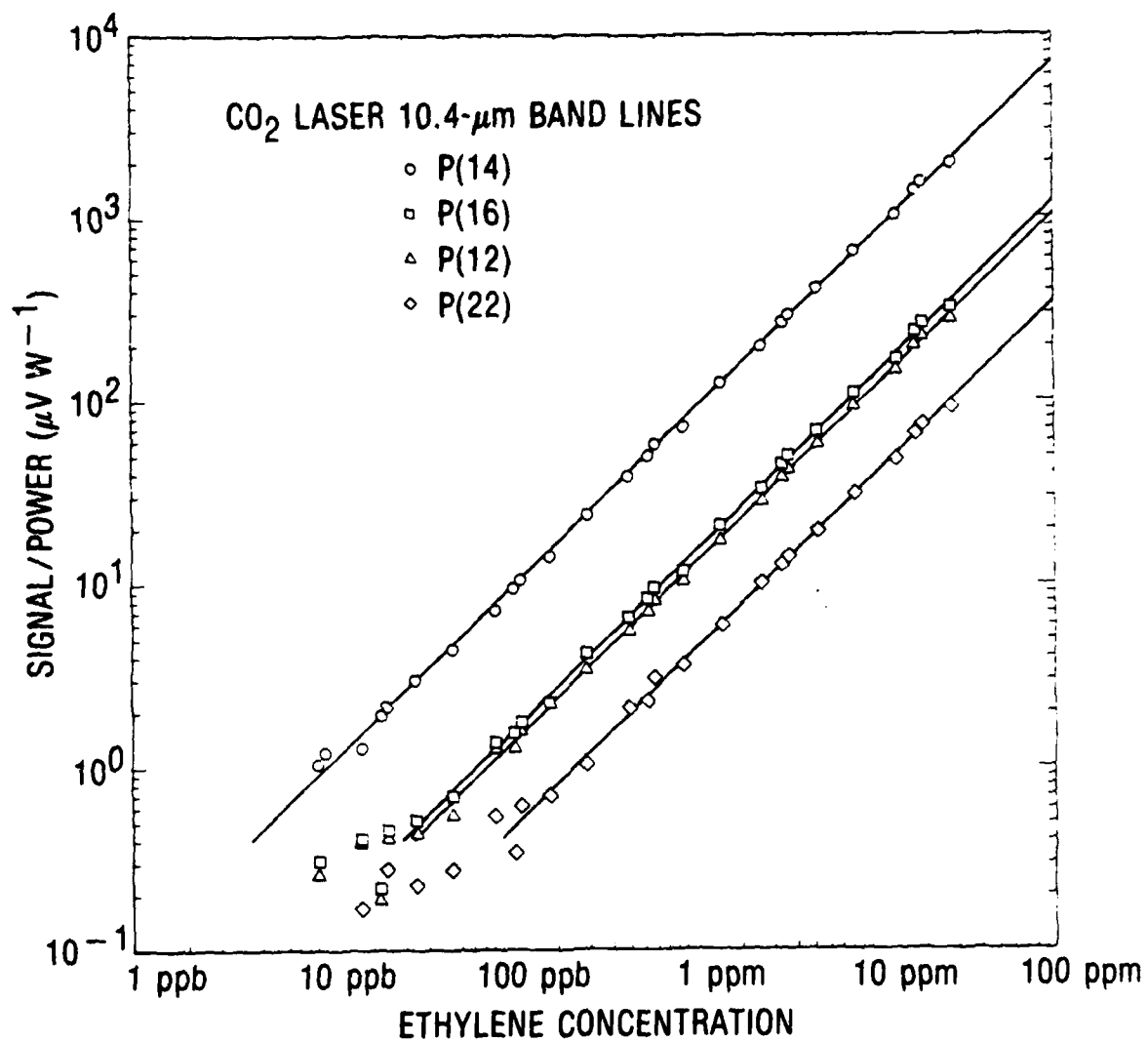
Fig. 6. Response of photoacoustic system at selected CO_2 laser lines versus ethylene concentration.

Based on these linear least-squares fit coefficients, the relative photoacoustic response of a 760-Torr nitrogen sample containing 0.10-Torr (131.6 ppm) ethylene would be predicted to be: P(12) = 0.145, P(14) = 1.000, P(16) = 0.174, and P(22) = 0.048. These relative response values are in good agreement with the absorption cross-section ratios $\sigma_{P(n)}/\sigma_{P(14)}$ obtained both in this study and by Persson and coworkers[71] (see Table II). Because (1) our measured ethylene cross section at the P(14) laser line agrees with the cross section of Christy and Faller[72] and is intermediate in value with the corresponding cross sections determined by Patty et al.[70] and Persson et al.,[71] and (2) as observed in Fig. 5, the ethylene cross section at the P(14) laser line is independent of ethylene concentration, we have selected the cross section measured at the P(14) laser line in the present study [$\sigma_{P(14)}$ = 34.76 cm^{-1} atm^{-1}] to calibrate the absolute response of our photoacoustic system. The absorption coefficients (in units per centimeter) measured for water-vapor—air mixtures were thus determined from the expression

$$\text{Abs. Coeff. Water—Air Mixtures} = \left\{ \text{antilog} \left[\frac{\log (\mu V\ W^{-1}\ \text{signal}) + 1.018}{0.974} \right] \right\} \times (34.76 \times 10^{-9})\ cm^{-1} \tag{1}$$

B. WATER-VAPOR ABSORPTION DATA MEASURED IN THE 10.4-μm CO_2 LASER BAND

Water absorption data were determined within the CO_2 laser 10.4-μm band in this study at temperatures of 27, 10, and -10°C for water-vapor—synthetic-air mixtures at 760-Torr total pressure. Initial measurements were performed at 27°C on mixtures containing 10-Torr water vapor. As Fig. 7 demonstrates, our data are in generally good agreement with data determined under similar conditions by Shumate and coworkers[14] and by Long and coworkers.[10,15,16] This agreement indicates consistency between the sample preparation and mixing procedures and photoacoustic responsivity calibration techniques used in this study and by the Shumate and Long groups.* The data of Shumate et al.[14] have

---

*Shumate and coworkers[14] used the photoacoustic technique to measure water absorption. As in the present study, they used ethylene to calibrate the photoacoustic responsivity. Long and coworkers[10,15,16] measured water absorption both by the photoacoustic technique and by the long-path absorption technique. They compared these measurements to establish the absolute magnitude of the water absorption by the photoacoustic technique.
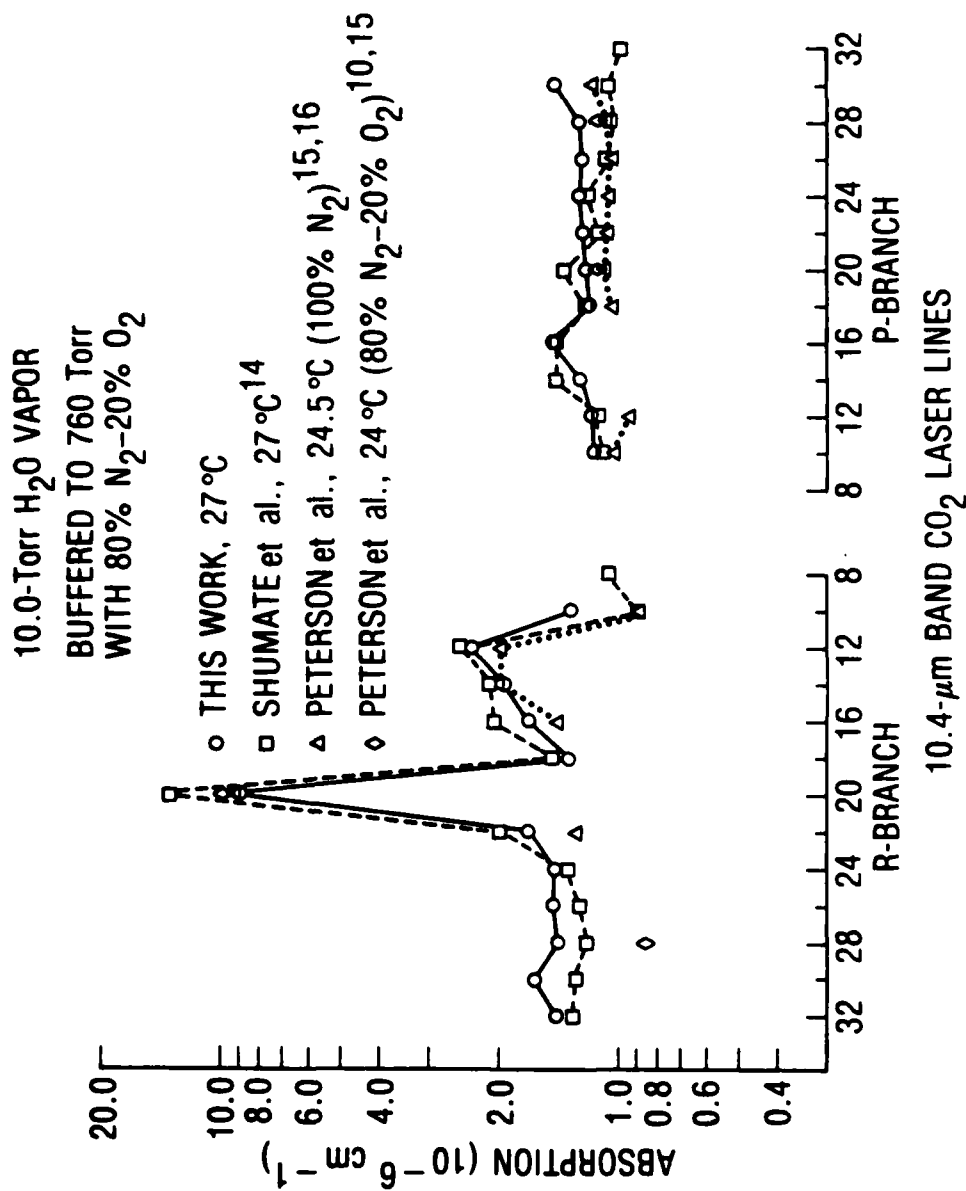
10.0-Torr H_2O VAPOR
BUFFERED TO 760 Torr
WITH 80% N_2-20% O_2

o THIS WORK, 27°C
□ SHUMATE et al., 27°C[14]
△ PETERSON et al., 24.5°C (100% N_2)[15,16]
◇ PETERSON et al., 24°C (80% N_2-20% O_2)[10,15]

ABSORPTION (10^{-6} cm^{-1})

20.0
10.0
8.0
6.0
4.0
2.0
1.0
0.8
0.6
0.4

R-BRANCH

32 28 24 20 16 12 8

P-BRANCH

8 12 16 20 24 28 32

10.4-μm BAND CO_2 LASER LINES

Fig. 7. Comparison of CO_2 laser absorption coefficient measurements on water-vapor--air mixtures by various workers. Data of Shumate et al. have been corrected here to the ethylene-absorption cross section of 34.76 cm^{-1} atm^{-1} determined in this study at the 10.4-μm band CO_2 laser P(14) line.

been corrected in Fig. 7 to the ethylene-absorption cross section of 34.76 cm^{-1} atm^{-1} determined here at the CO_2 laser 10.4-μm band P(14) line. Shumate et al. used the value of 29.10 cm^{-1} atm^{-1} determined by Patty et al.[70] for this cross section.

The sharp absorption peak at the CO_2 laser 10.4-μm band R(20) line above the water continuum in each spectrum in Fig. 7 has been proposed by McClatchey et al.[31] and Peterson[16] to result from a near-wavelength coincidence of the R(20) laser line and a weak local water-vapor pure rotational transition. This absorption feature can be used as a convenient calibration peak when measuring the weak water-continuum absorption. Limited measurements were thus performed in the present study to examine the temperature and water-partial-pressure dependences of this absorption feature. We briefly discuss the results obtained for this absorption peak before we present results on the temperature and water-pressure dependences of the continuum absorption.

1. WATER ABSORPTION PEAK AT THE CO_2 LASER 10.4-μm BAND R(20) LINE

Figure 8 shows CO_2 laser absorption spectra for water--air mixtures containing 7.5-Torr water vapor at temperatures of 27 and 10°C. Observe in Fig. 8 that the absorption feature at the R(20) laser line increases in intensity with increasing temperature, i.e., has a positive temperature coefficient. A positive temperature coefficient would be obtained for an absorption transition that originates from a thermally populated lower level. Accordingly, McClatchey et al.[31] have suggested that this transition originates from a lower rotational level with an energy of 1557.8 cm^{-1}. As illustrated in Fig. 9, this assignment is consistent with the magnitude of the temperature dependence observed between 18 and 35°C in the present study for the absorption peak at the R(20) laser line. The measurements in Fig. 9 were performed on mixtures containing 10 Torr of water vapor buffered to 760-Torr total pressure with air. From Fig. 9, it is observed that, at a fixed water partial pressure, the intensity of the absorption feature at the R(20) laser line can be monitored to verify independently the temperature of a water--air mixture.

The water-absorption feature at the CO_2 laser 10.4-μm band R(20) line has been assigned to a local water-vapor absorption line, so its intensity would
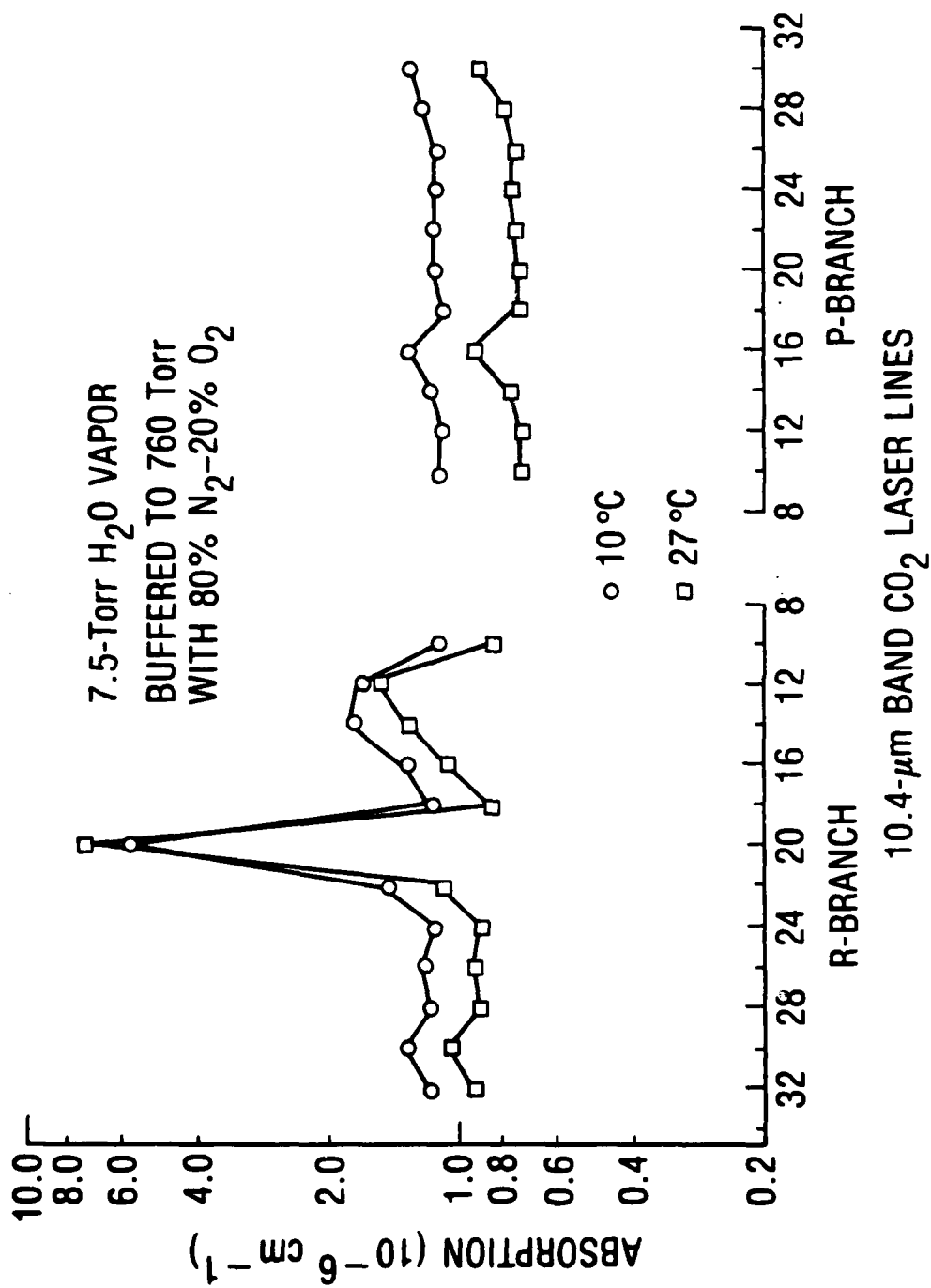
Fig. 8. CO_2 laser absorption spectra of water-vapor--air mixtures containing 7.5-Torr water vapor.
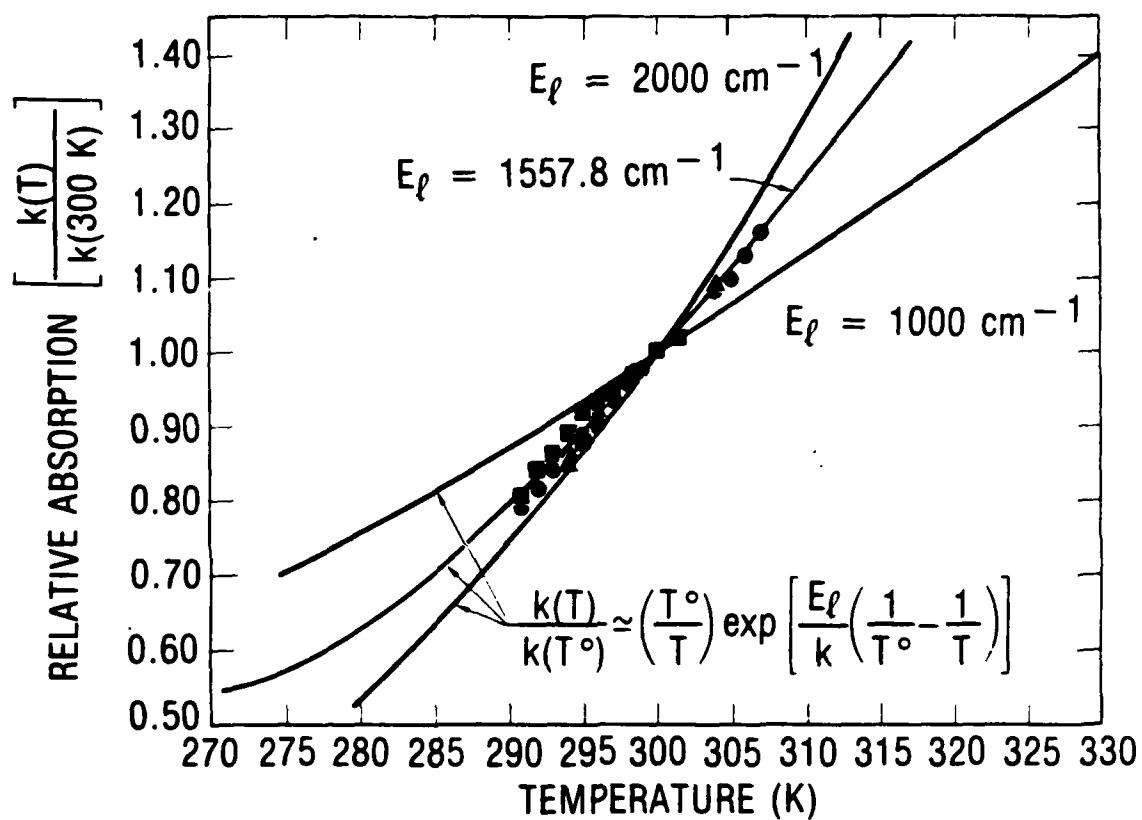
48

Fig. 9. Comparison of experimental with predicted temperature dependences
of water absorption peak at CO_2 laser 10.4-μm band R(20) line.
E_ℓ represents assumed lower-state energy level.

be expected to possess a nearly linear dependence on water partial pressure.[*] This is consistent with the water-partial-pressure dependence shown in Fig. 10 for this absorption peak in water—air mixtures at 10°C. (The linear photo-acoustic response obtained for water partial pressures up to close to the 9.2-Torr saturation vapor pressure for water at 10°C indicates that negligible water adsorptive losses occur on the photoacoustic cell walls for the conditions employed in this study.) From Fig. 10, it is observed that, at a fixed temperature, the intensity of the absorption peak at the R(20) laser line can be used to monitor the water partial pressure in a water—air mixture.

2. WATER ABSORPTION AT CO_2 LASER 10.4-μm BAND LINES WHERE CONTINUUM CONTRIBUTIONS DOMINATE

a. Temperature Dependence

Further examination of Fig. 8 reveals that the water absorption possesses a negative temperature coefficient within the CO_2 laser 10.4-μm band P-branch and the short-wavelength region of the R-branch, where absorption contributions from weak local water lines are small relative to continuum contributions. To examine the temperature dependence of the continuum absorption, extensive absorption measurements were performed at various temperatures on water—air mixtures at selected water pressures. In addition to the measurements performed at 27 and 10°C on water—air mixtures containing 7.5-Torr water vapor, shown in Fig. 8, measurements were performed at 27 and 10°C on mixtures containing 6.0-, 5.0-, and 3.0-Torr water vapor. The data obtained for these air mixtures are plotted in Figs. 11, 12, and 13, respectively. Also shown in Fig. 13 are absorption data on mixtures containing 3.0-Torr water vapor at 0°C. Data obtained at -10°C on mixtures containing 1.69-Torr water vapor are presented in Fig. 14.

These results show that the magnitude of the continuum-absorption negative temperature coefficient increases with increasing water pressure and decreasing temperature. The temperature coefficients between 27 and 10°C for mixtures containing 3.0-, 5.0-, 6.0-, and 7.5-Torr water vapor are -2.0 ± 0.4, -2.6 ± 0.3, -2.8 ± 0.3, and -2.9 ± 0.5%/°C, respectively. For mixtures with

---

[*]A pure linear dependence is observed only when the absorption strength of the local water line is significantly greater than the absorption strength of the underlying water continuum.
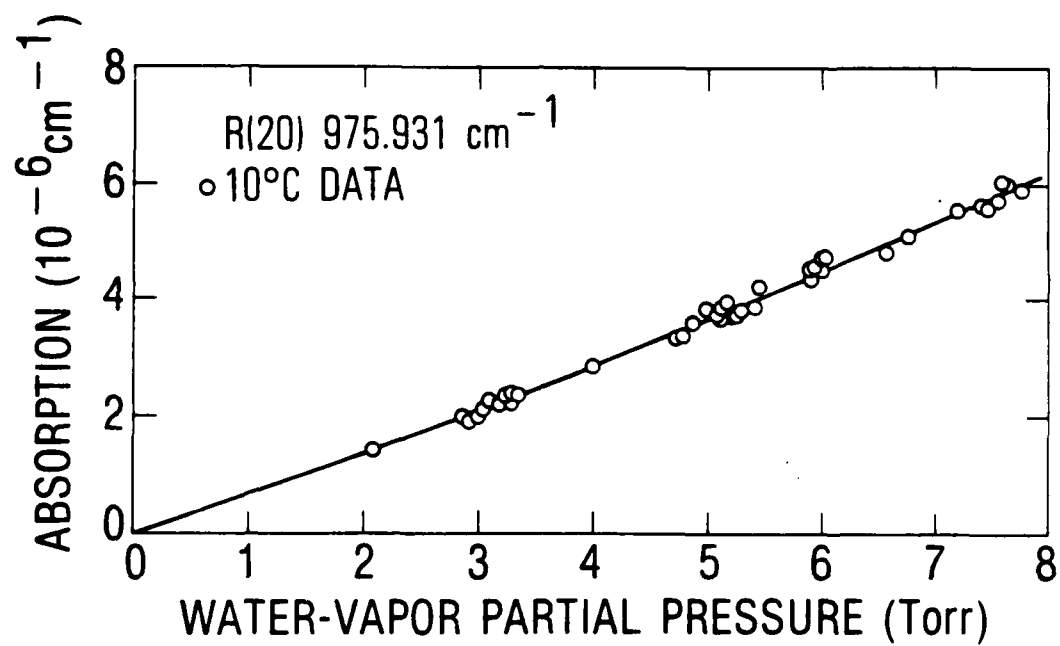
Fig. 10. Water-partial-pressure dependence at 10°C of water near line-center absorption at CO_2 laser 10.4-μm band R(20) line.
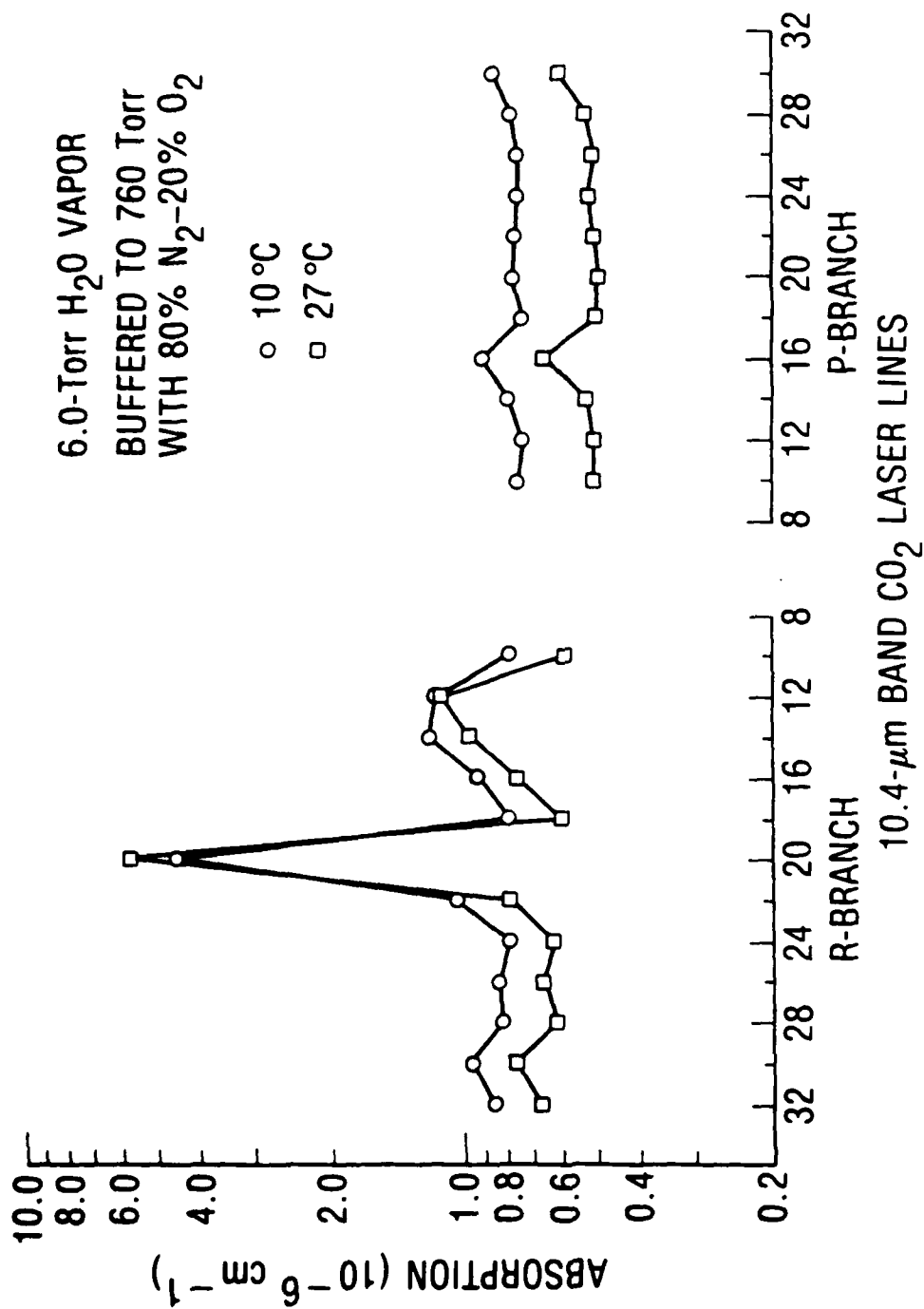
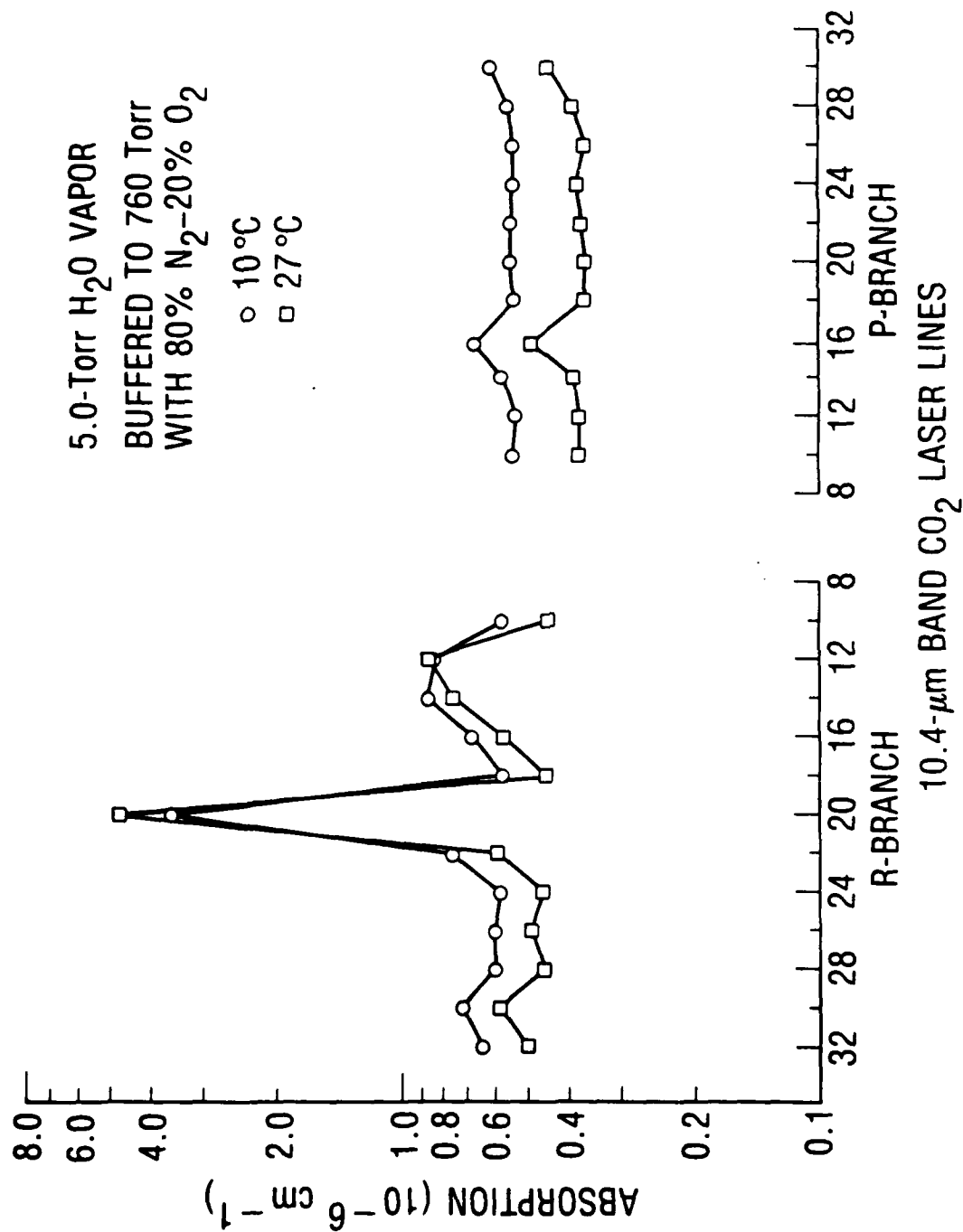Fig. 11. CO_2 laser absorption spectra of water-vapor—air mixtures containing 6.0-Torr water vapor.

52

Fig. 12. CO_2 laser absorption spectra of water-vapor–air mixtures containing 5.0-Torr water vapor.
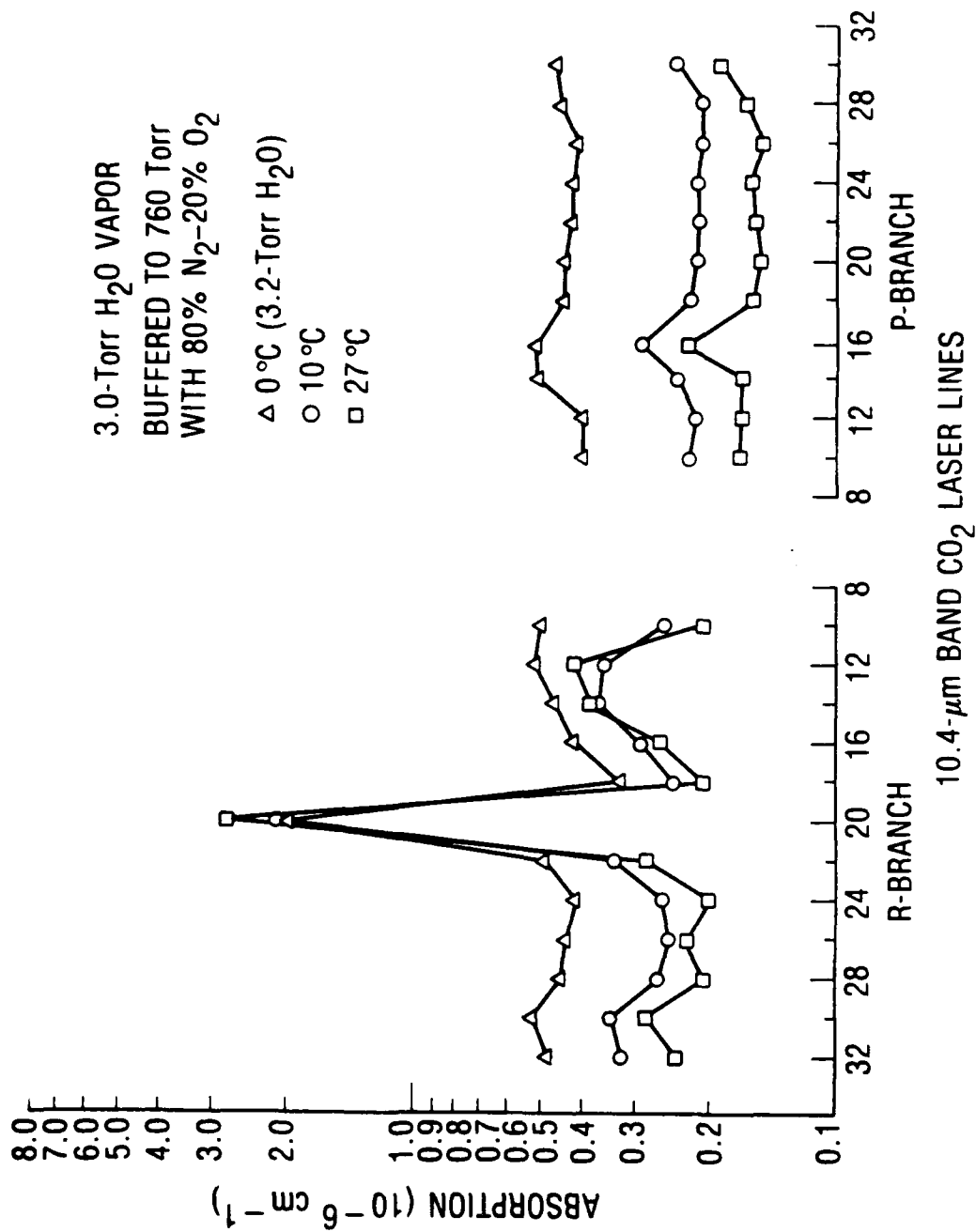
53

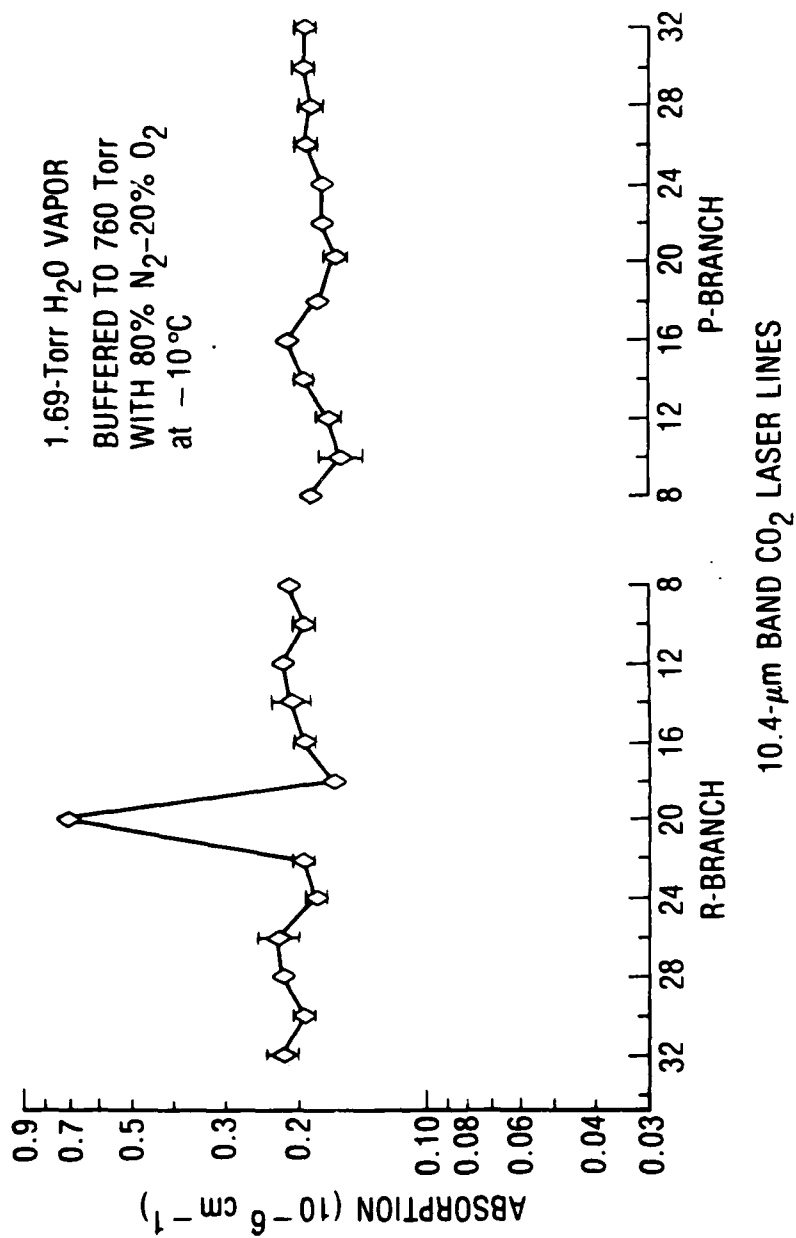Fig. 13. CO_2 laser absorption spectra of water-vapor-air mixtures containing 3.0-Torr water vapor.

54

Fig. 14. CO_2 laser absorption spectra of water-vapor--air mixtures containing 1.69-Torr water vapor.

3.0-Torr water the 10-to-0°C temperature coefficient is -7.7 ± 0.2%/°C. The 27 to 10°C temperature coefficients are in close agreement with the approximately -2%/°C value observed between 27 and 100°C.[6,9,12,15]

b. Water-Partial-Pressure Dependence

Work was also performed to determine the functional dependence of the water-absorption magnitude on water partial pressure in wavelength regions where continuum-absorption contributions are dominant. Extensive CO_2 laser absorption measurements were thus performed at 27 and 10°C on 760-Torr total pressure air samples containing a range of water pressures. These measurements were made at the CO_2 laser 10.4-μm band lines R(32) to R(10) and P(10) to P(30). The measurement results at the high-frequency 10.4-μm band line R(32) and the low-frequency line P(28), presented in Figs. 15 and 16, respectively, are representative of the results observed at 10.4-μm band laser wavelengths other than the R(20) line. The results of measurements at the 10.4-μm band laser lines other than R(32) and P(28) are shown in Figs. A-1 through A-21 in the Appendix. Examination of Figs. 15 and 16 and Figs. A-1 through A-21 reveals that, at those laser wavelengths where continuum-absorption contributions are most important [i.e., for laser lines other than R(20), Fig. A-6], the water absorption possesses a greater than linear but less than pure quadratic dependence on water-vapor partial pressure. Thus, the 27 and 10°C continuum absorption measured in the present study can be concluded to possess a dependence on water-vapor partial pressure that includes both linear and quadratic terms. As indicated above (cf., Section II.D), a similar water-vapor partial-pressure dependence has been observed for continuum absorption at room temperature and above.[5-10,14-16]

The 27 and 10°C water absorption data plotted in Figs. 15 and 16 and A-1 through A-21 were fit to the relation

$$abs.(\lambda, T) = a(\lambda, T)p_{H_2O} + b(\lambda, T)p^2_{H_2O}$$

where abs. (λ, T) represents the water absorption value measured at a particular temperature T and CO_2 laser wavelength λ; and p_{H_2O} is the water-vapor partial pressure in torr, employed in the measurements.
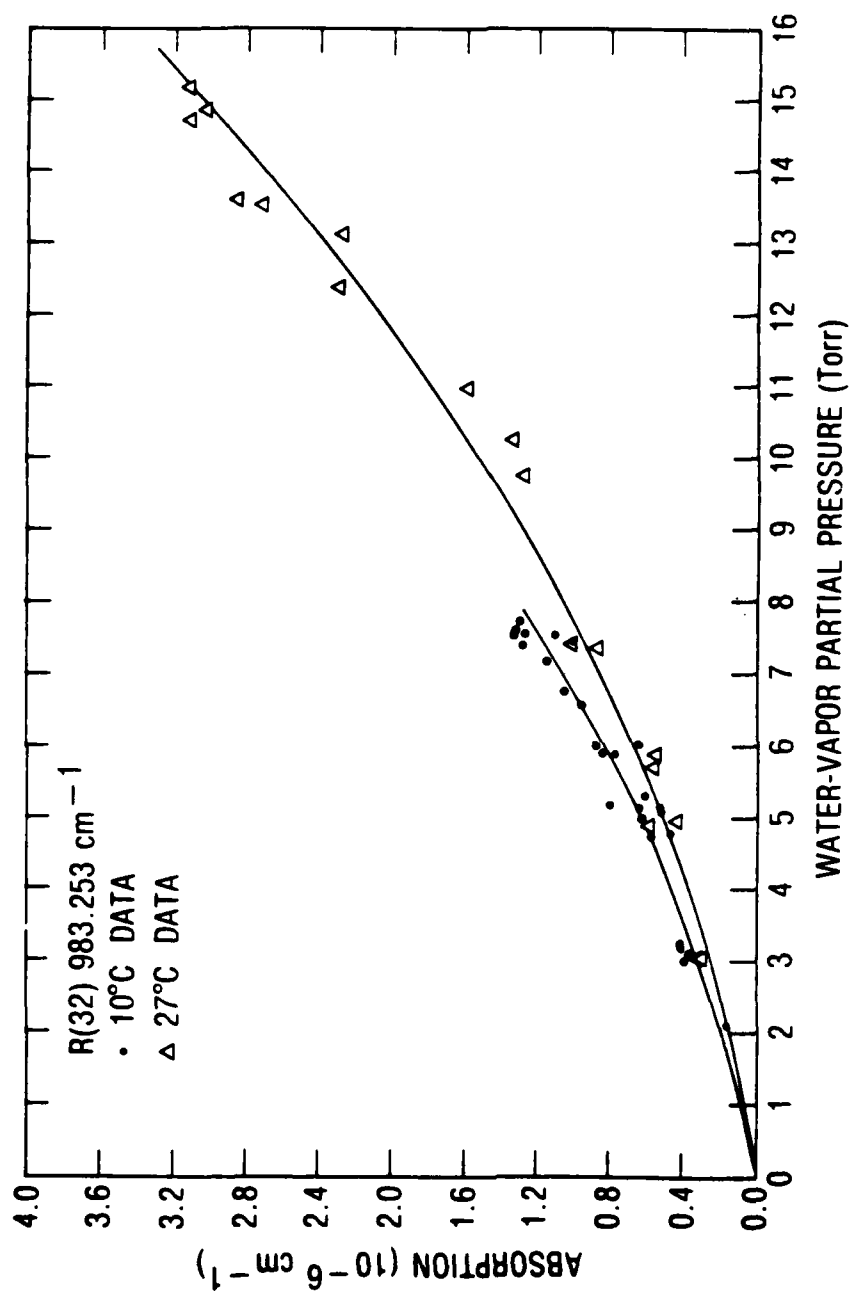
56

Fig. 15. Absorption coefficients of 760-Torr total pressure water-vapor--air mixtures versus water partial pressure at CO₂ laser 10.4-μm band R(32) line.
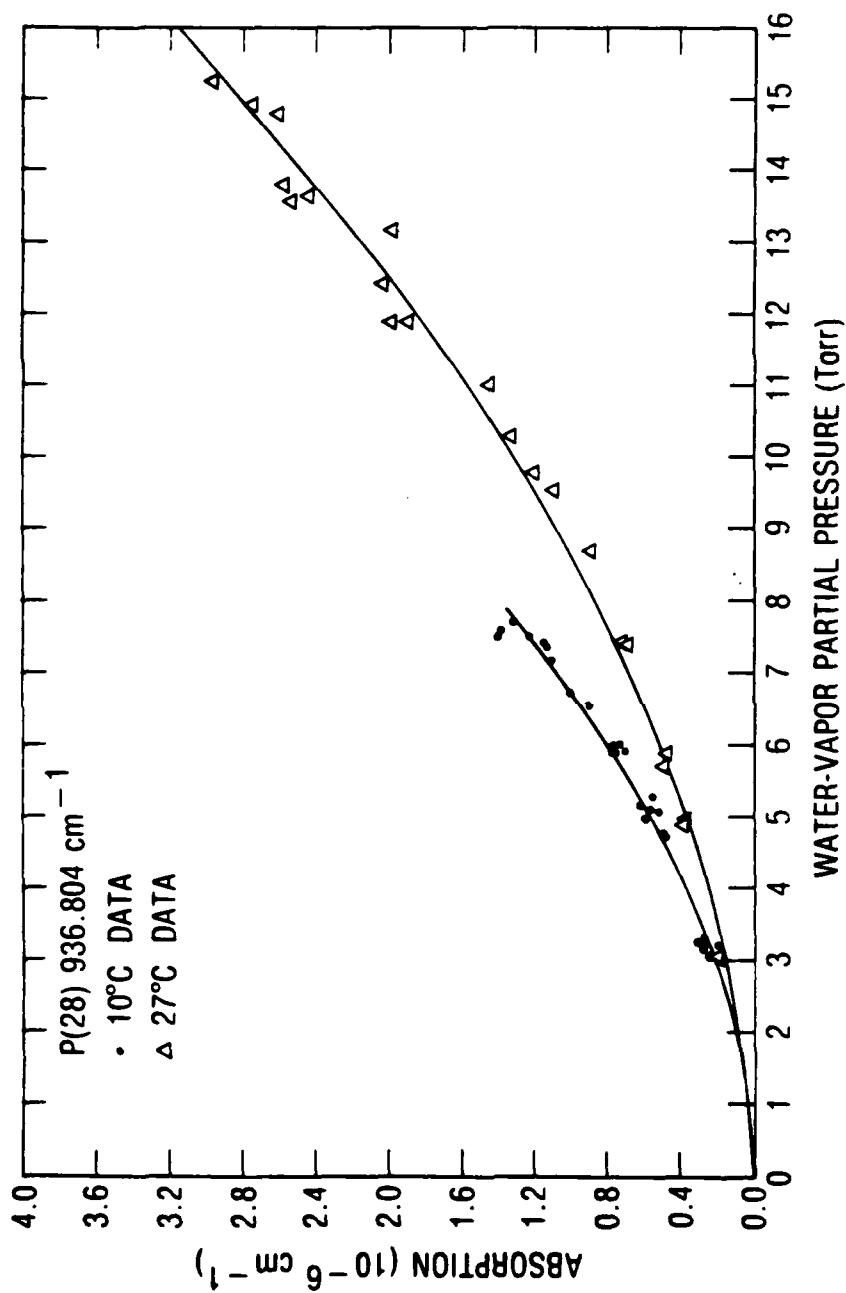
57

Fig. 16. Absorption coefficients of 760-Torr total pressure water-vapor–air mixtures versus water partial pressure at CO_2 laser 10.4-μm band P(28) line.

58

The $a(\lambda, T)$ and $b(\lambda, T)$ coefficients that correspond, respectively, to water-absorption contributions that have linear and quadratic dependences on water-vapor partial pressure are listed in Table III. The solid lines in Figs. 15 and 16 and A-1 through A-21 correspond to the absorption calculated from these coefficients. These coefficients, along with their standard deviations, were calculated from a linear least-squares fit of the abs.(λ, T) and P_{H_2O} data to the expression

$$\frac{\text{abs.}(\lambda, T)}{P_{H_2O}} = a(\lambda, T) + b(\lambda, T)P_{H_2O}$$

The linear coefficients $a(\lambda, T)$ and quadratic coefficients $b(\lambda, T)$ obtained at 27 and 10°C are displayed as a function of CO_2 laser wavelength in Figs. 17 and 18, respectively. [The error-bar limits associated with each $a(\lambda, T)$ or $b(\lambda, T)$ value in these figures are equal in magnitude to $a(\lambda, T)$ or $b(\lambda, T)$ plus or minus one standard deviation in their values.]

From Fig. 17 and Table III, it is observed that, throughout the CO_2 laser 10.4-μm band, the linear coefficients $a(\lambda, 10°C)$ are either the same as, within experimental uncertainty of, or (at a few laser wavelengths) smaller than the corresponding $a(\lambda, 27°C)$ values. The latter case [$a(\lambda, 10°C) < a(\lambda, 27°C)$] can be most easily observed at the R(20), R(14), and R(12) laser lines, where absorption contributions by thermally populated local water lines are thought to be important.[14] In contrast to the near constancy or decreasing behavior observed for the linear coefficients $a(\lambda, T)$ from 27 to 10°C, the quadratic coefficients $b(\lambda, T)$ are observed in Fig. 18 and Table III to clearly increase throughout the CO_2 laser 10.4-μm band as the temperature decreases from 27 to 10°C. It is this increase in the quadratic coefficients $b(\lambda, T)$ with decreasing temperature that is responsible for the larger water continuum absorption strengths observed at 10°C compared with 27°C.

C. **EVALUATION OF CONTINUUM DATA IN TERMS OF COLLISIONAL-BROADENING AND WATER DIMER MODELS**

The relative importance of the collisional-broadening and water-vapor aggregate mechanisms to water continuum absorption in the 8- to 12-μm region

TABLE III. COMPARISON AT 27°C AND 10°C OF THE LINEAR AND QUADRATIC WATER–PRESSURE DEPENDENCES OF CO_2 LASER ABSORPTION COEFFICIENTS FOR 760–TORR TOTAL PRESSURE WATER–VAPOR–AIR[a] MIXTURES

$C^{12}O_2^{16}$ Laser (00°1-[10°0]) Band			27°C Data		10°C Data		Ratio Linear Coefficient at 10°C and 27°C	Ratio Quadratic Coefficient at 10°C and 27°C
Transition	ν (cm⁻¹)	λ (µm)	Linear Coefficient a(λ, 27°C) (10⁻⁸ cm⁻¹/Torr H₂O)	Quadratic Coefficient b(λ, 27°C) (10⁻⁸ cm⁻¹/Torr² H₂O)	Linear Coefficient a(λ, 10°C) (10⁻⁸ cm⁻¹/Torr H₂O)	Quadratic Coefficient b(λ, 10°C) (10⁻⁸ cm⁻¹/Torr² H₂O)	a(λ,10°C)/a(λ,27°C)	b(λ,10°C)/b(λ,27°C)
R(32)	983.251	10.120	6.98 ± 0.93[b]	1.01 ± 0.09	7.25 ± 1.19	1.14 ± 0.20	1.46 ± 0.36	1.13 ± 0.22
R(30)	982.096	10.182	6.18 ± 0.39	1.09 ± 0.04	6.81 ± 0.92	1.53 ± 0.16	1.10 ± 0.16	1.40 ± 0.15
R(28)	980.914	10.194	3.30 ± 0.72	1.17 ± 0.07	3.96 ± 0.83	1.60 ± 0.14	1.20 ± 0.36	1.37 ± 0.15
R(26)	979.706	10.207	4.09 ± 0.75	1.14 ± 0.07	2.82 ± 0.65	1.83 ± 0.11	0.69 ± 0.20	1.61 ± 0.14
R(24)	978.473	10.220	2.94 ± 0.84	1.25 ± 0.08	4.02 ± 0.64	1.51 ± 0.11	1.37 ± 0.45	1.21 ± 0.12
R(22)	977.215	10.233	5.69 ± 0.74	1.21 ± 0.07	5.25 ± 0.89	1.98 ± 0.16	0.92 ± 0.20	1.61 ± 0.16
R(20)	975.931	10.247	87.93 ± 2.97	1.12 ± 0.28	64.39 ± 1.16	1.75 ± 0.21	0.73 ± 0.03	1.33 ± 0.12
R(18)	974.623	10.260	3.96 ± 0.62	1.01 ± 0.06	3.05 ± 0.66	1.67 ± 0.12	0.77 ± 0.20	1.65 ± 0.15
R(16)	973.289	10.274	4.79 ± 0.63	1.31 ± 0.06	3.88 ± 0.86	1.92 ± 0.15	0.81 ± 0.21	1.47 ± 0.11
R(14)	971.918	10.288	9.39 ± 0.93	1.14 ± 0.09	4.31 ± 1.85	2.58 ± 0.34	0.46 ± 0.19	2.26 ± 0.32
R(12)	970.548	10.303	9.15 ± 0.87	1.59 ± 0.08	4.78 ± 1.02	2.40 ± 0.18	0.52 ± 0.12	1.51 ± 0.14
R(10)	969.140	10.318	4.01 ± 1.02	0.98 ± 0.10	3.87 ± 1.62	1.53 ± 0.32	0.97 ± 0.48	1.56 ± 0.36
P(10)	952.882	10.494	2.90 ± 0.62	0.92 ± 0.06	2.48 ± 0.69	1.66 ± 0.12	0.86 ± 0.30	1.80 ± 0.18
P(12)	951.193	10.513	2.89 ± 0.65	0.92 ± 0.06	2.15 ± 0.72	1.69 ± 0.11	0.74 ± 0.30	1.84 ± 0.19
P(14)	949.480	10.532	2.49 ± 0.73	1.05 ± 0.07	2.72 ± 0.69	1.74 ± 0.12	1.09 ± 0.42	1.66 ± 0.16
P(16)	947.743	10.551	4.25 ± 0.59	1.10 ± 0.06	4.37 ± 0.81	1.77 ± 0.15	1.03 ± 0.24	1.61 ± 0.16
P(18)	945.981	10.571	2.21 ± 0.66	1.03 ± 0.06	2.46 ± 0.71	1.65 ± 0.12	1.11 ± 0.46	1.60 ± 0.15
P(20)	944.195	10.591	1.76 ± 0.50	1.09 ± 0.05	1.46 ± 0.94	1.89 ± 0.17	0.83 ± 0.58	1.73 ± 0.17
P(22)	942.384	10.611	1.95 ± 0.59	1.09 ± 0.06	1.49 ± 0.78	1.87 ± 0.14	0.76 ± 0.28	1.72 ± 0.16
P(24)	940.549	10.632	1.94 ± 0.58	1.17 ± 0.06	1.74 ± 0.71	1.81 ± 0.12	0.90 ± 0.46	1.62 ± 0.14
P(26)	938.689	10.653	1.61 ± 0.55	1.14 ± 0.05	1.30 ± 0.72	1.89 ± 0.13	0.81 ± 0.53	1.66 ± 0.14
P(28)	936.804	10.674	2.11 ± 0.57	1.13 ± 0.05	0.79 ± 0.20	2.05 ± 0.12	0.37 ± 0.14	1.81 ± 0.13
P(30)	934.895	10.696	2.48 ± 0.91	1.29 ± 0.08	1.59 ± 0.92	2.12 ± 0.16	0.64 ± 0.44	1.64 ± 0.16

Avg. = 0.88 ± 0.32   Avg. = 1.60 ± 0.18

[a] Synthetic air (80% N₂—20% O₂) was employed.

[b] Coefficient uncertainties are equal to one standard deviation of coefficient value.
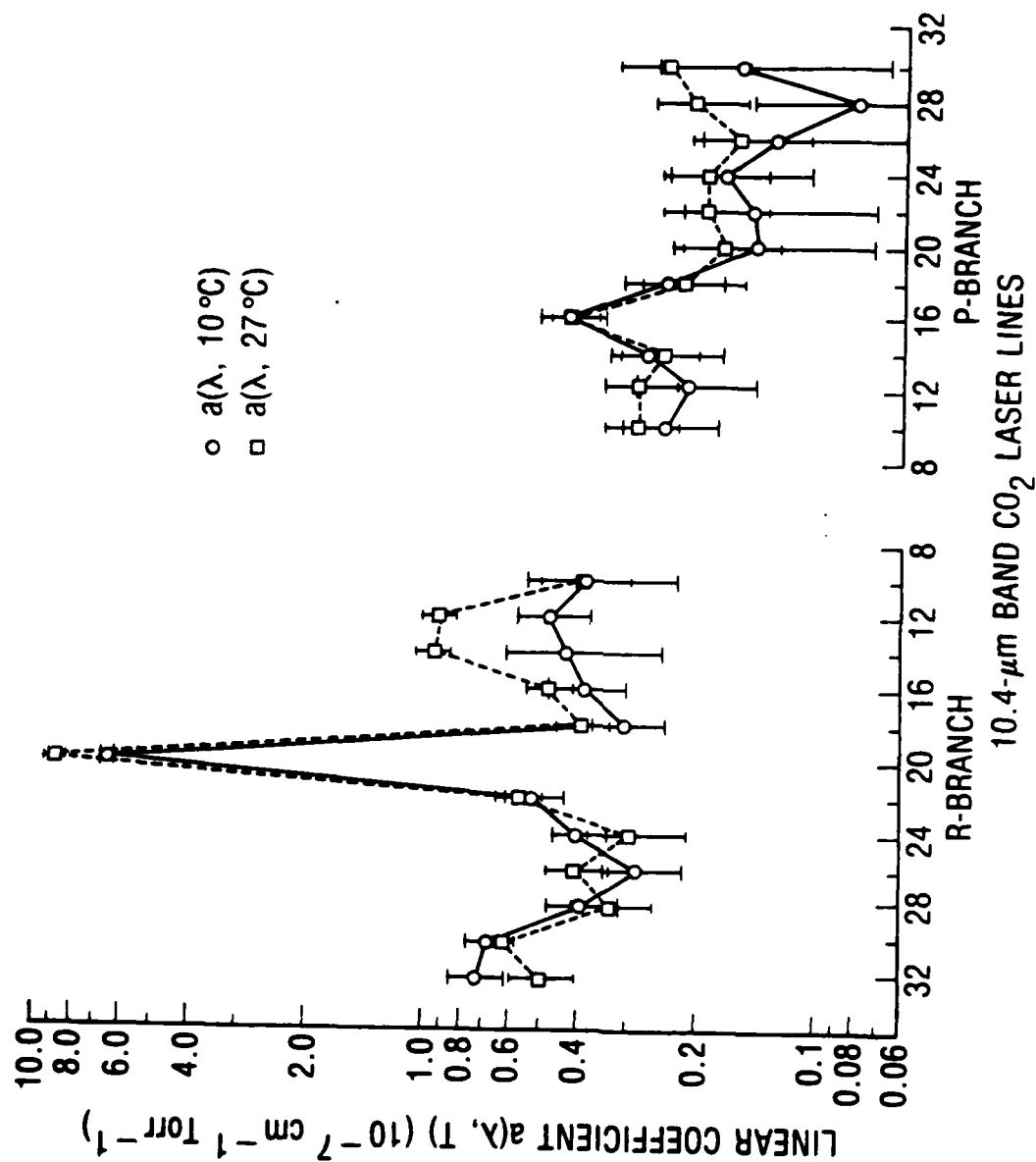
Fig. 17. Comparison of water-pressure linear coefficients as a function of laser wavelength at 10 and 27°C.
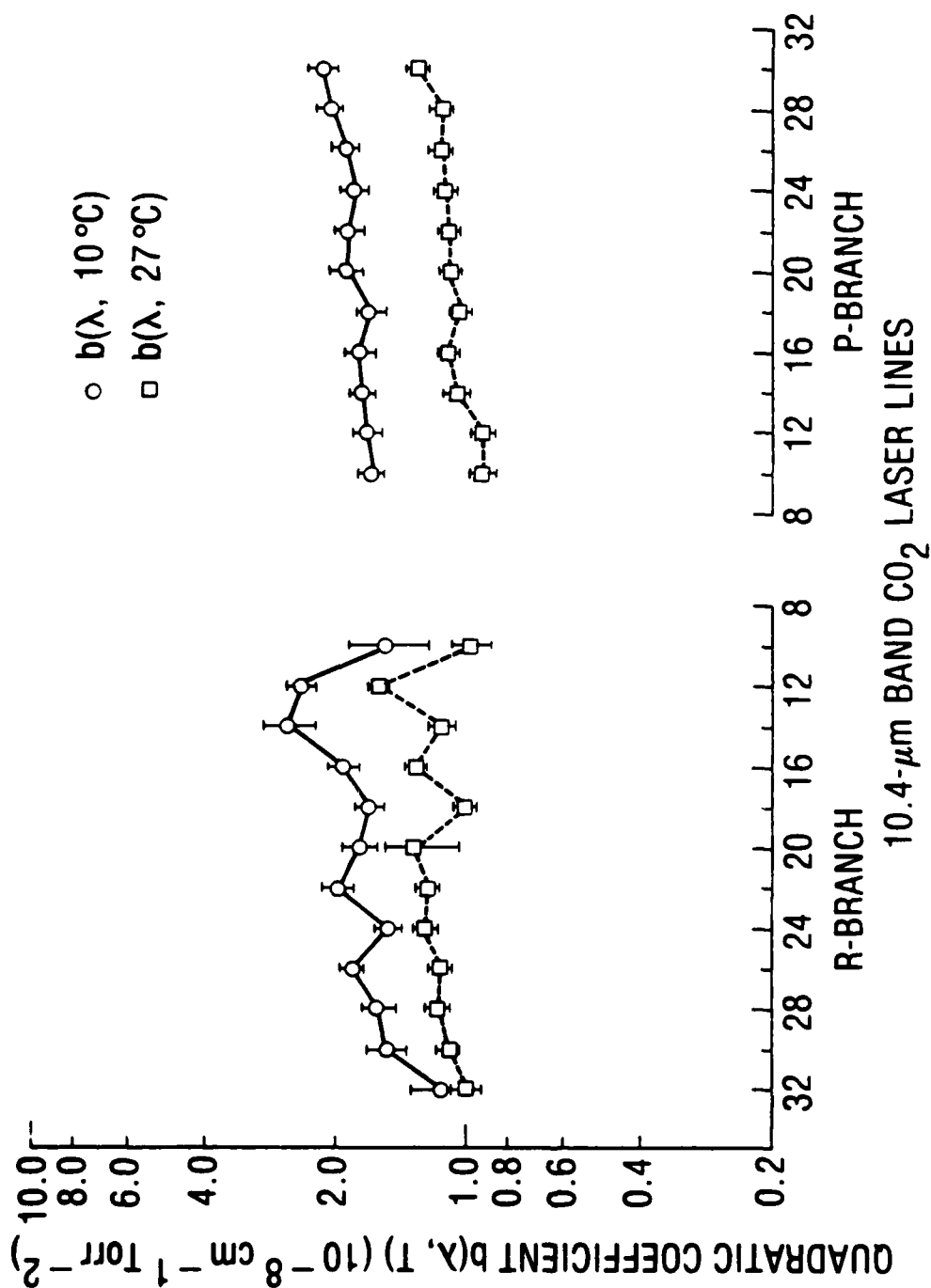
61

Fig. 18. Comparison of water partial-pressure quadratic coefficients as a function of CO_2 laser wavelength at 10 and 27°C.

under different possible atmospheric conditions is the subject of debate, as indicated in Section II.D. It is recalled that by the collisional-broadening mechanism, the continuum is attributed to the self- and foreign-collisionally broadened far wings of the water absorption lines on either side of the 8- to 12-µm region.[17,18,58] By the latter mechanism,[19,20] the continuum is attributed to the collisionally broadened far wings of absorption bands that are proposed to develop in the 16- to 18 µm region as the result of the formation of water-vapor aggregates, mainly water dimers.

For most atmospheric conditions, the magnitude of the continuum absorption is primarily governed by its water-pressure quadratic component.* Figure 19 compares the experimental and theoretically predicted temperature dependences of the water-pressure quadratic component of the 8- to 12-µm water continuum absorption. This figure is similar to Fig. 3, except that Fig. 19 also shows the data determined in this study, which extend the temperature dependence of the quadratic component to -10°C. Here, the water-pressure quadratic component of the continuum absorption determined by Montgomery[12] above 100°C can be observed to possess a very weak positive temperature coefficient. The continuum quadratic component determined by Burch et al.[6,34,55] and Montgomery[12] within the 100 to 27°C temperature regime, and by us between 27 and -10°C, can be observed to possess a strong negative temperature coefficient.

As indicated previously, Nordstrom and Thomas's[17,18] collisional-broadening model accurately predicts the observed linear- and quadratic-term functional dependences of continuum absorption on water-vapor partial pressure. As Fig. 19 shows, the present form of this model underestimates significantly the magnitude of the measured negative temperature coefficient for the water-pressure quadratic component between 100 and 27°C, but predicts properly the observed magnitude of the weak positive temperature coefficient above 100°C.

---

*From the linear and quadratic coefficients in Table III, one can conclude that the quadratic water-pressure component contributes predominantly to the total water-vapor absorption coefficient at 27 and 10°C for water pressures greater than about 3 and 2 Torr, respectively. For lower temperatures, the quadratic component would be the major contributor to absorption at even lower water pressures.
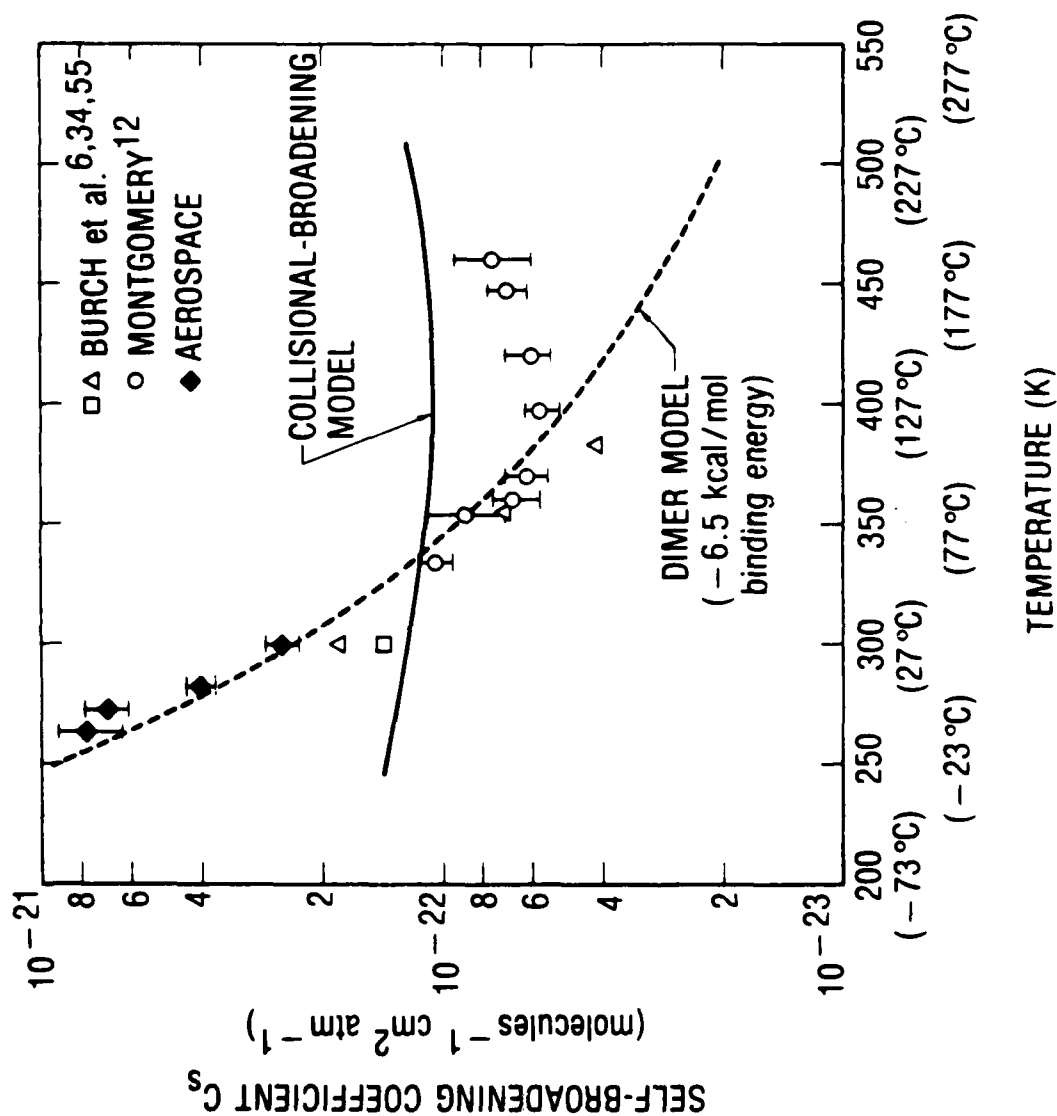
Fig. 19. Comparison of experimental and predicted temperature dependences of water-pressure quadratic component of 8- to 12-μm water continuum absorption. Here the magnitude of the continuum absorption predicted by the water dimer model has been increased by a factor of 1.3 from that shown in Fig. 3 to better match the absolute values of C_s measured between 100 and −10°C. The predicted dimer concentration temperature dependence, however, is identical to that shown in Fig. 3.

The water-vapor dimer model of Suck et al.,[19,20] on the other hand, predicts a pure quadratic water-vapor partial pressure dependence for the continuum absorption instead of the observed linear and quadratic water-pressure term dependences. The water dimer model is observed in Fig. 19 to correctly estimate the magnitude of the negative temperature coefficient for the quadratic component between 100 and 27°C, but fails to predict the weak positive temperature coefficient observed above 100°C. Both the collisional-broadening and water dimer models can predict the proper magnitude of the quadratic component near room temperature.

The magnitude of the negative temperature coefficient for the quadratic water-pressure component observed between 27 and -10°C in the present study is the same as that reported by Burch and coworkers and Montgomery between 100 and 27°C. Figure 19 shows that the magnitude of the negative temperature coefficient determined by us between 27 and -10°C is in very good agreement with that predicted by the water-vapor dimer model of Suck and coworkers.[19,20] Figure 19 further shows that, in its present form, the collisional-broadening model of Nordstrom and Thomas[17,18] severely underestimates the magnitude of the negative temperature coefficient measured here between 27 and -10°C. In our study, absolute values of the self-broadening coefficients have been determined only at 27 and 10°C. Our 27°C self-broadening coefficient of $(2.53 \pm 0.24) \times 10^{-22}$ molecules^{-1} cm^2 atm^{-1} is within experimental uncertainty of the value of $(2.25 \pm 0.41) \times 10^{-22}$ molecules^{-1} cm^2 atm^{-1} calculated from the 27°C data of Shumate et al.[14] [when corrected to our ethylene P(14) cross section of 34.76 cm^{-1} atm^{-1}] and the value of $(2.23 \pm 0.23) \times 10^{-22}$ molecules^{-1} cm^2 atm^{-1} calculated from the 24.5°C water—nitrogen absorption data of Peterson et al.[15,16] Our 0 and -10°C data in Fig. 19 are lower-limit esti-mates of the self-broadening coefficients at these temperatures.* The value at 0°C was calculated by multiplying the absolute value of the self-broadening coefficient at 10°C by the average ratio of the absorption coefficients at 0°C to those at 10°C. Similarly, the value at -10°C was calculated by multiplying the 10°C self-broadening coefficient by the average ratio of the absorption

---

*The "self-broadening" coefficient $C_s(\lambda, T)$ and "foreign-broadening" coefficient $C_f(\lambda, T)$ defined in the footnote on page 29 can be calculated from the linear and quadratic coefficients $a(\lambda, T)$ and $b(\lambda, T)$ in Table III through the following relations:

coefficients at -10°C to those at 10°C. The 0 to 10°C absorption-coefficient ratio was determined from continuum data on mixtures containing 3.20-Torr water vapor, whereas the -10 to 10°C absorption coefficient ratio was determined from data on mixtures containing 1.69-Torr water vapor.

One way to account for the temperature, pressure, and wavelength dependences observed in this and previous studies of the 8- to 12-μm continuum is, as suggested by Montgomery,[12] to assume the simultaneous contribution to the continuum of water-dimer and collisional-broadening mechanisms. The weak positive temperature dependence observed for the continuum above 100°C and the negative temperature dependence observed below 100°C are consistent with a model in which the collisional-broadening mechanism contributes more significantly to the continuum than the water dimer mechanism above 100°C, but in which the water dimer mechanism begins to make significant contributions to the continuum below 100°C. By this model the water dimer mechanism increases in importance with decreasing temperature relative to the collisional-broadening mechanism.

The simultaneous contribution of collisional-broadening and water dimer mechanisms to the water continuum would account for the continuum's observed linear and quadratic water-pressure dependences. The increase in importance of the quadratic component from 27 to 10°C observed in this study would also be consistent with an increasingly important water dimer contribution to the continuum absorption with decreasing temperature.

$$C_f(\lambda, T) = \frac{a(\lambda, T)}{P}\left(\frac{P_{H_2O}}{w_{H_2O}}\right)$$

and

$$C_s(\lambda, T) = \left(\frac{P_{H_2O}}{w_{H_2O}}\right)\left[\frac{b(\lambda, T) + a(\lambda, T)}{P}\right]$$

where p_{H_2O} is the water partial pressure and P is the total pressure in atmospheres, and w_{H_2O} is the density of water vapor in molecules per cubic centimeter. The C_s values shown at 27, 10, 0, and -10°C in Fig. 19 were calculated from averages of $C_s(\lambda, T)$ data determined within the laser 10.4-μm band P-branch, where local water absorption line contributions are negligible.

Further, the increase in the water-pressure quadratic coefficient between 27 and 10°C and the magnitude of the negative temperature coefficient below 27°C observed in this study are necessary (but not sufficient) requirements for a model in which the water dimer mechanism is more important at and below room temperature than a collisional-broadening mechanism. Because the intermolecular vibrational absorption bands of the water dimer are proposed to be located in the 16-μm region, a continuum model that assumes the simultaneous contribution of water-dimer and collisional-broadening mechanisms would also be consistent with the observed increase in the water continuum absorption coefficient with increasing wavelength. This effect is predicted by this model to become more important with increasing water pressure as has also been observed. Proponents of the collisional-broadening mechanism of continuum absorption,[58,17,18] on the other hand, have suggested that, with improved modeling of the H_2O-H_2O collisional interaction potentials and the use of more exact collisional scattering theory, it may be ultimately possible to account for the temperature, pressure, and wavelength dependences of the continuum by the collisional-broadening mechanism alone.

Definitive experimental information is still needed on the wavelength positions, intensities, and collision-broadened contours of the various intermolecular vibrational-rotational bands of the water dimer in the vapor phase to resolve absolutely the question of whether the 8- to 12-μm water continuum would be most correctly described by a collisional-broadening mechanism in combination with a water dimer mechanism or by a collisional-broadening mechanism alone. Direct absorption measurements of the vibrational-rotational lines of the water dimer in the vapor phase have not been performed to date,[20] because of the difficulty in spectroscopically distinguishing the dimer absorption lines from water monomer pure rotational lines in water—air mixtures, in which the monomer concentration is greater than the dimer concentration by three or more orders of magnitude.[19,20]

Collisional-broadening continuum models[58,17,18] treat only the collision-broadened shapes of absorption lines that already exist in the water monomer. Thus, collisional-broadening models of the water continuum based on even very accurate molecular collision theory would not be able to account for absorption contributions to the water continuum resulting from the development of intermolecular vibrational modes in an H_2O-H_2O collision complex. New

67

infrared absorption bands of this type might be expected for collision complexes with lifetimes of greater than even a few vibrational periods ($\gtrsim 10^{-13}$ sec). These bands would develop as the result of the loss of translational and rotational degrees of freedom by the water molecules forming the complex.

Although direct absorption measurements on the water dimer's intermolecular vibrational absorption bands have not been performed in the vapor phase, Bentwood et al.[74] have examined such bands in low-temperature matrices by matrix isolation vibrational spectroscopy. The water dimer out-of-plane bending intermolecular vibrational band (the high-frequency tail of which was proposed by Suck et al.[19,20] to be responsible for the water continuum in the 8- to 12-μm region) was found by Bentwood and coworkers to be centered near 19 μm in a nitrogen matrix at 20 K. The wavelength of this band is thus close to the vapor-phase position of between 16 and 18 μm predicted by Suck and coworkers. Evidence for the existence of water dimers in water-vapor—air mixtures comes from the observation by Gebbie and coworkers[75] of water dimer rotational-absorption features in the submillimeter-wavelength region. They showed that the integrated intensities of these water dimer rotational absorption features had a temperature dependence that indicated a dimer interaction energy of -6 ± 3 kcal/mol and a quadratic dependence on water pressure. On the basis of the spectrometer-limited linewidth observed for the strongest rotational feature of the water dimer, Gebbie et al. concluded that the dimer is stable in the vapor phase and calculated its lower-limit lifetime to be $\sim 10^{-11}$ sec.

The average thermal energy available at 27°C is about 0.6 kcal/mol. Given the strong (~ -5 kcal/mol) hydrogen-bond interaction energy that is known to exist between water molecules in solid, liquid, and vapor phases, thermodynamic considerations would also predict, as observed by Gebbie et al., that long-lived ($> 10^{-13}$ sec) H_2O—H_2O collision complexes are formed in water—air mixtures. The oscillator strengths of the water dimer intermolecular vibrational absorption bands and the magnitude of the vapor-phase water dimer concentration calculated by Suck et al.[19,20] also appear reasonable, so it seems likely that water dimer species contribute significantly to continuum absorption at and below room temperature.

68

In view of these considerations and the temperature and water-pressure dependences of the continuum observed below room temperature in this study, we believe that the 8- to 12-μm water continuum would best be modeled by the simultaneous operation of collisional-broadening and water dimer mechanisms.

V. CONCLUSIONS

Temperature and water-vapor partial pressure dependences have been measured for the water-vapor pure rotational transition superimposed on the water continuum at the CO_2 laser 10.4-μm band R(20) line. The temperature dependence observed for this sharp water-vapor absorption feature is consistent with assignments made by McClatchey et al.[31] for the energy of the originating state of this transition. It is concluded that the intensity of this absorption feature can be used to verify the temperature or water partial pressure during measurements of weak water-vapor continuum absorption.

Throughout the CO_2 laser 10.4-μm band, the water-vapor continuum absorption was found to have a functional dependence on temperature between 27 and -10°C that is similar to that observed between 100 and 27°C by previous workers. The negative temperature coefficient observed for the water continuum absorption between 27 and -10°C was determined to be more consistent with the predicted temperature dependence of a continuum absorption water-vapor dimer model than that of a recently developed collisonal-broadening continuum model.[17,18]

We feel that the temperature, pressure, and wavelength dependences observed for the 8- to 12-μm continuum in this study and in previous studies (reviewed in Section II.D) would be most correctly modeled by the simultaneous contributions to the continuum of water-dimer and collisional-broadening mechanisms. The temperature dependence observed in this study between 27 and -10°C and the increase in the water-pressure quadratic coefficient observed between 27 and 10°C are consistent with the water dimer mechanism being more important than the collisional-broadening mechanisms at room temperature and below.

71

REFERENCES

1. K. M. Haught and J. A. Dowling, Opt. Lett. 1, 121 (1977).

2. K. O. White, W. R. Watkins, C. W. Bruce, R. E. Meredith, and F. G. Smith, Appl. Opt. 17, 2711 (1978).

3. R. E. Roberts, J. E. A. Selby, and L. M. Biberman, Appl. Opt. 15, 2085 (1976).

4. M. T. Coffey, Q. J. Roy. Meteorol. Soc. 103, 685 (1977).

5. J. H. McCoy, D. B. Rensch, and R. K. Long, Appl. Opt. 8, 1471 (1969).

6. D. E. Burch, Investigation of the Absorption of Infrared Radiation by Atmospheric Gases, Semi-Annual Technical Report, No. U-4784 Aeronutronic (January 1970) (Contract F19628-69-C-0263).

7. K. J. Bignell, Q. J. Roy. Meteorol. Soc. 96, 390 (1970).

8. V. N. Arefev, V. I. Dianov-Klokov, V. F. Radionov, and N. I. Sizov, Opt. Spectrosc. 39 560 (1975).

9. V. N. Arefev and V. I. Dianov-Klokov, Opt. Spectrosc. 42, 488 (1977).

10. R. J. Nordstrom, M. E. Thomas, J. C. Peterson, E. K. Damon, and R. K. Long, Appl. Opt. 17, 2724 (1978).

11. D. A. Gryvnak, D. E. Burch, R. L. Alt, and D. K. Zgonc, Infrared Absorption by CH_4, H_2O, and CO_2, Report No. U-6275, Aeronutronic (December 1977) (AFGL-TR-76-0246, Contract F19628-76-C-0067).

12. G. P. Montgomery, Jr., Appl. Opt. 17, 2299 (1978).

13. United States Air Force, comp., Handbook of Geophysics, Macmillan and Company, New York (1960).

14. M. S. Shumate, R. T. Menzies, J. S. Margolis, and L. G. Rosengren, Appl. Opt. 15, 2480 (1976).

15. J. C. Peterson, A Study of Water Vapor Absorption at CO_2 Laser Frequencies Using a Differential Spectrophone and White Cell, dissertation, Ohio State University (June 1978).

16. J. C. Peterson, M. E. Thomas, R. J. Nordstrom, E. K. Damon, and R. K. Long, Appl. Opt. 18, 834 (1979).

17. M. E. Thomas, Tropospheric Water Vapor Absorption in the Infrared Window Regions, dissertation, Ohio State University (August 1979).

18. R. J. Nordstrom and M. E. Thomas, "The Water Vapor Continuum as Wings of Strong Absorption Lines," in Atmospheric Water Vapor, A. Deepak, T. D. Wilkerson, and L. H. Ruhnke, eds., Academic Press, New York (1980).

19. S. H. Suck, J. L. Kassner, Jr., and Y. Yamaguchi, Appl. Opt. 18, 2609 (1979).

20. S. H. Suck, A. E. Wetmore, T. S. Chen, and J. L. Kassner, Jr., Appl. Opt. 21, 1610 (1982).

21. H. R. Carlon, Appl. Opt. 17, 3192 (1978); H. R. Carlon, Infrared Phys. 19, 49 (1979); H. R. Carlon 19, 549 (1979); H. R. Carlon and C. S. Harden, Appl. Opt. 19, 1776 (1980).

22. V. E. Zuev, Propagation of Visible and Infrared Radiation in the Atmosphere, John Wiley and Sons, New York (1970).

23. L. S. Rothman, A. Goldman, J. R. Gillis, R. H. Tipping, L. R. Brown, J. S. Margolis, A. G. Maki, and L. D. G. Young, Appl. Opt. 20, 1323 (1981); D. J. Spencer, G. C. Denault, and H. H. Takimoto, Appl. Opt. 13, 2855 (1975).

24. M. M. Shapiro and H. P. Gush, Can. J. Phys. 44, 949 (1966); M. A. H. Smith, J. M. Russell, J. H. Park, C. P. Ringland, C. B. Farmer, "Measurements of Continuum Absorption Near 2400 cm^{-1} in the Lower Stratosphere," Proc. Amer. Meteorol. Soc., 4th Conf. Atmos. Radiat. (June 1981).

25. S. A. Clough, F. X. Kneizys, L. S. Rothman, W. O. Gallery, "Atmospheric Spectral Transmittance and Radiance: FASCOD1B," Proc. Soc. Photo-Opt. Instr. Eng. 277, 152 (1981).

26. F. X. Kneizys, E. P. Shettle, W. O. Gallery, "Atmospheric Transmittance and Radiance: the LOWTRAN 5 Code," Atmospheric Transmission, Proc. Soc. Photo-Opt. Instr. Eng. 277, 116 (1981).

27. J. A. Logan, M. J. Prather, S. C. Wofsy, and M. B. McElroy, J. Geophys. Res. 86, 7210 (1981).

28. M. T. Coffey, W. G. Mankin, and A. Goldman, J. Geophys. Res. 86, 7331 (1981).

29. H. S. Stoker and S. L. Seager, Environmental Chemistry: Air and Water Pollution, Scott, Foresman and Company, Glenview, Illinois (1972).

30. S. I. Rasool, ed., Chemistry of the Lower Atmosphere, Plenum Press, Inc., New York (1973).

31. R. A. McClatchey, W. S. Benedict, S. A. Clough, D. E. Burch, R. F. Calfee, K. Fox, L. S. Rothman, and J. S. Garing, AFCRL Atmospheric Absorption Line Parameters Compilation Report, Report AFCRL-TR-73-0096, Air Force Geophysics Laboratory, Bedford, Massachusetts (1973).

32. L. S. Rothman, S. A. Clough, R. A. McClatchey, L. G. Young, D. E. Snider, and A. Goldman, "AFGL Trace Gas Compilation," Appl. Opt. 17, 507 (1978).

74

33.	L. S. Rothman, "High-Resolution Atmospheric Transmittance and Radiance: HITRAN and the Data Compilation," Proc. Soc. Photo-Opt. Instr. Eng. 142, 2 (1978).

34.	H. J. P. Smith, D. J. Dube, M. E. Gardner, S. A. Clough, F. X. Kneizys, and L. S. Rothman, FASCODE - Fast Atmospheric Signature Code (Spectral Transmittance and Radiance), Report AFGL-TR-78-0081, Air Force Geophysics Laboratory, Bedford, Massachusetts (1978).

35.	J. E. A. Selby, E. P. Shettle, and R. A. McClatchey, Atmospheric Transmittance from 0.25 to 28.5 μm: Supplement LOWTRAN 3B (1976), Report AFGL-TR-76-0258, Air Force Geophysics Laboratory, Bedford, Massachusetts (1 November 1976).

36.	J. E. A. Selby, F. X. Kneizys, J. H. Chetwynd, Jr., and R. A. McClatchey, Atmospheric Transmittance/Radiance: Computer Code LOWTRAN 4, Report AFGL-TR-78-0053, Air Force Geophysics Laboratory, Bedford, Massachusetts (1978).

37.	R. C. Shirkey, L. D. Duncan, and D. Clayton, Interim Electro-Optical Systems Atmospheric Effects Library, Vol. 2: User's Manual, Report ASL-TR-0048, Atmospheric Sciences Laboratory, White Sands Missile Range, New Mexico (1979).

38.	K. Tomiyama, J. H. Pierluissi, and R. B. Gomez, "Atmospheric Model for Laser Transmission in the Infrared," Atmospheric Transmission, Proc. Soc. Photo-Opt. Instr. Eng. 277, 136 (1981).

39.	L. L. Smith and T. Hilgeman, "High-Resolution Lower Atmospheric Transmission Predictions Over Long Paths," Atmospheric Transmission, Proc. Soc. Photo-Opt. Instr. Eng. 277, 141 (1981).

40.	A. S. Zachor, "Whatever Happened to Band Models," Atmospheric Transmission, Proc. Soc. Photo-Opt. Instr. Eng. 277, 105 (1981).

41.	C. K. N. Patel, Phys. Rev. Lett. 12, 588 (1964); Phys. Rev. 136, A1187 (1964).

42.	R. Beck, W. Englisch, and K. Gürs, Table of Laser Lines in Gases and Vapors, Springer Series in Optical Sciences, Vol. 2, Springer, Berlin (1978).

43.	G. L. Loper and J. A. Gelbwachs, "Below Room Temperature Measurements of the 8-12 μm Water Vapor Continuum Absorption," Atmospheric Transmission, Proc. Soc. Photo-Opt. Instr. Eng. 277, 40 (1981).

44.	C. K. N. Patel and R. J. Kerl, Appl. Phys. Lett. 30, 578 (1977).

45.	T. F. Deaton, D. A. Depatie, and T. W. Walker, Appl. Phys. Lett. 26, 300 (1975).

46.	M. S. Shumate, U. S. Patent 4,067,653 (10 January 1978).

47. C. F. Dewey, Jr., R. D. Kamm, and C. E. Hackett, Appl. Phys. Lett. 23, 633 (1973).

48. C. W. Bruce, B. Z. Sojka, B. G. Hurd, W. R. Watkins, K. O. White, and Z. Derzko, Appl. Opt. 15, 2970 (1976).

49. W. M. Elsasser, Phys. Rev. 34, 126 (1938).

50. A. Adel, Astrophys. J. 89, 1 (1939); R. Anthony, Phys. Rev. 85, 674 (1952); W. T. Roach, and R. W. Goody, Q. J. Roy. Meteorol. Soc. 84, 319 (1958); K. Bignell, F. Saiedy, and P. A. Sheppard, J. Opt. Soc. Amer. 53, 466 (1963).

51. J. H. Taylor and H. W. Yates, J. Opt. Soc. Amer. 47, 223 (1957); H. W. Yates and J. H. Taylor, Infrared Transmission of the Atmosphere, Report 5453, Naval Research Laboratory (1960).

52. H. J. Bolle, F. Möller, and W. Zdunkowski, Tech. Rpt. No. 2, Cambridge Research Laboratory, OAR (Contract AF 61 (052)-488); F. Vigroux, Ann. Geophys. 15, 453 (1959).

53. P. Varanasi, S. Chou, and S. S. Penner, J. Quant. Spectrosc. Radiat. Transfer 8, 1537 (1968).

54. D. E. Burch, D. A. Gryvnak, and G. H. Piper, Infrared Absorption by H_2O and N_2O, (Contract No. F19628-73-C-0011), Report U-6026, Aeronutronic (July 1973).

55. D. E. Burch, D. A. Gryvnak, and F. J. Gates, Continuum Absorption by H_2O Between 330 and $825 cm^{-1}$, Report No. U-6095, Aeronutronic (September 1974) (AFCRL-TR-74-0377).

56. D. E. Burch and D. A. Gryvnak, "Continuum Absorption by H_2O Vapor in the Infrared and Millimeter Regions," in Atmospheric Water Vapor, A. Deepak, T. D. Wilkerson, and L. H. Ruhnke, eds., Academic Press, New York (1980).

57. D. E. Burch, "Continuum Absorption by Atmospheric H_2O," Atmospheric Transmission, Proc. Soc. Photo-Opt. Instr. Eng. 277, 28 (1981).

58. S. A. Clough, F. X. Kneizys, R. Davies, R. Gamache, and R. Tipping, "Theoretical Line Shape for H_2O Vapor; Application to the Continuum," in Atmospheric Water Vapor, A. Deepak, T. D. Wilkerson, and L. H. Ruhnke, eds., Academic Press, New York (1980).

59. P. G. Wolynes and R. E. Roberts, Appl. Opt. 17, 1484 (1978).

60. P. A. Kollman and L. C. Allen, J. Chem. Phys. 51, 3286 (1969); K. Morokuma and J. R. Winnick, J. Chem. Phys. 52, 1301 (1970); J. Del Bene and J. A. Pople, J. Chem. Phys. 52, 4858 (1970); G. H. F. Diercksen, W. P. Kraemer, and B. O. Roos, Theor. Chim. Acta 36, 249 (1975); O. Matsuoka, E. Clementi, and M. Yoshimine, J. Chem. Phys. 64, 1351 (1976).

61. F. H. Stillinger and C. W. David, J. Chem. Phys. 69, 1473 (1978); J. C. Owicki, L. L. Shipman, and H. A. Scheraga, J. Phys. Chem. 79, 1794 (1975); L. A. Curtiss and J. A. Pople, J. Mol. Spectrosc. 55, 1 (1975); C. Braun and H. Leidecker, J. Chem. Phys. 61, 3104 (1974).

62. T. R. Dyke, K. M. Mack, and J. S. Muenter, J. Chem. Phys. 66, 498 (1977); T. R. Dyke, J. Chem. Phys. 66, 492 (1977).

63. K. J. Laidler, Chemical Kinetics, 2nd ed., McGraw-Hill Book Company, (1965).

64. G. E. Walrafen, Water: A Comprehensive Treatise, Vol. 1, F. Franks, ed. Plenum, New York (1972).

65. P. W. Anderson, Phys. Rev. 76, 647 (1949); C. J. Tsao and B. Curnutte J. Quant. Spectrosc. Radiat. Transfer 2, 41 (1962).

66. J. H. Van Vleck and D. L. Huber, Rev. Mod. Phys. 49, 939 (1977); D. L. Huber and J. H. Van Vleck, Rev. Mod. Phys. 38, 187 (1966).

67. H. M. Foley, Phys. Rev. 69, 616 (1949); V. V. Fomin and S. D. Tvorogov, Appl. Opt. 12, 584 (1973).

68. R. K. Long, F. S. Mills, G. L. Trusty, Tech. Rpt., Advanced Research Projects Agency (1973) (Contract Number F30602-72-C-0016).

69. W. R. Watkins, R. L. Spellicy, K. O. White, B. Z. Sojka, and L. R. Bower, Appl. Opt. 18, 1582 (1979).

70. R. R. Patty, G. M. Russwurm, W. A. McClenny, and D. R. Morgan, Appl. Opt. 13, 2850 (1974).

71. U. Persson, B. Marthinsson, J. Johansson, and S. T. Eng, Appl. Opt. 19, 1711 (1980).

72. E. H. Christy and K. H. Faller, 2nd Joint Conf. on Sensing of Environmental Pollutants, Paper 23, Washington, D. C. (10-12 December 1973).

73. G. Herzberg, Molecular Spectra and Molecular Structure: II. Infrared and Raman Spectra of Polyatomic Molecules, Van Nostrand Reinhold Company, New York (1945).

74. R. M. Bentwood, A. J. Barnes, and W. J. Orville-Thomas, J. Mol. Spectrosc. 84, 391 (1980).

75. H. A. Gebbie and W. J. Burroughs, Nature, Lond. 217, 1241 (1968); J. E. Harries, W. J. Burroughs, and H. A. Gebbie, J. Quant. Spectrosc. Radiat. Transfer 9, 799 (1969).

APPENDIX

FIGURES A-1 THROUGH A-21

The following figures show the dependence of the water absorption
coefficient on water partial pressure for various CO_2 laser 10.4-μm band
lines. Similar plots for the R(32) and P(28) laser lines appear in the text
(Figs. 15 and 16). The solid lines in Figs. A-1 through A-21 correspond to
the absorption calculated from the $a(\lambda, T)$ and $b(\lambda, T)$ coefficients, which
were determined from a linear least-squares fit of the abs. (λ, T) and
P_{H_2O} data to the expression

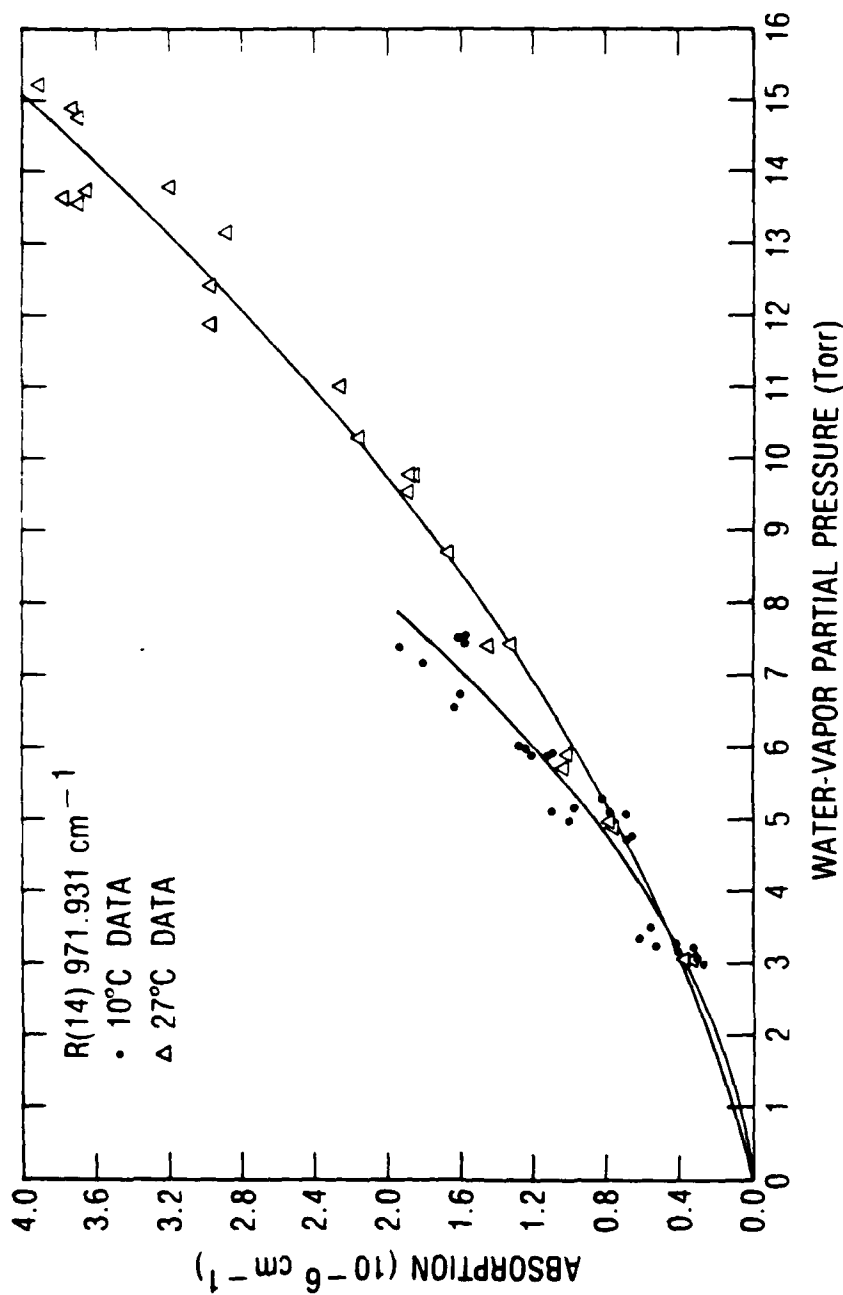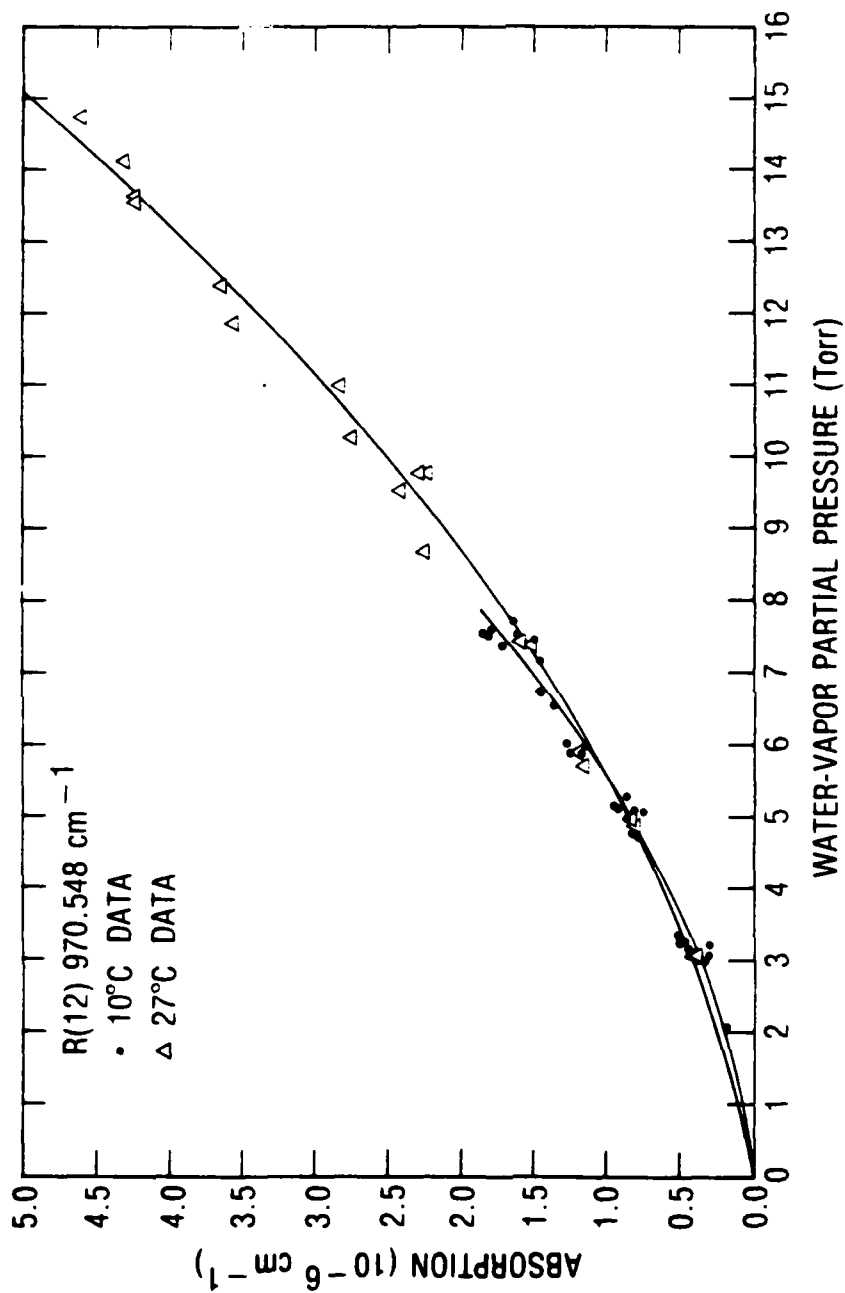$$\frac{\text{abs.}(\lambda, T)}{P_{H_2O}} = a(\lambda, T) + b(\lambda, T)P_{H_2O}$$
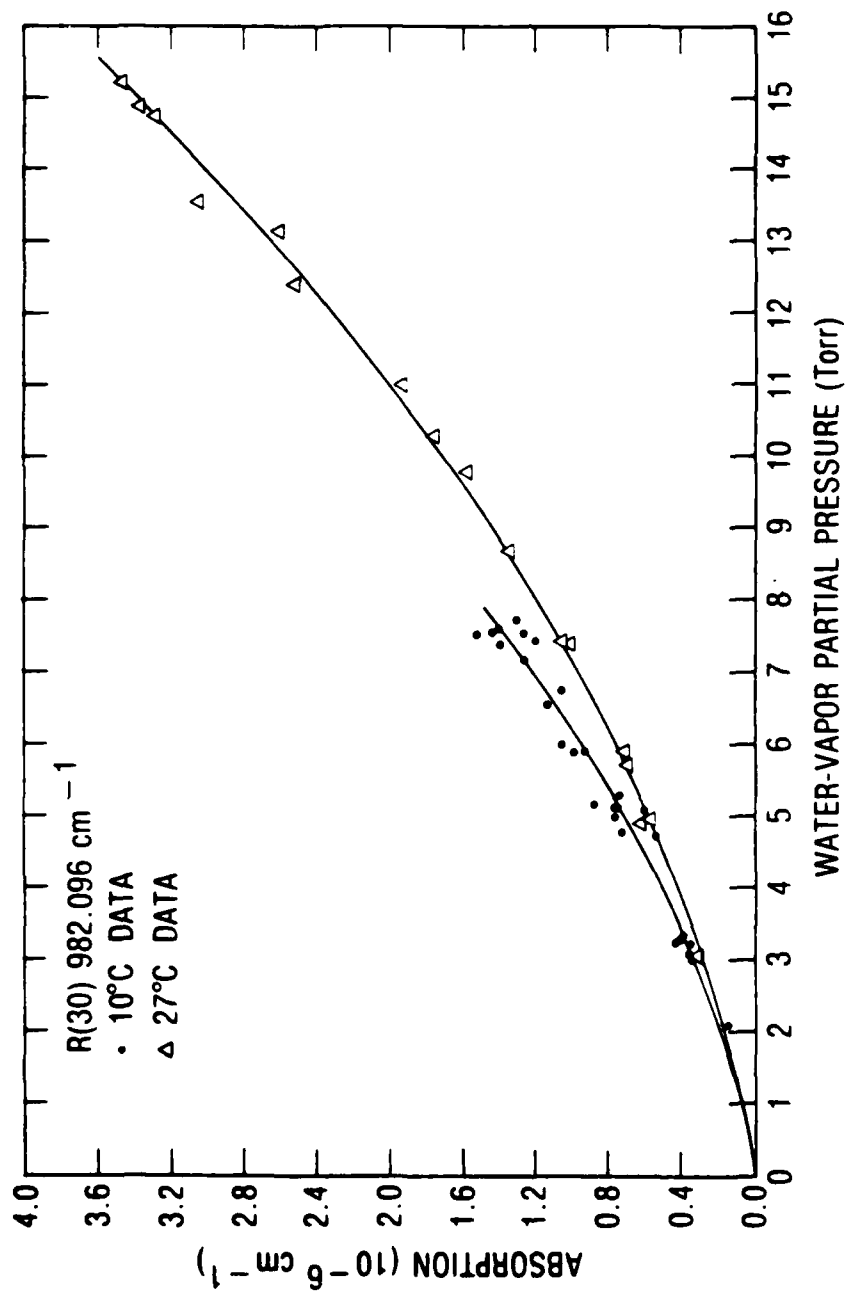
Fig. A-1. Dependence of absorption coefficients of 760-Torr total pressure water-vapor--air mixtures on water partial pressure at CO_2 laser 10.4-μm band R(30) line.
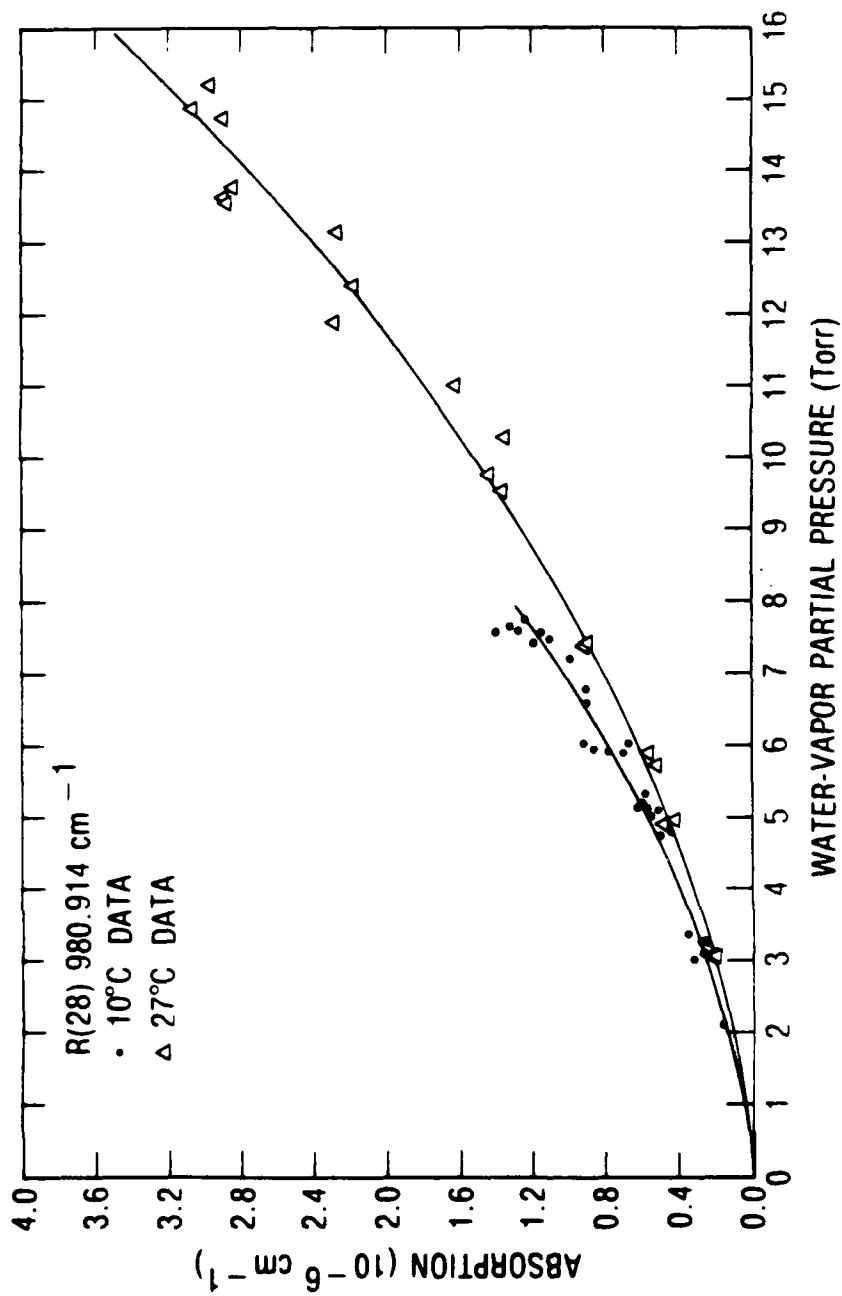
Fig. A-2. Dependence of absorption coefficients of 760-Torr total pressure water-vapor—air mixtures on water partial pressure at CO_2 laser 10.4-μm band R(28) line.
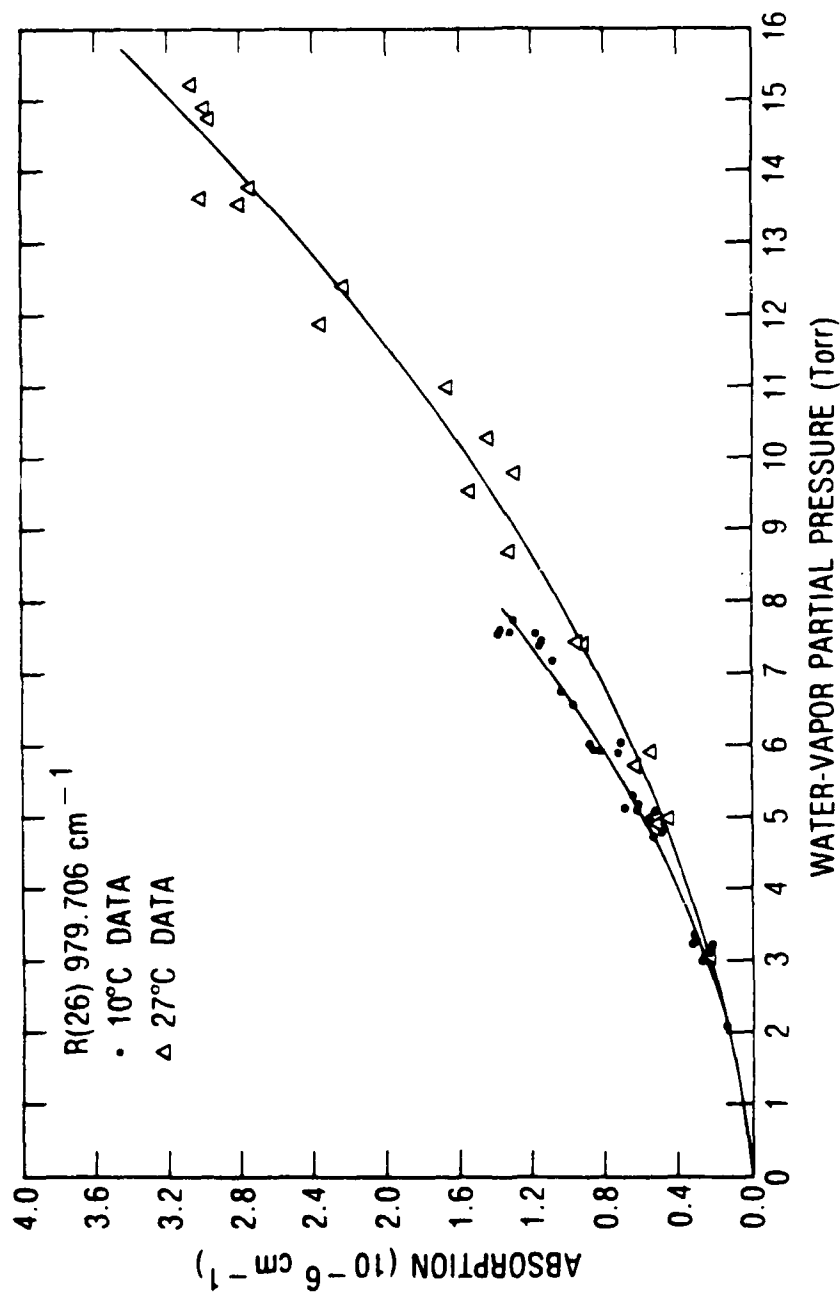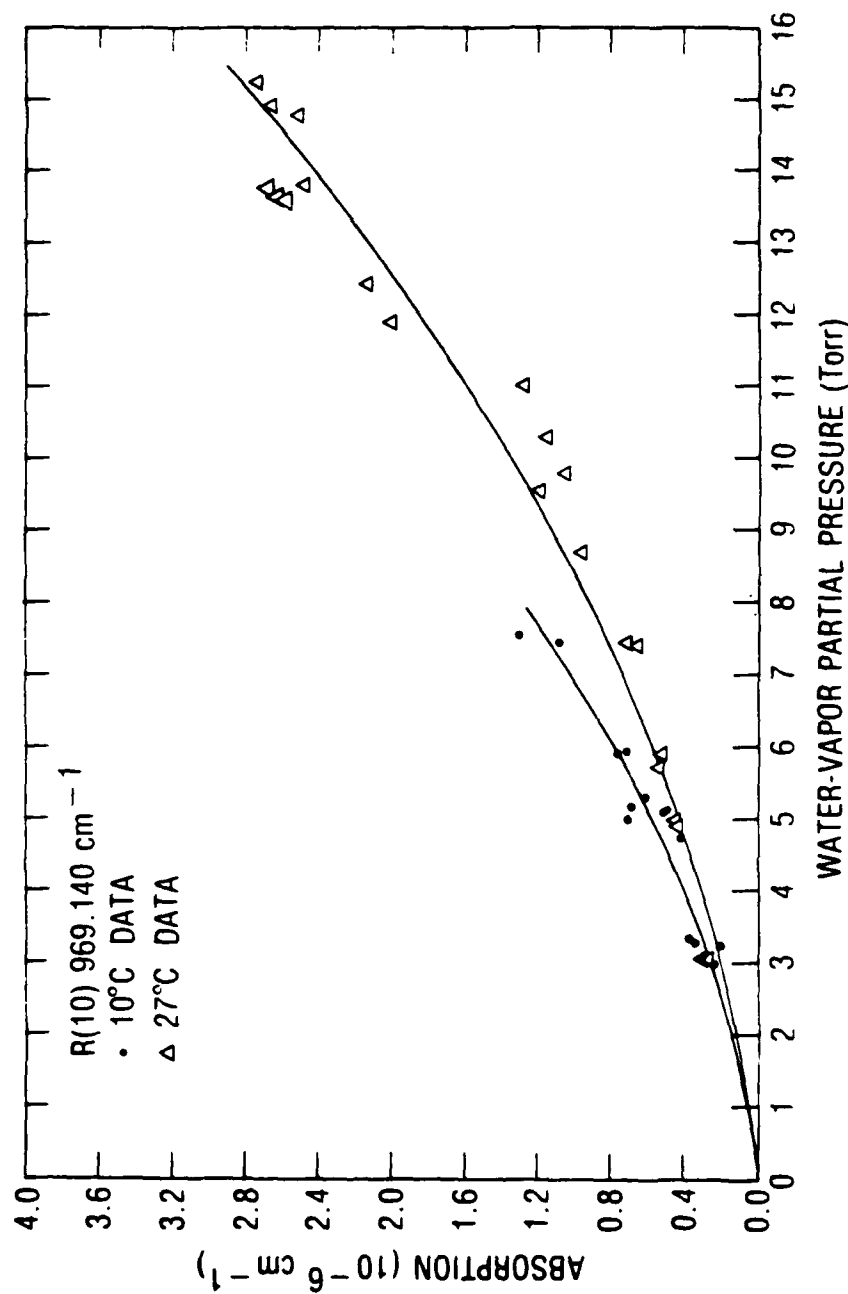
Fig. A-3. Dependence of absorption coefficients of 760-Torr total pressure water-vapor—air mixtures on water partial pressure at CO_2 laser 10.4-μm band R(26) line.
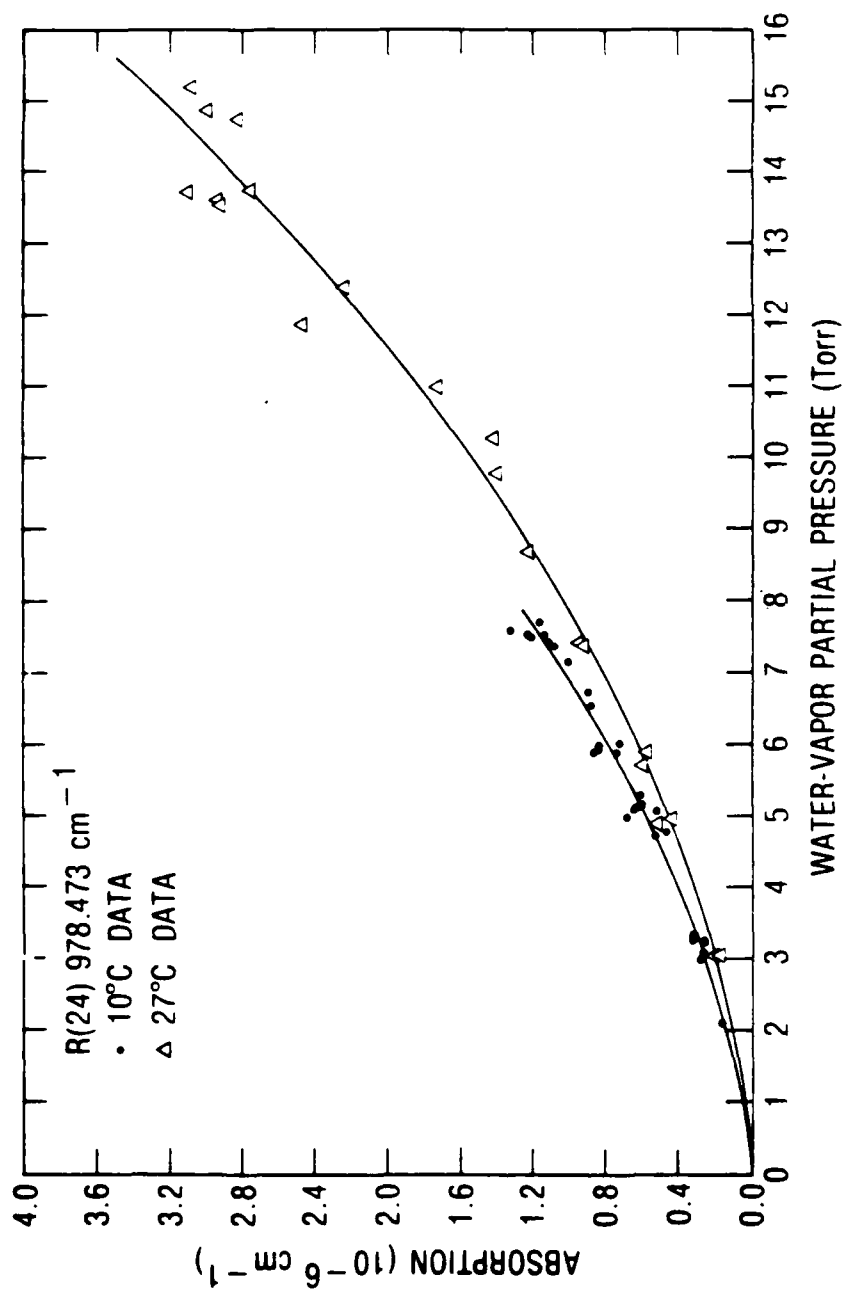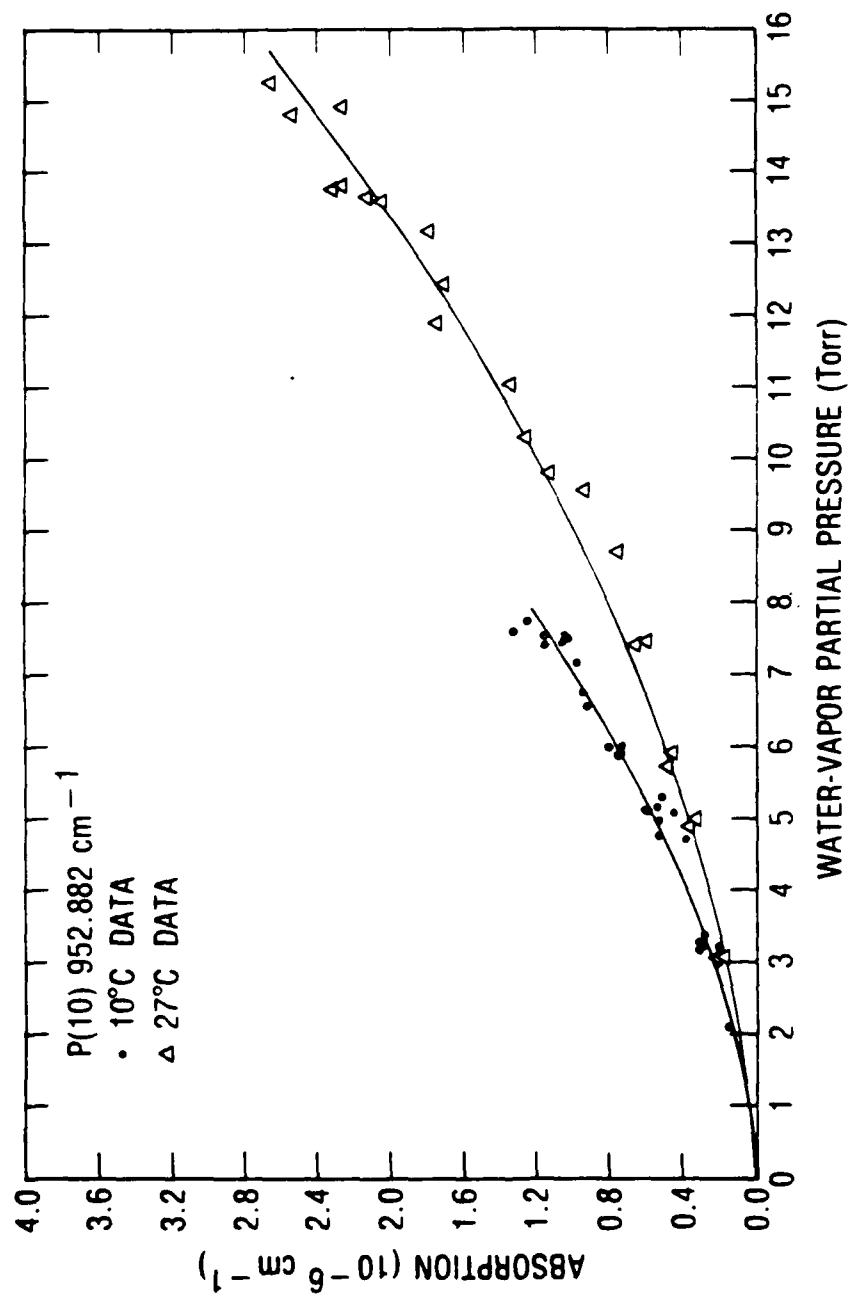
Fig. A-4. Dependence of absorption coefficients of 760-Torr total pressure water-vapor--air mixtures on water partial pressure at CO_2 laser 10.4-μm band R(24) line.
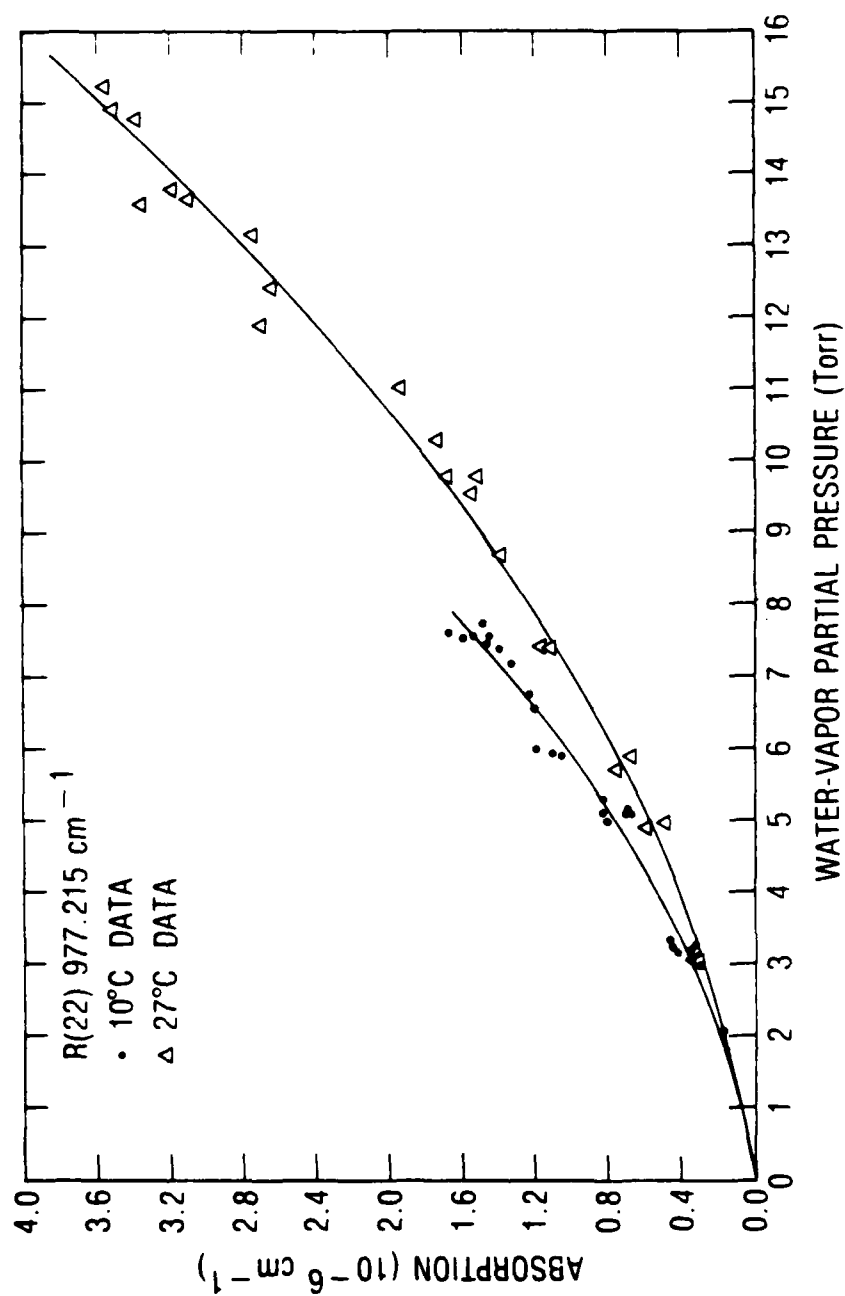
Fig. A-5. Dependence of absorption coefficients of 760-Torr total pressure water-vapor—air mixtures on water partial pressure at CO_2 laser 10.4-μm band R(22) line.
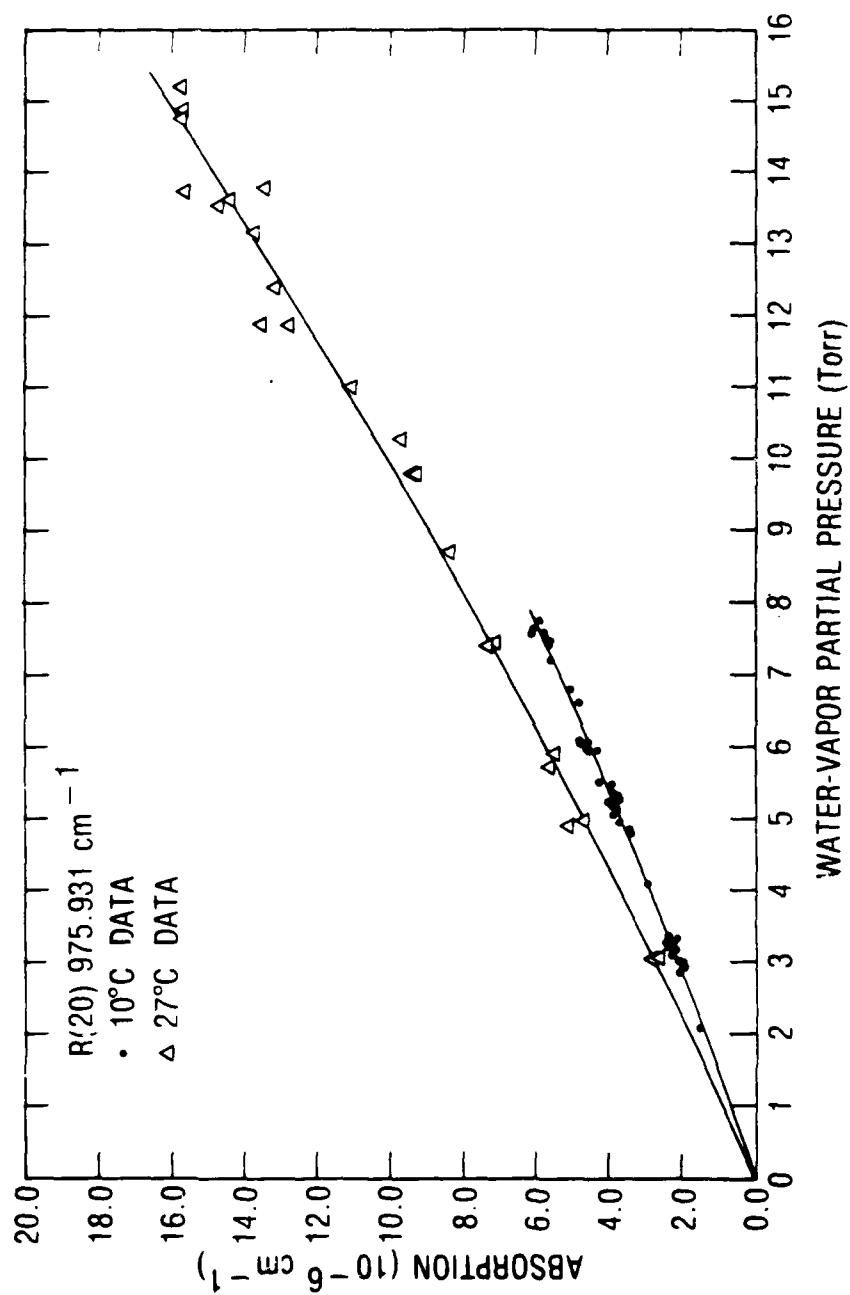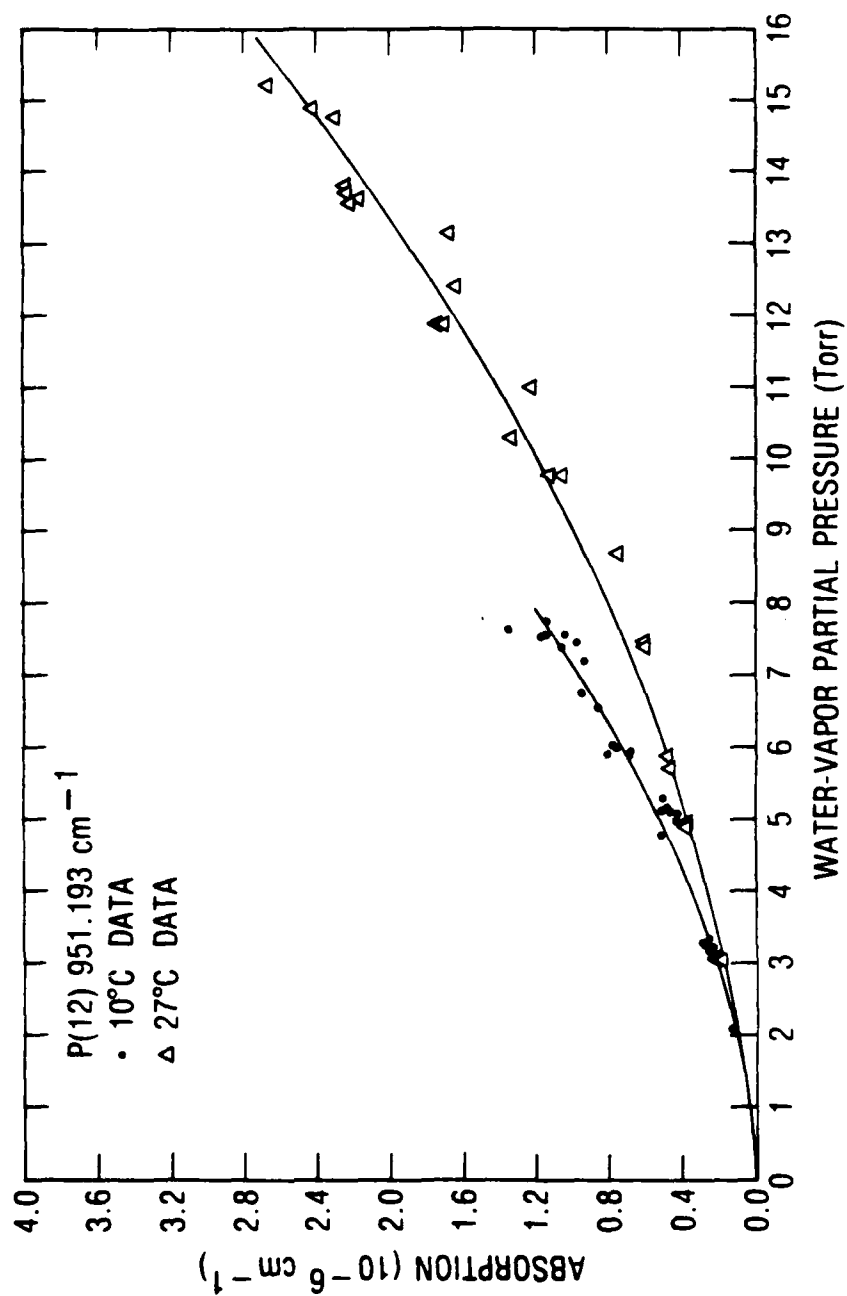
Fig. A-6. Dependence of absorption coefficients of 760-Torr total pressure water-vapor--air mixtures on water partial pressure at CO_2 laser 10.4-μm band R(20) line.
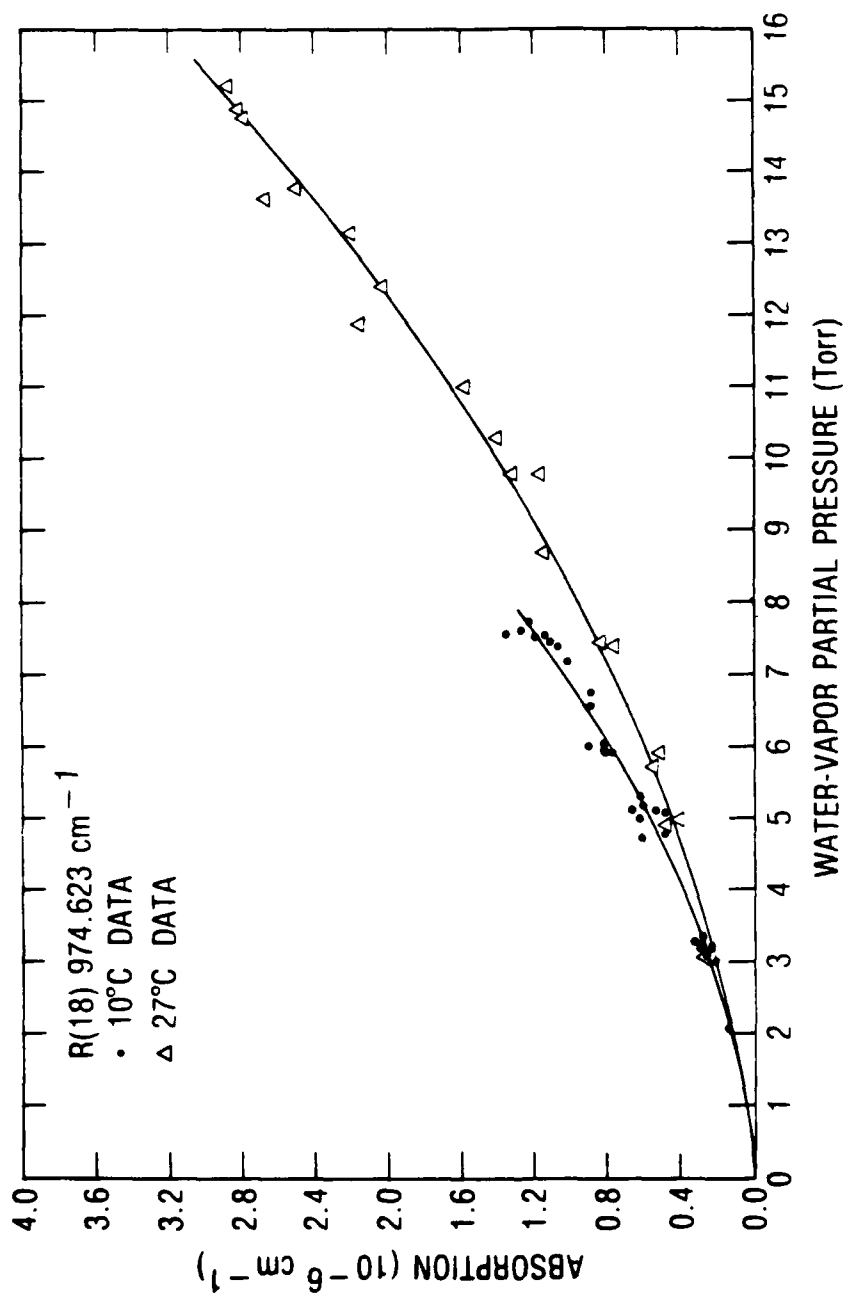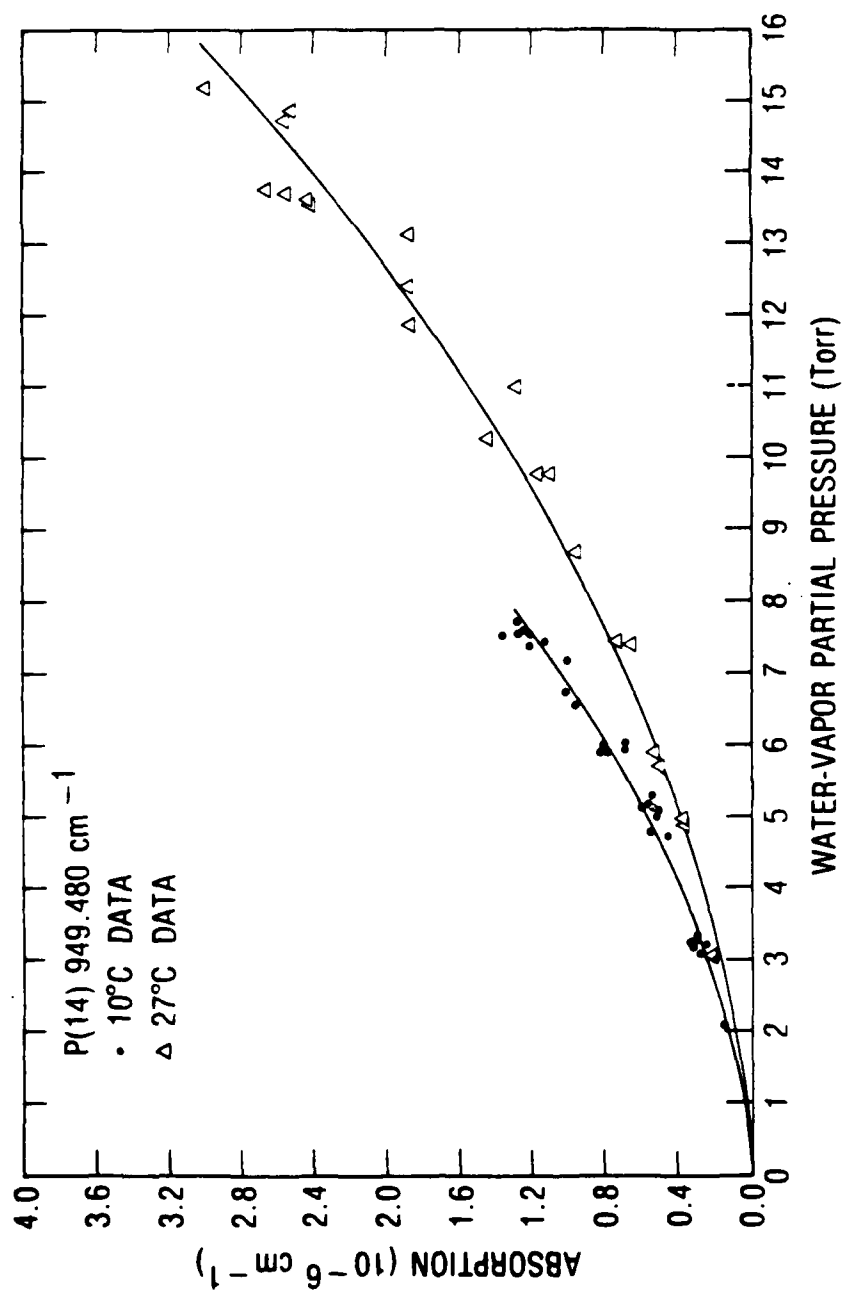
Fig. A-7. Dependence of absorption coefficients of 760-Torr total pressure water-vapor--air mixtures on water partial pressure at CO_2 laser 10.4-μm band R(18) line.
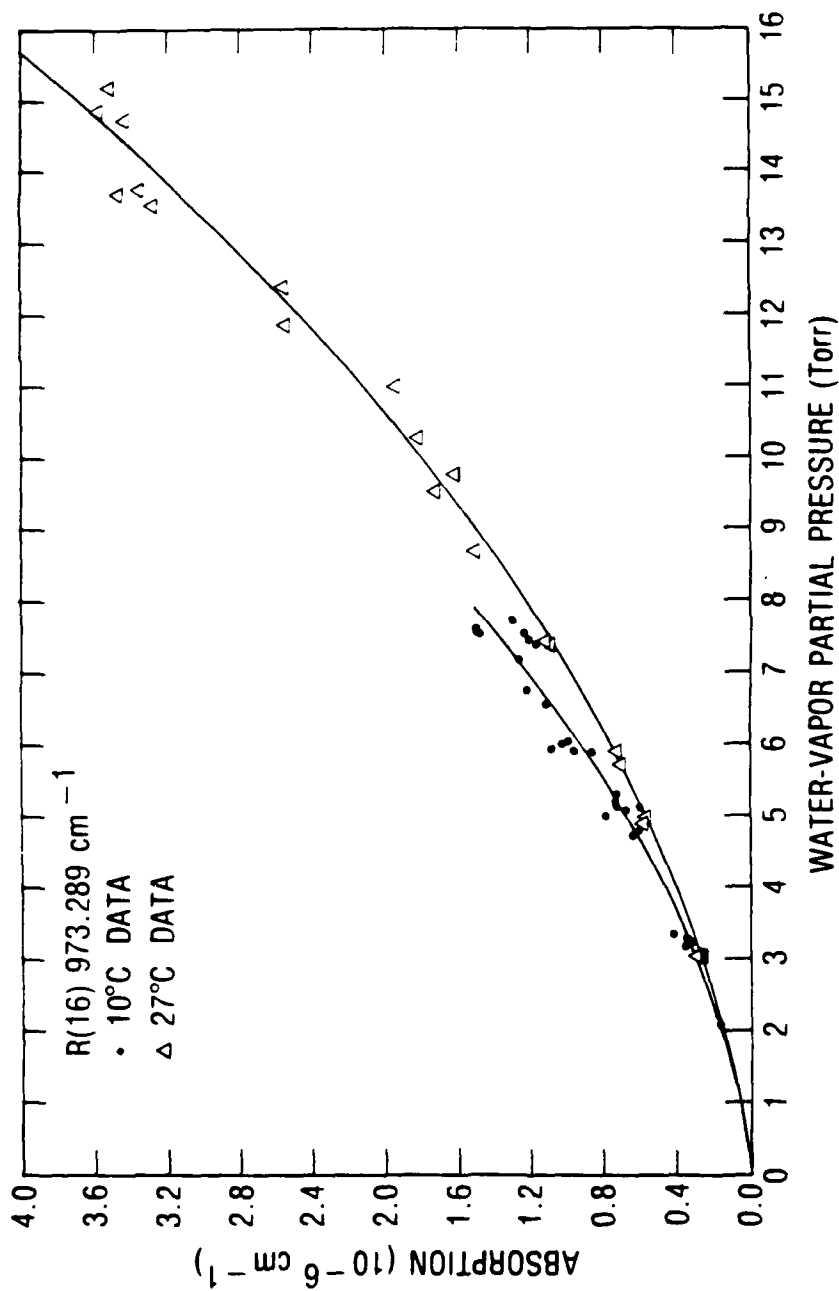
Fig. A-8. Dependence of absorption coefficients of 760-Torr total pressure water-vapor—air mixtures on water partial pressure at CO_2 laser 10.4-μm band R(16) line.
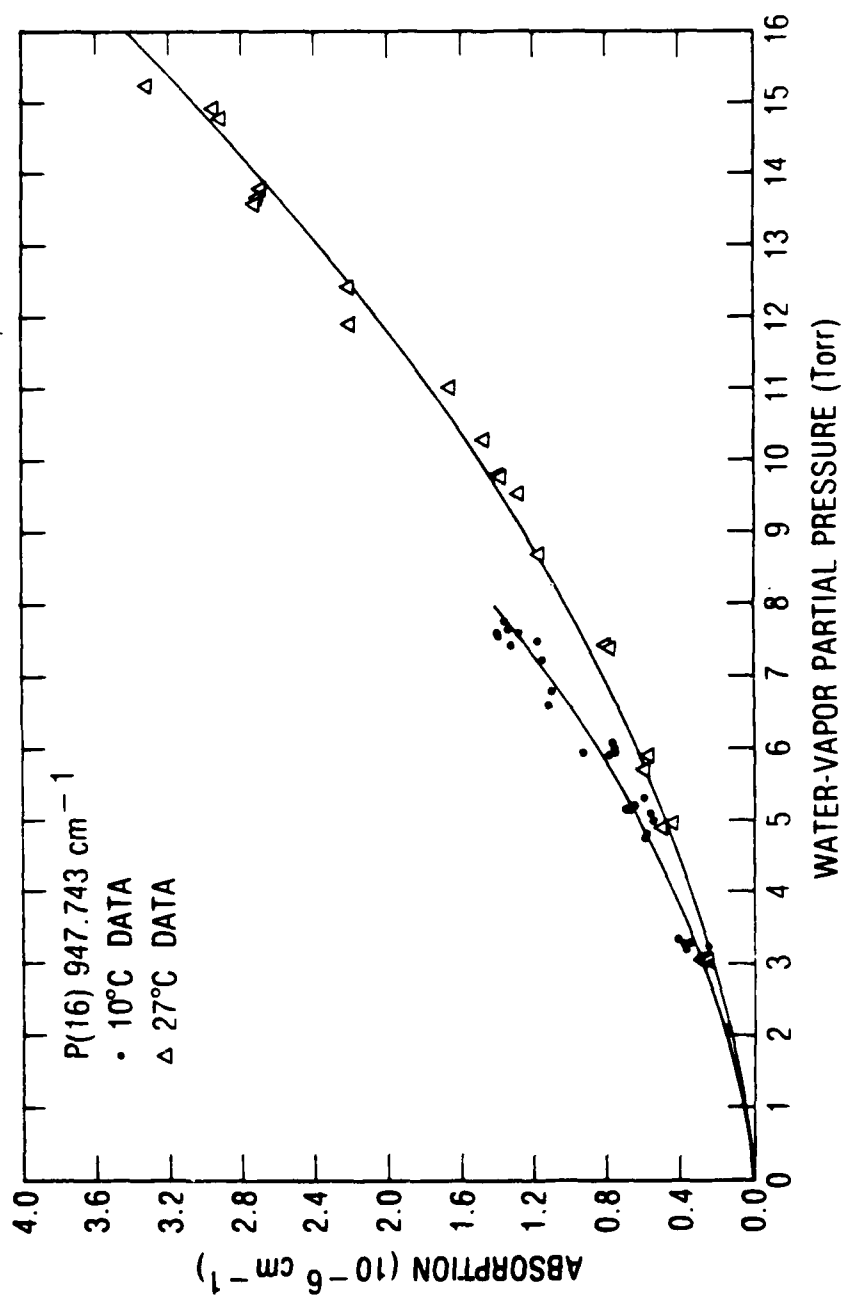
87

Fig. A-9. Dependence of absorption coefficients of 760-Torr total pressure water-vapor--air mixtures on water partial pressure at CO_2 laser 10.4-μm band R(14) line.

88

Fig. A-10. Dependence of absorption coefficients of 760-Torr total pressure water-vapor—air mixtures on water partial pressure at CO_2 laser 10.4-μm band R(12) line.
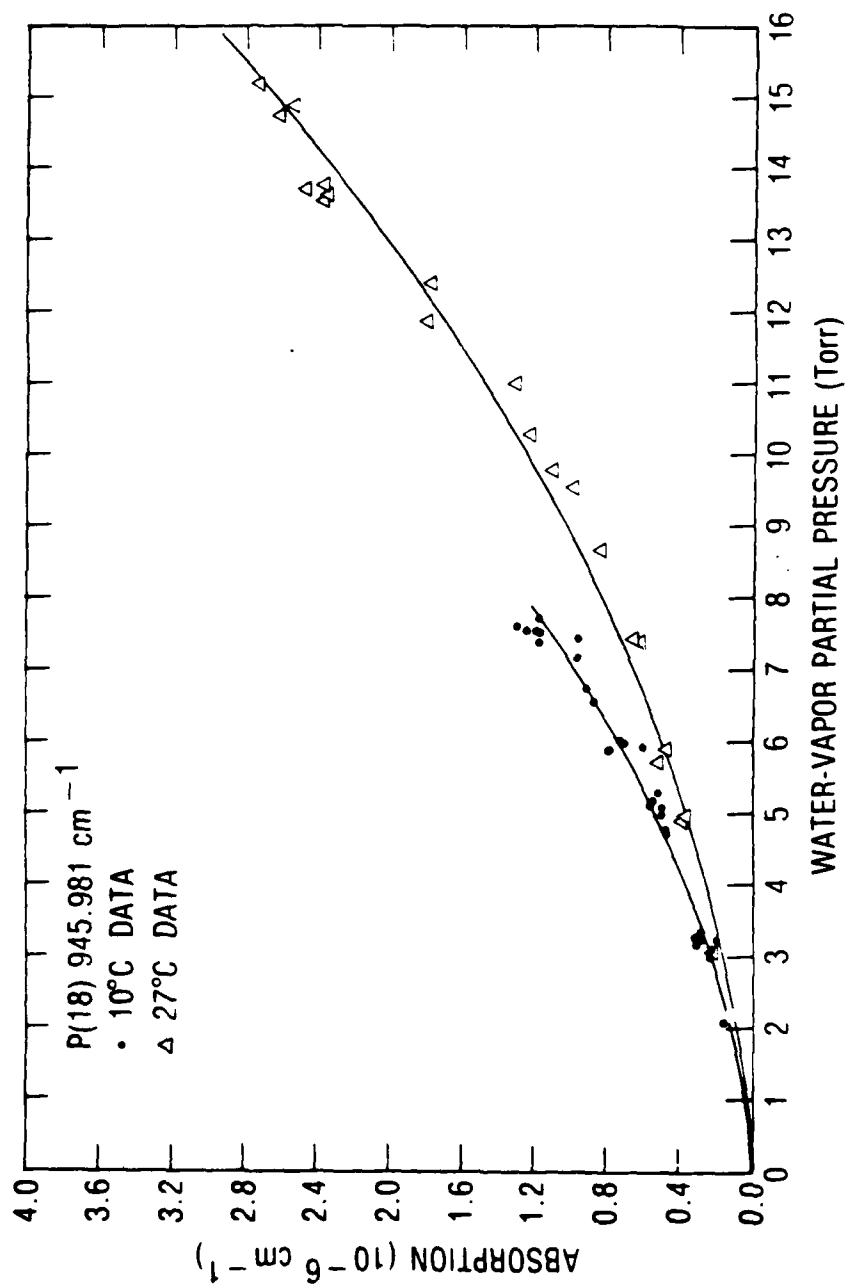
Fig. A-11. Dependence of absorption coefficients of 760-Torr total pressure water-vapor—air mixtures on water partial pressure at CO_2 laser 10.4-μm band R(10) line.

Fig. A-12. Dependence of absorption coefficients of 760-Torr total pressure water-vapor—air mixtures on water partial pressure at CO_2 laser 10.4-μm band P(10) line.
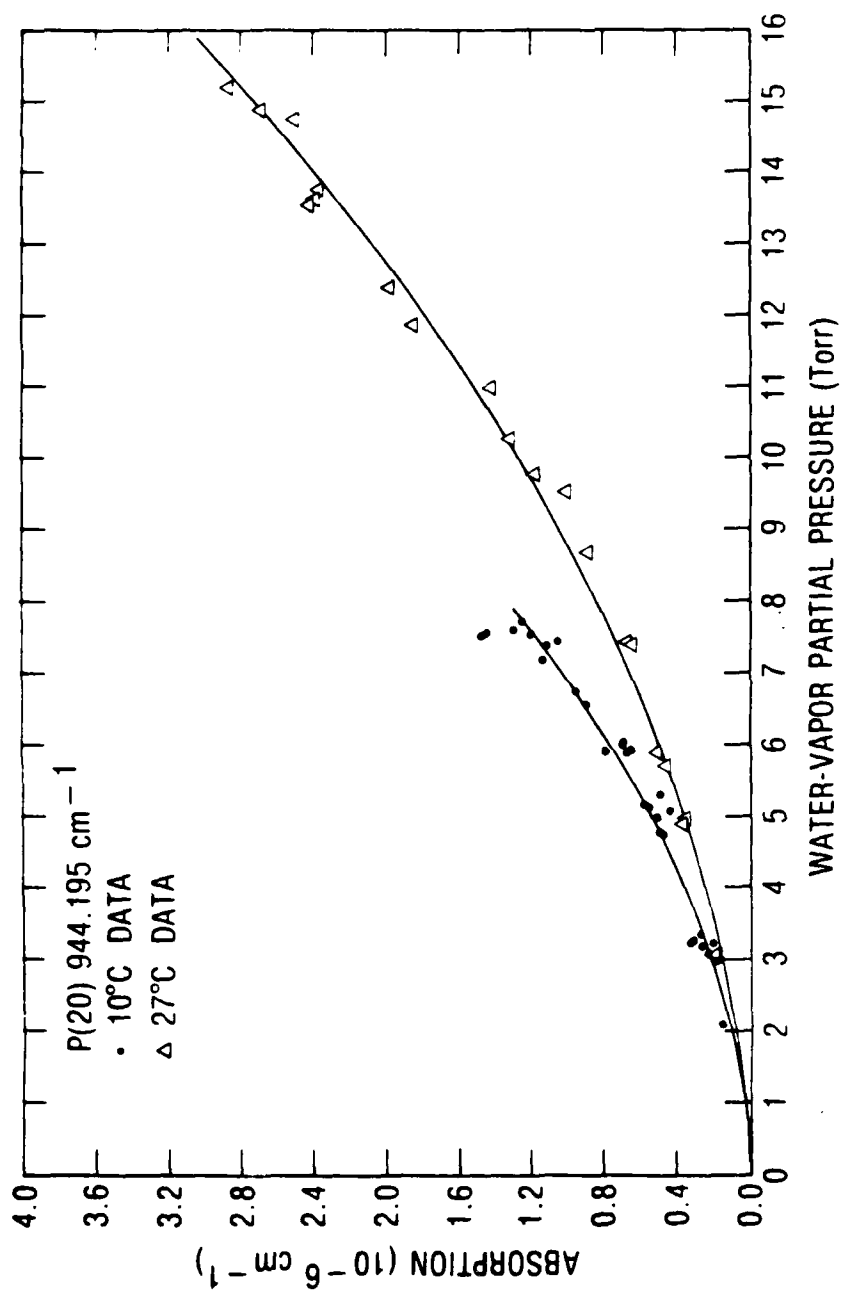
Fig. A-13. Dependence of absorption coefficients of 760-Torr total pressure water-vapor--air mixtures on water partial pressure at CO_2 laser 10.4-μm band P(12) line.

Fig. A-14. Dependence of absorption coefficients of 760-Torr total pressure water-vapor--air mixtures on water partial pressure at CO_2 laser 10.4-μm band P(14) line.
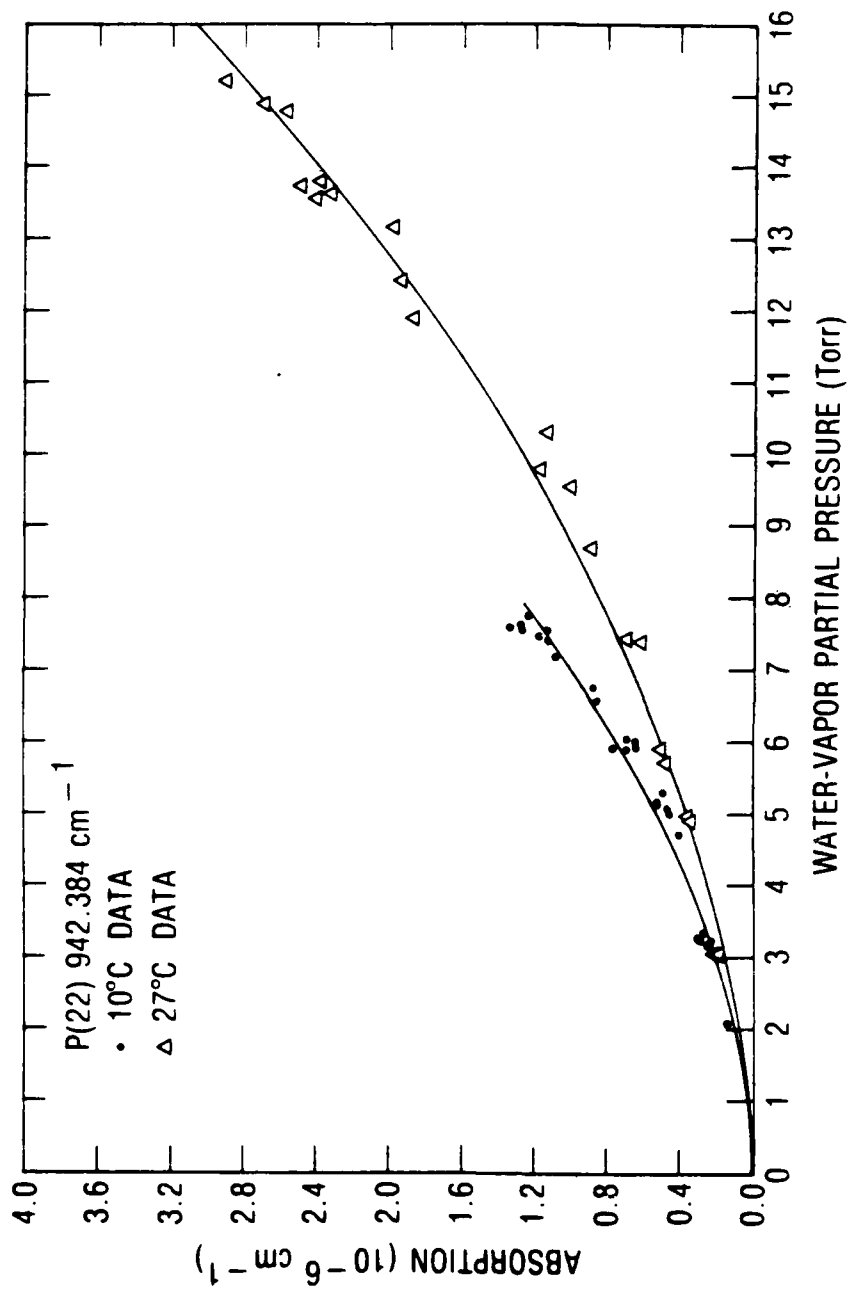
93

Fig. A-15. Dependence of absorption coefficients of 760-Torr total pressure water-vapor--air mixtures on water partial pressure at CO_2 laser 10.4-μm band P(16) line.
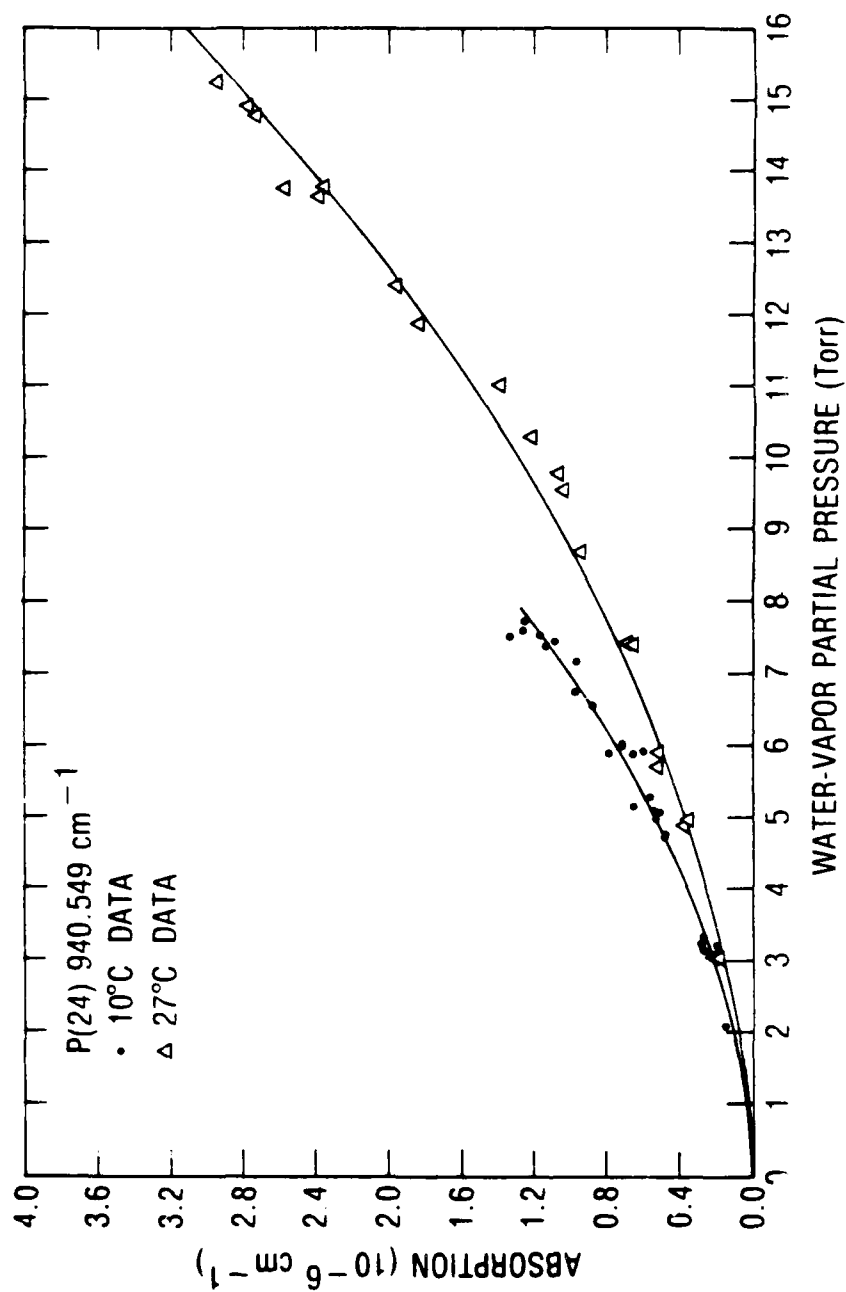
Fig. A-16. Dependence of absorption coefficients of 760-Torr total pressure water-vapor--air mixtures on water partial pressure at CO_2 laser 10.4-μm band P(18) line.

Fig. A-17. Dependence of absorption coefficients of 760-Torr total pressure water-vapor--air mixtures on water partial pressure at CO_2 laser 10.4-μm band P(20) line.

Fig. A-18. Dependence of absorption coefficients of 760-Torr total pressure water-vapor--air mixtures on water partial pressure at CO_2 laser 10.4-μm band P(22) line.

Fig. A-19. Dependence of absorption coefficients of 760-Torr total pressure water-vapor—air mixtures on water partial pressure at CO_2 laser 10.4-μm band P(24) line.
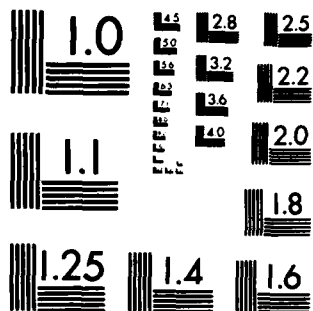
END
DATE
FILMED
7 84
DTIC

MICROCOPY RESOLUTION TEST CHART
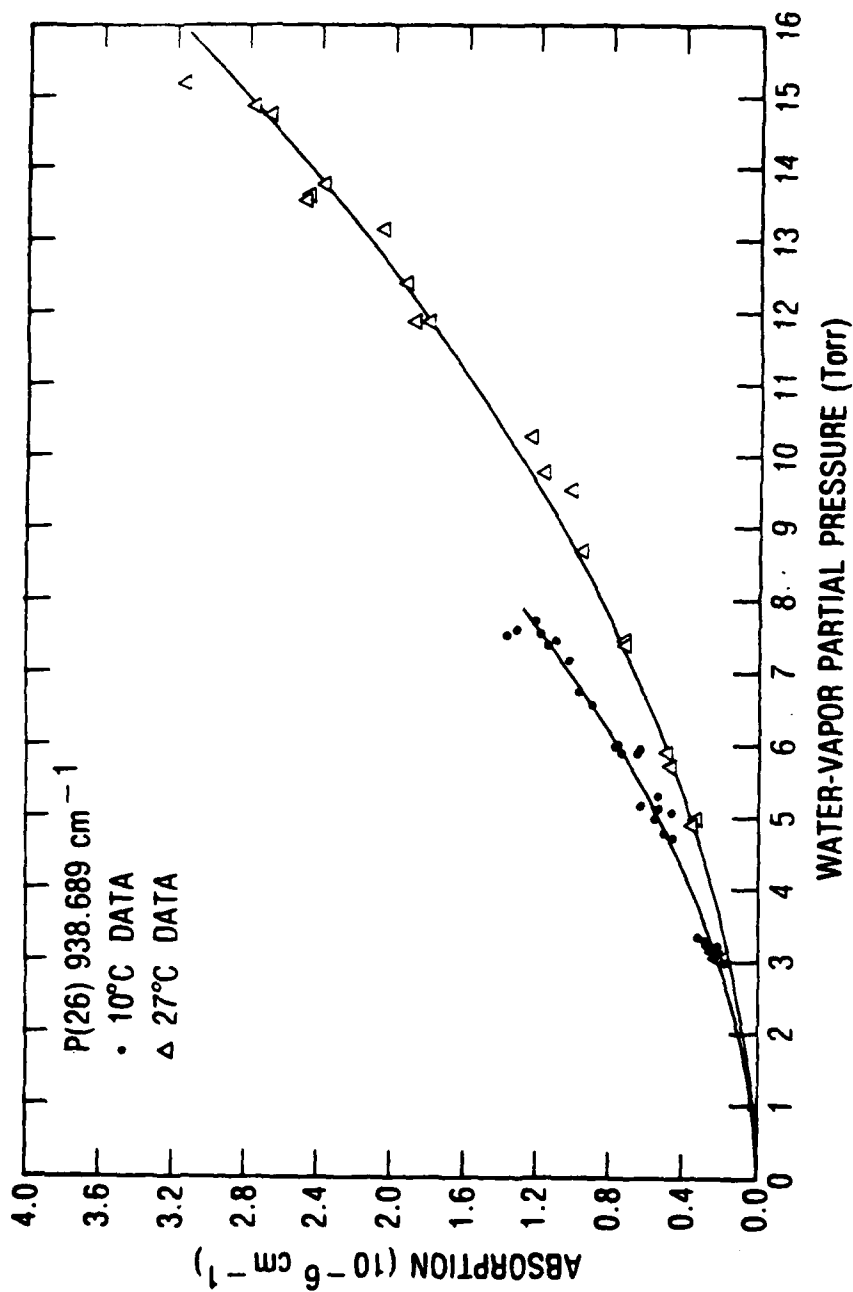NATIONAL BUREAU OF STANDARDS-1963-A

Fig. A-20. Dependence of absorption coefficients of 760-Torr total pressure water-vapor—air mixtures on water partial pressure at CO_2 laser 10.4-μm band P(26) line.
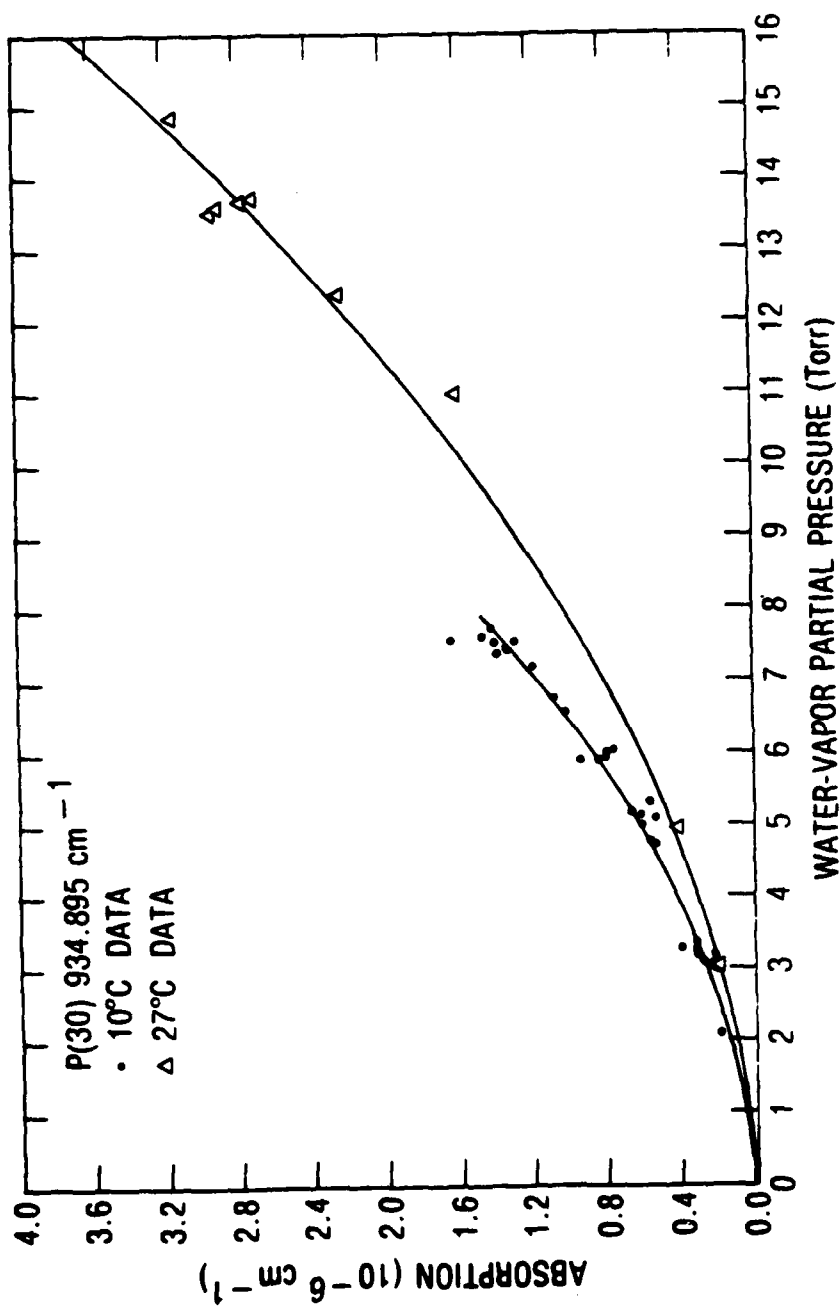
Fig. A-21. Dependence of absorption coefficients of 760-Torr total pressure water-vapor--air mixtures on water partial pressure at CO_2 laser 10.4-μm band P(30) line.

LABORATORY OPERATIONS

The Laboratory Operations of The Aerospace Corporation is conducting exper-
imental and theoretical investigations necessary for the evaluation and applica-
tion of scientific advances to new military space systems. Versatility and
flexibility have been developed to a high degree by the laboratory personnel in
dealing with the many problems encountered in the nation's rapidly developing
space systems. Expertise in the latest scientific developments is vital to the
accomplishment of tasks related to these problems. The laboratories that con-
tribute to this research are:

Aerophysics Laboratory: Launch vehicle and reentry aerodynamics and heat
transfer, propulsion chemistry and fluid mechanics, structural mechanics, flight
dynamics; high-temperature thermomechanics, gas kinetics and radiation; research
in environmental chemistry and contamination; cw and pulsed chemical laser
development including chemical kinetics, spectroscopy, optical resonators and
beam pointing, atmospheric propagation, laser effects and countermeasures.

Chemistry and Physics Laboratory: Atmospheric chemical reactions, atmo-
spheric optics, light scattering, state-specific chemical reactions and radia-
tion transport in rocket plumes, applied laser spectroscopy, laser chemistry,
battery electrochemistry, space vacuum and radiation effects on materials, lu-
brication and surface phenomena, thermionic emission, photosensitive materials
and detectors, atomic frequency standards, and bioenvironmental research and
monitoring.

Electronics Research Laboratory: Microelectronics, GaAs low-noise and
power devices, semiconductor lasers, electromagnetic and optical propagation
phenomena, quantum electronics, laser communications, lidar, and electro-optics;
communication sciences, applied electronics, semiconductor crystal and device
physics, radiometric imaging; millimeter-wave and microwave technology.

Information Sciences Research Office: Program verification, program trans-
lation, performance-sensitive system design, distributed architectures for
spaceborne computers, fault-tolerant computer systems, artificial intelligence,
and microelectronics applications.

Materials Sciences Laboratory: Development of new materials: metal matrix
composites, polymers, and new forms of carbon; component failure analysis and
reliability; fracture mechanics and stress corrosion; evaluation of materials in
space environment; materials performance in space transportation systems; anal-
ysis of systems vulnerability and survivability in enemy-induced environments.

Space Sciences Laboratory: Atmospheric and ionospheric physics, radiation
from the atmosphere, density and composition of the upper atmosphere, aurorae
and airglow; magnetospheric physics, cosmic rays, generation and propagation of
plasma waves in the magnetosphere; solar physics, infrared astronomy; the
effects of nuclear explosions, magnetic storms, and solar activity on the
earth's atmosphere, ionosphere, and magnetosphere; the effects of optical,
electromagnetic, and particulate radiations in space on space systems.

LMED